12-2023

Assessing The Thermodynamic Potential of Deep Eutectic Solvents in The Absorption of Greenhouse Gases Through Computational Methods

Thomas Michael Quaid
Florida Institute of Technology, tquaid2018@my.fit.edu

Title:

Assessing the thermodynamic potential of deep eutectic solvents in the absorption of greenhouse gases through computational methods.

by

Thomas Michael Quaid

A dissertation submitted to the Department of Chemistry and
Chemical Engineering of
Florida Institute of Technology
in partial fulfillment of the requirements
for the degree of

Doctor of Philosophy
in
Chemical Engineering

Melbourne, Florida
December, 2023

We the undersigned committee hereby approve the attached dissertation, "Assessing the thermodynamic potential of deep eutectic solvents in the absorption of greenhouse gases through computational methods" by Thomas Michael Quaid.

M. Toufiq Reza, Ph.D.
Associate Professor
Chemistry and Chemical Engineering
Major Advisor

Maria E. Pozo de Fernandez, Ph.D.
Assistant Professor
Chemistry and Chemical Engineering

Manolis M. Tomadakis, Ph.D.
Professor
Chemistry and Chemical Engineering

Nasheen Nur, Ph.D.
Assistant Professor
Electrical Engineering and Computer Science

Paul Yelvington, Ph.D.
Graduate faculty
Chemistry and Chemical Engineering

Jessica Smeltz, Ph.D.
Associate Professor and Department Head
Chemistry and Chemical Engineering

Abstract

Title: Assessing the thermodynamic potential of deep eutectic solvents in the absorption of greenhouse gases through computational methods.

Author: Thomas Quaid

Advisor: M. Toufiq Reza, Ph.D.

Greenhouse gas (GHG) capture is a fundamental technology in the fight against climate change. Some species of devastating GHGs like fluorinated compounds are released directly to the air from industrial processes. Some GHGs are co-produced in sustainably derived biofuels which require absorptive upgrading. The development of more efficient, cost effective, and environmentally friendly methods of capturing GHG's from pollutant sources and industrial streams is of utmost importance in the fight against climate change. Deep eutectic solvents have entered the separations stage as potential disruptors to conventional solvent choices for a variety of applications. Deep eutectic solvents (DES) are compounds of a hydrogen bond donor (HBD) and a hydrogen bond acceptor (HBA) that contain a depressed melting point compared to their individual constituents. These solvents are generally described as room temperature green tunable solvents. This dissertation explores the

thermodynamic potential of DES-GHG systems for their use as absorbents. Through examination of the various combinations of DES's a mechanistic understanding is developed which offers insights into which solvent components work best for a given application and why. The applications include absorption of fluorinated GHG R-32, CO_2 capture from biogas and the effects impurities have on the system, siloxane capture as an inhibitor to CO_2 uptake and biogas utilization, use of DES in upgrading model syngas systems, and the procedure required to make thermodynamic predictive software (COSMO-RS) accurate for studying more exotic systems of R-134a.

For each outlined topic a host of DES candidates from the type 3 or type 5 database was studied dependent upon the solutes energetic structure as computed through Turbomole software using density functional theory. A search for novel DES combinations and compositions was undertaken through the computation of thermodynamic parameters such as ln activity, solubility, and henry's constants with the use of COSMO-RS. An understanding of absorption mechanisms was arrived at through the examination of energetic structures, enthalpic mixing analysis, and comparisons of the resulting thermodynamic absorption values. Influence of independent systematic parameters were examined through varying pressure, temperature, and compositions while comparing resulting thermodynamics. EHS analyses were performed on the viable

DES candidates per system using VEGA KNN predictive software and Fischer Scientific SDS databases to understand the environmental and human worker safety/impacts of utilizing the DES components in industry. Aspen Plue V12 was utilized to compare DES system with conventional adsorbents on performance and energy requirements. Parameters for Aspen Plus V12 were found through literature, generated with COSMO-RS, and neural networks when necessary.

Table of Contents

List of Figures

List of Tables

Acronyms

AARD: average absolute relative deviation

AD: anaerobic digestion

a_{eff}: effective contact area

BCF: bioconcentration factor

BTACl: benzyltriethylammonium chloride

C: concentration

CFC's: chloro-fluorinated carbons

CO_2: carbon dioxide

CO: carbon monoxide

COSMO-RS: Conductor-like screening and modeling of real solvents

DEA: dimethanolamine

def2-TZVP: default-2 Valence Triple-Zeta Polarization

DES: Deep Eutectic Solvents

DFT: density functional theory

D3: hexamethylcyclotrisiloxane

D4: octamethylcyclotetrasiloxane

EHS: environmental health and safety

E_{misfit}: Misfit energy

GHG: greenhouse gas

G_{solv}: Gibbs free energy of solvation

GWP: Global warming potential

HBA's: hydrogen bond acceptors

HBD's: hydrogen bond donors

HCS: Hazard Communication Standard

H: Henry coefficients

H_2: hydrogen gas

H_{int}: excess enthalpy of interaction

HFC: Hydrofluorocarbons

HPWS: high pressure water scrubbing

H_2S: hydrogen sulfide

IL: Ionic liquid

KNN: K-nearest neighbors

LD_{50}: lethal dose 50

L2: hexamethyldisiloxane

L3: octamethyltrisiloxane

lnγ: activity coefficients

MEA: monoethanolamine

MDEA: methyldiethanolamine

MOF's: metal organic frameworks

M: sigma moment

MTOA: methyltrioctylammonium bromide

N4Br: tetrabutylammonium Bromide

N8Br: tetraoctylammonium Bromide

NFPA: National Fire Protection Association

OSHA: Occupational Safety and Health Administration

PEG: polyethylene glycol

P: pressure

R32: difluoromethane

RSS: residual sum of squares

SDS: safety data sheet

STP: standard temperature pressure

Syngas: synthesis gas

VOC's: volatile organic compounds

QSAR: quantitative structure-activity relationship

QSPR: quantitative structure-property relationships

μ: chemical potentials

$p_s(\sigma)$: distribution function

σ: sigma

Acknowledgements

I would like to acknowledge the patience, grace, and devotion to the successes of others of my mentor and advisor Dr. Toufiq Reza. Through him I have been given an example of how to meet people where they are in both their professional and personal journey. Through him I have learned to walk side-by-side with someone in facing and surpassing their limitations. This document bears the fruit of my efforts in seeking a PhD in chemical engineering, of which considerable personal setbacks and growth were necessary to produce. The emotional vicissitudes of this undertaking would not have been bearable without the support of an excellent faculty who truly care about the individual before them, rather than solely the task at hand. The people who have had a special part in setting premium examples in work ethic, persistence, professionalism, and compassion are found in the names of my committee members. I am thankful for the crossing of our paths and the lasting impressions bestowed upon me for having met and worked with each of you; Dr. Tomadakis, Dr. Pozo, Dr. Nur, and Dr. Yelvington. Most important is my wife Alesia Quaid who has made this possible through her continued support and sacrifices. May any success from this experience encourage you all to continue brightening the lights of others.

Chapter 1
Background

1.1. Greenhouse Gases

The term “climate change” was a re-branding of the “global warming” phenomena introduced by scientists and politicians in decades past. Climate change is the long-term alteration of consistently recorded weather patterns on a global scale. Several independent events have been responsible for invoking climate change in the earth’s history such as volcanic activity, solar activity, and other greenhouse gas emitting events [1], [2]. When excessive greenhouse gases are released into the atmosphere, the retention time for heat caused by radiation from the sun increases [3]. Long-term increases in global average temperature through this mechanism is what the earth is currently experiencing. Of the various causes for climate change, anthropogenically

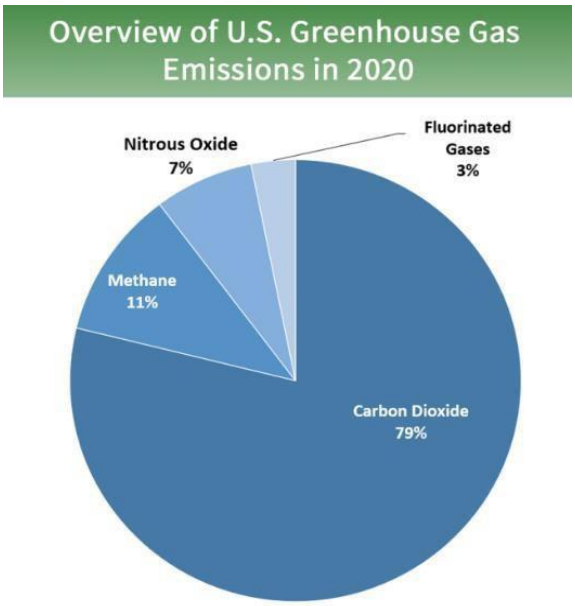

Figure 1: Compositional chart of GHG emissions [12]

sourced greenhouse gas emissions have been shown to be the main contributor to the recent warming event currently taking place which started in the 1800's [4]–[6]. During this period, global average temperature has increased by 1.1 °C [7]. As the temperature continues to climb significant impacts to Earths biosphere, natural resources, and human civilization will become increasingly evident [8]. In an attempt to mitigate anthropogenic contributions to climate change, several policies have been enacted by western governments which call for the remediation of some GHG's and phasing out from industry of others [9]–[11]. CO_2, CH_4, N_2O, and fluorinated gases are considered the "main" GHG's by the EPA with global annual makeup emissions of 79%, 12%, 6%, and 3% respectively as depicted in figure 1 [12]. In 2019 it was estimated that ~34,000 million metric tons of carbon dioxide were released from anthropogenic sources [13]. Much attention has been given to CO_2 in the climate change discussion due to the sheer volume of output from human sources. However, each gas has its own global warming potential (GWP) metric which is a measure of the greenhouse potential of the molecule in relation to CO_2. While fluorinated gases comprise only 3% of annual GHG emissions globally, some have GWP's of ~25,000, making them ~25,000 times more potent than CO_2 per mol [14]. Table 1 exhibits various literature values for GWP's, persistence lifetimes, and emission makeup percent for the U.S.

along with common contaminants and their compositional impact in biofuels like biogas and syngas.

Table 1: Greenhouse gases, their atmospheric lifetimes, global warming potentials (GWP), compositional ranges for biogas and syngas with common contaminants [3],[12],[14],[18],[43].

Species	Abbreviation	Lifetime	GWP (20yrs)	Annual U.S. Emission %	Biogas %	Syngas %
Carbon Dioxide	CO_2	1	1	79.4	25-50	1-17
Methane	CH_4	12	86	11.5	50-75	0-6
Nitrous Oxide	N_2O	120	280	6.2	-	-
Fluorinated Gases	HFC, PFC, SF_6, NF_3	50,000 ≥ X	25,000 ≥ X	3	-	-
Nitrogen	N_2	-	-	-	2-8	0.5-50
Hydrogen	H_2	-	-	-	0-1	2-34
Carbon Monoxide	CO	-	-	-	0-1	15-60
Hydrogen Sulfide	H_2S	-	-	-	0-1	0-1
Siloxanes	L2, L3, L4, etc.	-	-	-	0-1	-
Ammonia	NH_3	-	-	-	0-1	-

Anthropogenic emissions of GHG's are released from both centralized and de-centralized sources. It is estimated by the EPA [15] that 62% of emissions are from centralized sources of power generation, industrial, commercial, and residential zones. While the remaining comes from transportation, agricultural practices, and forestry. The distribution may be seen graphically in figure 2. However, the fight against climate change does not only exist at source emissions. The utilization of sustainably sourced fuels to supplement or replace fossil fuels has grown substantially, especially in the energy and transportation sectors. In the energy sector, adoption of biogas in place of fossil fuel derived natural gas has produced 18 GW of power globally with a growth of 4% per year over the last decade [16]. Syngas has been deemed a sustainable resource for generating hydrogen gas that may fuel the transportation industry [17]. However, the production of these cleaner alternate fuels results in the co-production of greenhouse gases which must be separated prior to combustion.

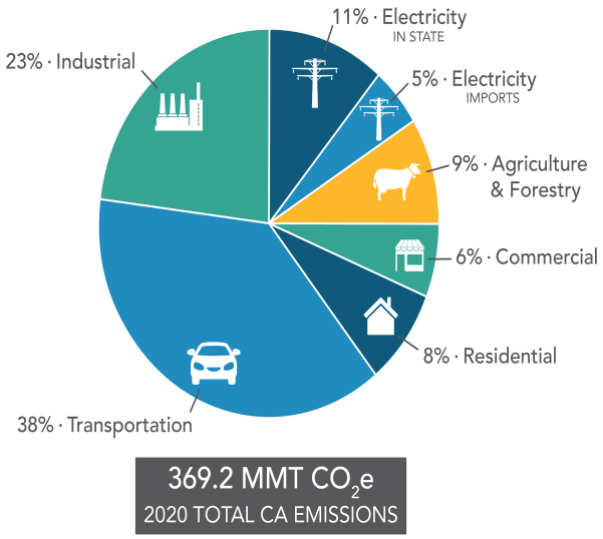

Figure 2: CO2 emissions and their sources for California in 2020. [18]

1.2. Biogas

Through a natural process called anaerobic digestion (AD), waste streams such as manure, agricultural chaff, and food wastes may be converted to a combustible fuel termed biogas [19]. AD is the process of breaking down organic substances in anoxic conditions by bacteria [20]. Organic macro-molecules such as fats, carbohydrates, and proteins are digested into micro-molecules during AD, which results in a nutrient-rich solid for plants (fertilizer) and biogas [21]. This process occurs naturally in landfills, but also in a controlled environment in equipment called anaerobic digestors. The feedstock for AD are materials that are otherwise considered waste, such as agricultural waste, manure, organic waste from animal processing plants, food waste, and many others [22], [23]. The growing adoption of AD offers a new approach to these waste streams which supports a recycling economy that increases market efficiency and bolsters the renewable energy industry as the globe shifts towards green fuel.

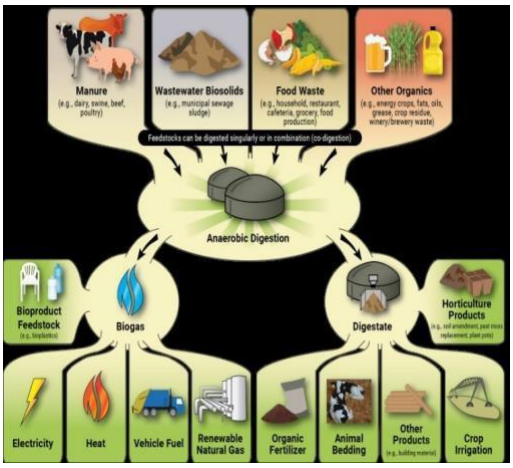

Figure 3: Feedstocks and product streams of anaerobic digestion [24].

Figure 3 is a simplified schematic of anaerobic digestion which displays the various feed sources and the wide array of usages for the products [24]. The range of sources for the feed leads to the variability of composition in the gaseous output stream as found in table 1. The point use determines the specific purity requirements for the product biogas.

During AD, several reactions occur, but the process can be categorized into four stages: hydrolysis, acidogenesis, acetogenesis, and methanogenesis. During hydrolysis, long-chain polymers like cellulose are hydrolyzed into fermentable forms like glucose. Acidogenesis and acetogenesis are characterized by the generation of hydrogen gas and carbon dioxide from monomers and glucose. The final stage, methanogenesis, is the stage where most of the methane is produced. Apart from CH_4 and CO_2, several other impurities are formed dependent upon the feed, such as ammonia, hydrogen sulfide, water, nitrogen, and siloxanes. The presence of CO_2 and the impurities lower the overall energy content of the biogas and can cause premature failure of point-of-use equipment [25]. For these reasons, carbon capture and biogas upgrading are often required prior to biogas application. Currently, biogas upgrading is conventionally performed through amine-based ionic liquid absorption or water scrubbing [26]. Ionic liquid (IL) amine-based absorption is desirable due to the solvents having a high selectivity for CO_2 over CH_4, which can achieve ~99% CH_4 purity [26]–[29]. However, the high viscosity, high cost, and

toxicity of these solvents suggest the need for an alternative [29]–[31]. Water scrubbing has a high efficiency (~97% CH_4 purity achieved), but it has been associated with bacterial growth issues, massive water consumption, and its necessity for additional processes in series to remove feed impurities [26], [29]. Other processes have also been developed for CO_2 removal, such as solid sorbents. These solid-based sorbents are found to have a large range of CO_2 capacity that reach up to 80 weight percent but have high operating temperatures that exceed 500 °C [32], [33]. However, due to the low combustive properties of some impurities, low-temperature solid adsorbents like zeolites are the only feasible option, which have significantly lower capacities [34], [35].

1.3. SynGas

The escalating global demand for sustainable and clean energy sources has led to a surge in research efforts focusing on alternative energy production methods, such as syngas (synthesis gas) generation from biomass and waste materials [36]–[38]. Syngas is a mixture of hydrogen (H_2), carbon monoxide (CO), carbon dioxide (CO_2), and hydrogen sulfide (H_2S), and serves as a valuable feedstock to produce a wide range of chemicals and fuels [39], [40]. However, the presence of impurities like CO_2 and H_2S can negatively impact the efficiency and environmental performance of syngas utilization processes [41], [42]. Consequently, it is

essential to develop effective and environmentally friendly methods for cleaning syngas to enhance its quality and applicability.

Figure 4 depicts a simplified process flow diagram of syngas feeds, syngas upgrading, and syngas usage in various industries [43]. The feeds are typically carbon-based wastes in the form of coal, biomass, petroleum coke, and carbon rich waste streams from other industries. After solid feeds are gasified the syngas must be upgraded to the purity standards of the facilities that would utilize it which changes for each type (energy, transportation, etc.). After upgrading syngas may be directly burned for heat, sold for use in chemical development, or sent through a generator to create electricity.

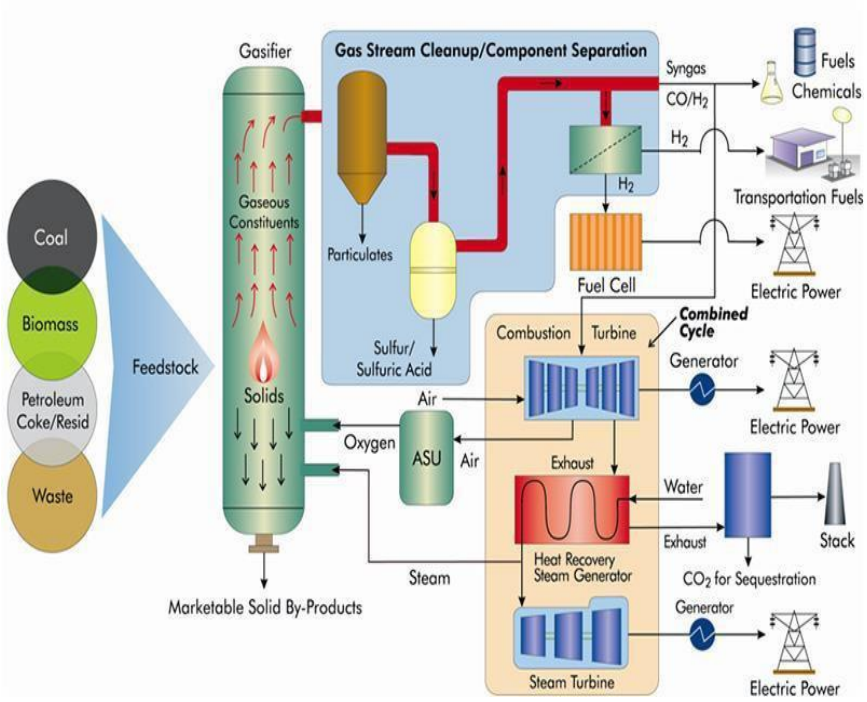

Figure 4: PFD of a syngas treatment plant, feed sources for syngas production, and point use destinations [43].

The significance of syngas as an alternative to fossil fuels comes in the value product of H_2 gas which can be used as a fuel whose only waste stream is water as the energy is provided through the fusion of hydrogen and oxygen [44]. However, The cost to produce the energy equivalent of a gallon of gasoline (1kg H_2) in 2020 was reported as between $3-8/kg [45]. Although it is reported that separation costs alone using conventional methods may reach up to $8/kg [46]. Whereas gasoline costs less than $1 to transport, refine, and less than $1 for crude feed totaling in <$2 for the entire operation [47]. Due to the high cost of hydrogen fuel much work must be done in production efficiency to make it competitive with conventional fossil fuel systems.

1.4. GHG separation

Adsorbing GHG's to solid materials such as zeolites, metal organic frameworks (MOF's), silica gels, and activated carbons is a method currently being developed and studied as a solution to improving the cost of alternate fuel purifications and pre/post combustion CO_2 capture [48]. These methods may undergo both physical or chemical adsorption mechanisms at both high and low temperature conditions. While these are generally a relatively cleaner technology, research is still being done to overcome their issues of chemical instability, low working capacity, low selectivity, high

regenerative costs, and abrasive resistance in fixed and fluidized beds [49], [50].

Absorption based GHG capture encompasses two main routes: chemical and physical. In chemical absorption, amine solvents like MEA react with CO_2 and form carbamates or bicarbonates which are reversed in a regeneration unit. Equations 1 and 2 show the main reactions found between CO_2 and monoethanolamine (MEA) in a chemical scrubbing procedure. MEA is considered a conventional solvent for acid gas capture due to its high absorption load and rate [51]. Though the regeneration procedure is high cost due to extreme energy demands and it is sensitive to other acidic impurities which would readily react with it [52]. Due to its reactivity and the strong alkaline nature of MEA, simple steel construction is not permitted for the procedure resulting in higher capital cost equipment [53]. As seen in figure 5 the typical absorption system consists of a desulfurization section, an absorption column, and a regeneration column with recycling for lean solvent assuming the feed is dehydrated.

$$2\ RNH_2 + CO_2 \rightleftharpoons RNH_3^+ + RNHCOO^- \quad \text{(Carbamate Formation)} \quad (1)$$

$$RNH_2 + CO_2 + H_2O \rightleftharpoons RNH_3^+ + HCO_3^+ \quad \text{(Bicarbonate Formation)} \quad (2)$$

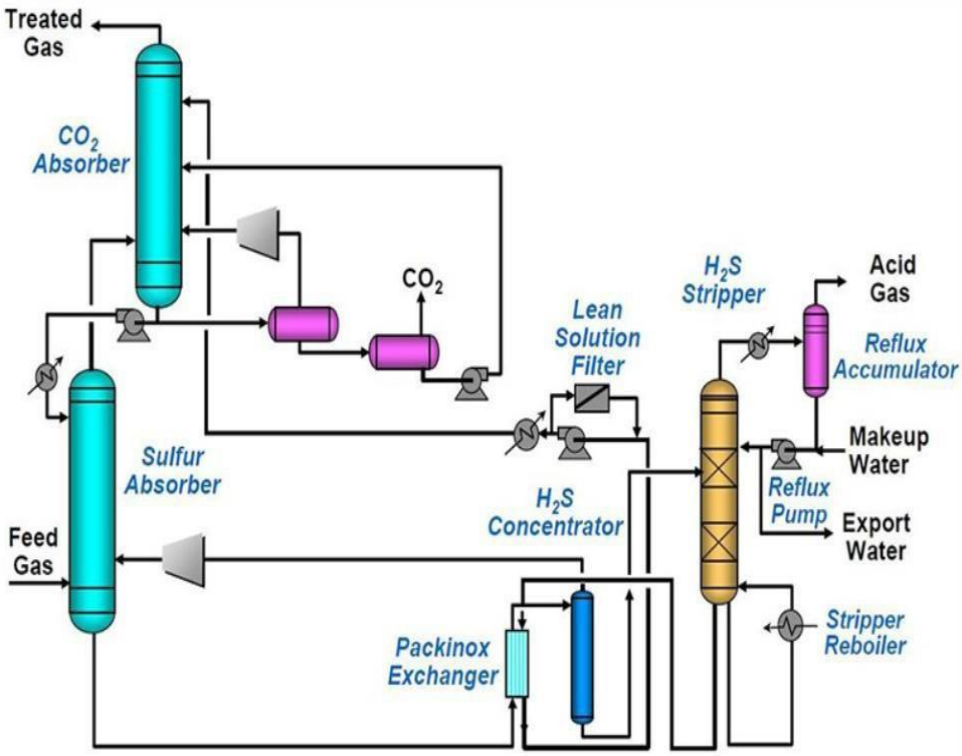

Figure 5: A common PFD system for upgrading biogas or syngas which includes a multistage absorption system for sulfuric compound remediation and ghg removal.

Physical absorption relies on selectively dissolving a gaseous species in a solvent rather than covalent bond formations found in chemical absorption [54]. These solvents rely on mechanisms such as Vander Wals interactions, hydrogen bonding, and physical entrainment to remove components from a gaseous stream [55]. Physical absorbents are commonly used for GHG capture in the form of water scrubbing or organic solvents when concentrations of the solute are high, as found in feed streams of syngas and biogas where CO_2 is a co-product [56]. These absorbents have

the advantage of relatively low regeneration energy requirements, low toxicity, and high selectivity [57]. Among this class is high pressure water scrubbing (HPWS) and organic solvents like Selexol. While this method generally operates at close to room temperature, requires less energy to regenerate, has lower solvent loss due to low vapor pressures, and is significantly less corrosive than the chemical absorbents, they tend to have higher viscosities which can make them difficult to process [53], [58], [59].

1.5. Novel Solvents

Ionic liquids are solvents that are comprised of complementary ionized components whose combination results in a material with a melting point below 100 °C. This class of solvents have gained tremendous popularity among the scientific community in the past two decades due to their "designer" attribute which allows a mixing of varying components to develop highly suitable solvent properties for a given application [60]. Ionic liquids have several favorable characteristics which make them appealing as a replacement for conventional GHG capture solvents such as thermal stability, wide application, low flammability, non-volatility, and recyclability [61], [62]. Works have shown IL's possess the ability to effectively absorb GHG's like Perumal et al. [63] who reported IL blends increased absorption efficiency of CO_2 by up to 30% over baseline of a MEA. Zachello et al. [64] report results of IL assisted absorption to decrease regeneration energy demands by up to 11% in carbon capture vs

conventional MEA systems. Huang et al. [65] reported IL assisted capture of CO_2 to reduce the regeneration costs by up to 15% with comparable uptake efficiency. While IL's are thermodynamically capable of absorbing GHG's comparably to the conventional solvent MEA, they tend to suffer from issues such as high viscosity, toxicity, long-term instability, corrosive nature, and expense limit them to be useable as a pure solvent and are often mixed with the conventional MEA as an approach to lower overall operating costs [66], [67].

Deep Eutectic Solvents (DES) are considered analogues of ionic liquids with the main difference being that they are room temperature solvents and comprised of organic compounds with a single associated ion rather than two ionized species. These are a relatively new class of green solvents defined by their composition of two or more chemicals which, when added together, incur a significant eutectic point depression [68]. These parts are categorized as being hydrogen bond acceptors (HBA's) and hydrogen bond donors (HBD's) as no covalent or ionic bonding takes place. For example, HBA like choline chloride (melting point, ~302 °C) and HBD like urea (~133 °C) in a mixture of 1:2 M ratio form DES with a melting point of 12 °C [69], [70]. Figure 6A [69] depicts a prototypical phase diagram for a eutectic solvent mixture, where a significant eutectic depression point exists when two solids are mixed in a 1:2 molar ratio. Figure 6B [69] shows the cluster formation that develops between ChCl and

urea when mixed in a 1:2 molar ratio. The hydrogen bonding complex between the cation associated with the choline molecule and the urea molecules has been determined as the driving factor of the eutectic depression [71]. It is this hydrogen bonding complex which offers the extensive variability of physical properties found in the myriad of DES combinations which is visually depicted in figure 6B [69]. DES have thus been termed a “tunable solvent” [72]. Not only can DES be tuned in terms of viscosity, melting point, polarity, etc. through manipulation of molar ratios and components, but they have been able to take on fundamentally different characteristics which has led to several new classifications such as hydrophobic/hydrophilic, magnetic, switchable hydrophobicity, and natural DES [73]–[76]. DES may be categorized into five main types as available in table 2.

Table 2: Classification of DES types.

Type	General Formula
1	Quaternary Halide + Metal Chloride
2	Quaternary Halide + Metal Chloride Hydrate
3	Quaternary Halide + Hydrogen Bond Donor
4	Metal Halide Hydrate + Hydrogen Bond Donor
5	Non-Ionic Species + Non-Ionic Species

Among the five types of DES, only type 3 and 5 DESs are considered as environmentally benign and are generally cheaper alternatives to conventional solvents used in industry [77]–[79]. New solvent combinations are continually being discovered and added to the library of DES. So far, most of the components for type 3 and 5 (which are of special consideration due to their "greenness") can be classified by a select few species for HBA and HBD. For HBA most chemicals fall under quaternary ammonium salts, quaternary phosphonium salts, terpenoid/phenolic, acids, and imidazoles [80]–[82]. HBD components may generally be found to exist in chemical groups of carbamates, acids, alcohols/polyols, and terpenoid/phenolic [68], [83]–[85].

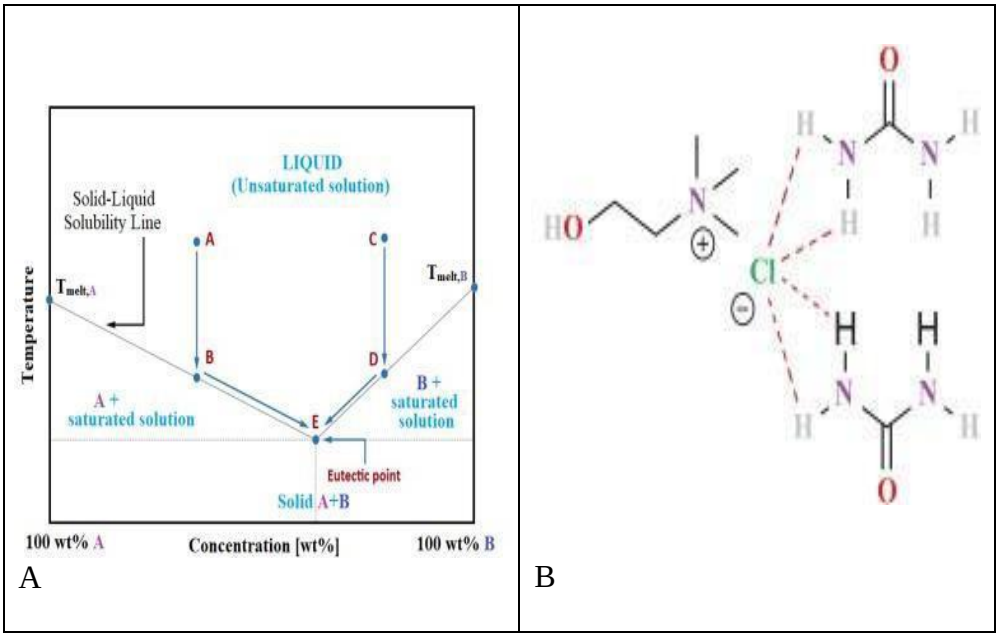

Figure 6 A&B: Figure 6A is a phase diagram of ChCl:Urea DES where the eutectic point is found at a mixture of 1:2 molar ratio respectively. Figure 6B is a molecular diagram of ChCl:Urea in a 1:2 molar composition.

Much research has been done on the feasibility of using deep eutectic solvents in place of conventional and novel ones for GHG capture with promising results. Liu et al [86] analyzed the CO_2 solubility in several DES vs several IL's and concluded that DES surpass IL's in absorptivity in finding up to 12.9 mol CO_2/kg solvent in TBD-EG. Works by Castro et al [87] determine several DES as suitable candidates for hydrofluorocarbon separation and capture due to high absorptivity and selectivity for common

contaminants, namely quaternary ammonium salt and imidazole based DES. Gu et al. [88] tested hydrophobic DES like [TEPA]Cl-thymol for CO_2 capture with findings of a high molar absorptive capacity of 1.355 and no regenerative losses after 5 cycles. Wang et al studied ChCl:Urea for absorption of CO_2 post combustion and found a promising exergy analysis of 74.28%, a purity of CO_2 capture stream of 99.42%, and a selectivity ratio of 97.33% for a coal power plant.

1.6. Computational Screening of DES

Of the research already performed involving DES in GHG capture and biofuel upgrading many promising results have been found for replacing the conventional solvents for these generally cheaper, lower toxicity, biodegradable, greener solvents which promise not only an improvement in efficiency but also a more environmentally sustainable option. However, nearly all studies to date have been narrowly focused on a select few popular DES out of the vast library of potential combinations. Conducting research experiments is a time-consuming costly measure which greatly limits the scope of the solvents studied. Considering this, computational procedures greatly reduce the demand placed on the researcher and may expedite the development of new technologies. Computational methods in the field of DES may assist in predicting physical characteristics for potential solvents like viscosity, density, conductivity, vapor pressure, and surface tension [89]–[92]. These methods

may be used to predict the thermodynamics of systems involving DES like activity coefficients, solubilities, partition coefficients, and henry law constants [93]–[95]. The conventional method for engineers to predict aspects of a solvent are through group contribution methods like UNIFAC and NRTL. However, due to the relative novelty of DES the library of experimentally determined coefficients required to use these methods is severely lacking [55], [96]. Therefore, new methods have begun to be applied to the study of novel solvents such as ab initio and machine learning. In 2022, Boublia et al. [97] published a neural network developed for predicting the conductivity of deep eutectic solvents with an R^2 = 0.993 training value of and an R^2 testing value of 0.984 using 2266 data points based on quantitative structure-property relationships (QSPR). In 2023, Mohan et al. [98] published a neural network for predicting CO_2 capture in DES with an average absolute relative deviation (AARD) of 2.72%. In 2022, Yu et al. [99] published a transition state theory inspired neural network for predicting the viscosities of DES with an AARD of 6.84% and R^2 value of 0.98 on the test set. Some researchers like Linke et al. [100] have used K-nearest neighbors (KNN) models to predict environmental health and safety (EHS) properties of deep eutectic solvents like toxicity, bioaccumulation factor, and various persistence measures.

1.7. Conductor-like screening and modeling of real solvents (COSMO-RS)

While these modern machine learning models offer excellent quantitative results, much of the predicting qualities are not preserved or presented that drive the reasoning for why certain DES combinations work better than others for any given application or what characteristics determine physical properties of the different combinations. To this end, the ab initio methods of molecular modeling provide significant insights into where other computational routes fail. One such modeling approach is called Conductor-like screening and modeling of real solvents (COSMO-RS). This modeling software has received several scientific achievement awards for its innovative and accurate use in predicting the thermodynamics of chemical systems and providing significant insights into the determination of these results [101]. This software has been utilized extensively with ionic liquids. Sosa et al. [102] used COSMO-RS to successfully design novel ionic liquid combinations for the capture of hydrofluorocarbons by screening 600 potential combinations before confirming results experimentally and determining significant insights like the anions were the more significant contributor to absorption capacity in the IL's. Moya et al. [103] successfully applied COSMO-RS to model the isotherms of 15 IL-CO_2 systems and validated them with experimental literature with an R^2 value of 0.9. Islam et al. [104] successfully utilized

COSMO-RS to screen 720 novel combinations of IL's for the purpose of GHG capture in the form of CO_2, CH_4, and N_2O with an insight that phosphonium, ammonium, and choline anions were the most suitable for the task and confirmed the findings of Sosa et al. [102] that the anion was the determinant component for thermodynamic properties of the systems.

1.8. Literature Gap

From the literature review above, DES has been shown to be a viable candidate to disrupt the status quo in GHG capture technology. DES contain various attributes which endow them with the ability to do so such as tunability, being environmentally benign, and their availability/cost. However, due to the novel nature of these solvents, their potential has yet to be fully explored. A significant literature gap exists in the scope of DES applied to specific separations and absorption problems where most studies test less than ten DES out of the infinite combinations and compositions available. This leads to a significant understatement on the practicality of utilizing DES. Another literature gap is presents itself as the systems studied are generally focalized on single absorbents namely CO_2. Little consideration has been given to the separations of GHGs and rather been focused on pure gas absorption.

This dissertation seeks to push the cutting edge of deep eutectic solvent analysis for the utilization within the scope of greenhouse gas capture. This is done through a near exhaustive scope of DES combination

analysis of thermodynamic potential for absorption of select GHG's and co-contaminants found in industry which require absorptive separations. R-32, Siloxane, H_2S, CO, etc, have rarely been studied in the context of DES as DES has been almost exclusively applied to the absorption of CO_2 in the gaseous realm. This dissertation looks at these important molecules and complex systems of multi-component separations to forward the topic of study.

A commonly used refrigerant (R32) that is notoriously difficult to capture without the use of vacuum extraction and cryogenic distillation will be tested against type 5 DES. ***Chapter 2*** focuses on understanding the absorption mechanics and suitability of DES/R32 systems through thermodynamic and EHS analyses utilizing COSMO-RS, VEGA, and available SDS's.

It has been found that exotic absorbents like R-134a are unable to meet the scientific standard of accuracy in COSMO-RS without intervention by the user. Preliminary results suggest an AARD of 400% associated with R134a and ionic liquid/DES systems. ***Appendix A*** offers a re-parameterization of the COSMO-RS software to pave the way for systems where it fails to offer meaningfully accurate results. The use of COSMO-RS and Python was critical in this project.

Selective GHG capture in the context of biogas upgrading imposes a large cost to the development of sustainable fuels. DES have been shown to

be strong novel candidates to conventional methods. However, the sensitivity of the commonly studied DES with regards to varying contaminants has not been explored. ***Chapter 3*** fills the literature gap to offer clear insight into not only which solvents may be strong absorbents of GHG's in biogas but also how they may be selectively applied to systems of varying compositions using COSMO-RS, VEGA, and available SDS's.

Siloxane has been shown to be a highly influential contaminant in DES/GHG systems in chapter 4. ***This chapter*** explores the absorption mechanisms of four commonly encountered siloxanes. A representative group of type 3 and type 5 DES are used to determine which solvents might be most suitable in the use of solvating these siloxanes using COSMO-RS. Thermodynamics are compared to conventional solvents for reference. An EHS analysis is performed for insights into sustainability of the solvents using VEGA and available SDS's.

Selective GHG capture in the context Syngas imposes a large cost to its usage as a sustainable fuel. ***Chapter 5*** investigates utilizing DES as a potential candidate of selectively absorbing CO_2 and H_2S in the presence of syngas products: H_2 and CO. Nearly 1000 solvent combinations are explored which effectively represent the known groups of known DES components and mixing them in novel combinations. Insights into the absorption mechanics and EHS characteristics are provided using COSMO-RS, VEGA, and available SDS's. Finally, a process flow diagram is

modelled in ASPEN which compares the selected physical absorbents to a conventional DEPG solvent. Some missing parameters for the ASPEN simulation are predicted using a neural network.

1.9 Significance

The significance of this dissertation may be described in two facets: First the research herein excels the cutting edge of greenhouse gas (GHG) capture with regards to novel absorbent separations, second it provides a means of not only applying but also enhancing the accuracy and scope of modern computational tools which offer utility for and beyond GHG capture.

The first statement of significance is actualized through the modelling of highly novel absorbent systems comprised of deep eutectic solvents (DES) and various GHG's along with relevant industrial stream components. DES research is currently in the infancy stage where specific promising component combinations are repeatedly applied to mainstream separations problems theoretically and at the bench scale. While the popular DES combinations like reline have been repeatedly proven to outperform conventional solvents in a wide array of applications, the narrow scope of the DES that receives attention is a grievous error in the pursuit of developing the process efficiency required to make biofuels a competitor to fossil fuels or for application as an industrial GHG remediate. Within this dissertation one will find an ambitious scope has been undertaken to explore

the real potential of DES in a wide range of applications. This has been realized by solving thermodynamic systems for hundreds of novel DES combinations at each venture, exploring what the driving forces of selective absorption is for these systems for future development, and comparing results to industrially relevant data when able. Thus, this dissertation excels the cutting edge of GHG capture with regards to novel absorbent separations.

The second statement of significance is realized through the synergistic application of multiple computational approaches and rigorous evaluation of accuracy. The marriage of quantum mechanical computational software (COSMO-RS), process modelling computational software (ASPEN), predictive machine learning models (neural network), predictive KNN models (VEGA), and statistical evaluation logically interwoven provides a uniquely modern approach to solving large scale chemical engineering problems which others may adopt or enhance upon. Evaluating computational approaches like COSMO-RS for accuracy have exposed weaknesses in applicability which have been remedied in this dissertation with Python-based statistical enhancements. Thus, this dissertation provides a means of not only applying but also enhancing the accuracy and scope of modern computational tools which offer utility for GHG capture and beyond.

Chapter 2
Mechanistic understanding of difluoromethane absorption on DES using COSMO-RS

2.1. Introduction

Hydrofluorocarbons (HFC) are a class of fluorinated compounds used primarily in refrigeration, foam-blowing agents, aerosol propellants, solvents and fire suppressants [105]. These compounds were encouraged after policy change through the Montreal Accord on conventional chloro-fluorinated carbons (CFCs) due to ozone depletion properties [106]–[108]. While HFCs are considered a better alternative to the previous components regarding ozone depletion, due to the hydrogen allowing for much faster breakdown periods in the atmosphere, they are still persistent in the air, lasting between 15 and 270 years compared to CFCs that can last over 1000 years [109], [110]. These gases also have an extreme global warming potential (GWP), being 677 times as potent as carbon dioxide in their greenhouse potential per 100 years in the atmosphere [109], [111]. In 2020, the US reportedly emitted the CO_2 equivalent of 190 million metric tons of fluorinated gases [109]. Thus, providing recycling alternatives to the current separation processes is of great and immediate importance [112].

Difluoromethane is among the most used HFC today for refrigeration and fire suppression. Difluoromethane has received attention from the scientific community for capture and separation through absorption and adsorption, recently through the use of ionic liquids [113]. Complex novel solvents are required for processing HFC refrigerants such as difluoromethane [114], [115]. Ionic liquids, a group of novel solvents, are generally composed of expensive, toxic, or non-biodegradable chemicals which can be detrimental to the environment [55], [87]. Contrarily, deep eutectic solvents (DES) are considered analogues of ionic liquids as they possess many similar physicochemical properties, yet offer cheap, non-toxic, and environmentally benign alternatives [55]. Rather than ionic pairs, DES are formed through combinations of hydrogen bond acceptors (HBA) and hydrogen bond donors (HBD), which develop a significantly depressed eutectic point generally causing them to be liquid at room temperature [70], [116]. DES are currently separated into five types. Two of these types (3 and 5) are attributed with being green solvents, while the other classes contain potentially hazardous metal components [117]. Type five DES are also termed hydrophobic DES or HDES. Due to the relatively nonpolar nature of fluorinated compounds, HBA and HBD, which are prevalent HDES, are examined in this study as they likely ensure the best solubility.

Thus far, DES have been extensively studied in their capacity as common greenhouse gas absorbents such as CO_2 and CH_4, gaseous

pollutants such as siloxanes, and sulfur contaminants, continuously outperforming conventional solvents in studies [70], [116]–[118]. DES have been proven to be highly effective in the capture of greenhouse gases (GHG) [34], [119]. However, the application of DES for HFCs, and especially difluoromethane, has yet to be explored as best to the authors knowledge. One barrier for the experimental investigation of DES in this application is the vast number of available HBA, HBD, combinations, and mixture compositions. Thus, to aid in initial explorations of DES–difluoromethane systems, many researchers have relied upon thermodynamic property prediction methods [120]–[122]. The conductor-like screening model (COSMO) suite is a thermodynamic property prediction method which employs quantum mechanical calculations, density functional theory, and QSPR methods in order to determine ab initio predictions [123]. COSMO is especially popular among researchers studying ionic liquids and DES, as one remarkable trait of these solvents is their tunability, leading to virtually infinite possible combinations of components and compositions [124]–[127].

The objectives of this study are to determine the feasibility of difluoromethane absorption using type 5 DES, determine what types of solvent components work through ln activity coefficient analysis, determine why these solvent components work through energetic absorption mechanism analysis with the use of sigma analysis, and to determine

whether the promising candidates are indeed “green” alternatives through an environmental health and safety (EHS) analysis, utilizing chemical SDS and the VEGA model. The sigma analysis includes a sigma profile and sigma potential investigation. A sigma profile is the probability distribution of a molecular surface segment having a specific charge density as computed for a molecule [122], [128]. A sigma potential plot is the graphing of the chemical potential resulting from the computed molecule being placed in an environment of a specific charge [122], [128].

2.2. Computational Methods

Thermodynamic properties of absorbed compounds, DES, and act of absorption will be predicted through COSMO-RS. If available, molecule files for analyte and DES components (HBAs and HBDs) will be gathered from the onboard database of COSMO-RS. Otherwise, molecules will be imported as SMILES files from PubChem. Files imported from PubChem will be run in TmoleX (version 4.5.3N) to solve for the lowest energetic geometric conformation and the sigma surface charges. All DFT calculations will be performed at the basis point density functional theory b-p DFT level and Karlsruhe (Ahlrichs) def2-TZVP (default-2 Valence Triple-Zeta Polarization) basis set [129]. HBA salts will be modelled in a single .cosmo extension file. The output files from TmoleX will be uploaded to COSMOConf18 for conformational analysis. The outputs of COSMOConf18 will be uploaded to COSMOthermX to predict

thermodynamic properties including chemical potentials (μ). Equation 3 shows how separate functions of the sigma segments (E_{misfit}, E_{HB}, and p_s) are responsible for the prediction of chemical potential.

$$\mu_s(\sigma) = -\frac{RT}{a_{eff}} \ln\left[\int p_s(\sigma') e^{\left(\frac{a_{eff}}{RT}(\mu_s(\sigma') - E_{misfit}(\sigma,\sigma') - E_{HB}(\sigma,\sigma'))\right)} d\sigma'\right] \quad (3)$$

Where $\mu_s(\sigma)$ is the chemical potential as a function of sigma (σ). σ and σ' are two interacting surface segments between two molecules prime and non-prime. a_{eff} is the effective contact area. E_{misfit} is the energetic penalty for charge and steric misfits of the segments. E_{HB} is the energy resulting from hydrogen bonding. $p_s(\sigma)$ is the distribution function. R is the gas constant and T is absorption temperature. These chemical potentials are further used as a basis for COSMO-RS calculations. Further description of the COSMO-RS software fundamentals may be found elsewhere [129]–[132].

Next the calculated sigma potentials are used to determine the chemical potential of compound i in the DES (S). This is achieved through equation 4 where the potential of the system is integrated over the surface of the compounds. C is a designated combinatorial term that accounts for area and volume geometric characteristics of differing molecules.

$$\mu^i_S = \mu^i_{C,S} + \int p^i(\sigma)\mu(\sigma)d\sigma \quad (4)$$

The activity coefficients ($\ln\gamma$) are calculated through equation 5 in COSMOthermX which represent the affinity between solvent and solute and are strong indicators of solubility [121], [133].

$$\ln \gamma_s^i = \frac{(\mu^i_s - \mu^i_p)}{RT} \quad (5)$$

COSMOthermX uses the chemical potentials (μ) to determine $\ln \gamma_s^i$ of siloxane compound (i) in DES (s) at infinite dilution. R is the gas constant, and T is the absorption temperature of the system which was kept at 25°C as similar studies report lower temperatures equate to better solubilities among DES and gaseous compounds [134], [135]. Equation 6 is used to convert $\ln \gamma_s^i$ into solubility capacity in some instances [136].

$$C_s^i = \frac{1}{\gamma_s^i} \quad (6)$$

In equation 7, Henry coefficients (H) used for the validation procedure are calculated through an iterative process of varying the pressures (P) with the concentration (C).

$$C=H*P \quad (7)$$

Similar to the ln activity coefficient, Gibbs free energy of solvation (G_{solv}) is computed as a difference in chemical potentials. G_{solv} is the result from the difference of the chemical potential of the siloxane compound i in its pure phase μ_p^i and its chemical potential in the solvent phase μ_s^i at infinite dilution. Equation 8 describes the process.

$$G_{solv} = \mu_s^i - \mu_p^i \text{ (8)}$$

The predicted solubility of analyte in DES is produced through equation 9. Where j is the gaseous analyte compound, p_j is the partial pressure of analyte in solvent system, p_j^o is the partial pressure of analyte in its pure form, x_j is the solubility of analyte in solvent, and γ_j is the activity coefficient of analyte in solvent.

$$p_j = p_j^o x_j \gamma_j \text{ (9)}$$

Along with activity coefficients, another powerful indicator of solubility and interactions is the excess enthalpy of interaction (H_{int}) for the absorption [137]. Where ln gamma draws its importance from its relation to Hildebrand solubility, excess enthalpy of interaction (H_{int}) is a temperature derivative of Gibbs free energy, allowing for a more precise study of the contributions from each interaction type (hydrogen bond and van der Waals bond) [138], [139]. These interaction types are represented through COSMOthermX parameters used to measure the total enthalpy of mixing as expressed in equation 10.

The excess enthalpy of a system was solved through equation 11. Where H_{int} is the excess enthalpy of mixing or excess enthalpy of interaction for each molecule in the system, $H_{i,mix}$ and $H_{i,pure}$ are the enthalpies of the molecule i in the mixture and in pure form respectively. x_i is the composition of component i.

$$H_{int} = \sum x_i (H_{i,mix} - H_{i,pure}) \quad (10)$$

$$H_{int} = H_{mf} + H_{hb} + H_{vdw} \, (11)$$

Where H_{mf} is the enthalpic penalty of a misfit factor which accounts for structural, steric hindrances, and charge misalignment [128]. H_{HB} is the enthalpic contribution from hydrogen bond interactions when mixing, and H_{vdw} is the Vander walls contribution [140].

Quantitative structure property relationships (QSPR) descriptors can be generated from sigma potential profiles reported in .cosmo files [141]. These moments (*M*) consist of σ polynomial function ($f_i(\sigma)$) which are reported in equation 12 and can be used in several property predictions in COSMOthermX like density and viscosity [131]. An analyte specific moment (M_i) is computed through equation 13 from the σ profile (p(σ)) of the siloxane and $f_i(\sigma)$.

$$f_i(\sigma) = \sigma^i \; for \; i \geq 0 \quad (12)$$

$$M_i^s = \int p(\sigma) f_i(\sigma) d\sigma \quad (13)$$

Some of these moments have been correlated with the chemical's properties while others remain as simple regression parameters. The zeroth order moment (M_0^s, where i=0) is the total surface area of the analyte "s", the first order moment (M_1^s, where i=1) is the total COSMO polarization charge on the surface of the given analyte, the second moment (M_2^s, where

i=2) is a vector of total COSMO polarization energy of the molecule, the third moment (M_{ξ}^{i}, where i=3) correlates to the measure of sigma profile symmetry, and the hydrogen bond donating and hydrogen bond accepting moments (M_{Hdon}^{s} and M_{Hacc}^{s} respectively) are measurements of the analytes ability to act as each, respectively [128].

2.2.1. VEGA KNN models

The quantitative structure-activity relationship (QSAR) based software VEGA [60] was used to evaluate the EHS factors for each solvent based upon five properties:persistence, bioconcentrationfactor (BCF), mutagenicity, carcino genicity, and acute toxicity. Persistence is measured in days chemical is retained in the medium. Toxicity is measured in lethal dose 50 (LD50) of units mg/kg. BCF is measured in half-life nits of L/kg. Mutagenicity is measured in revertants per microgram (rev/µg). Carcinogenicity is measured in concentrations per lifespan ([C]/time). VEGA has been used extensively in literature for EHS property analysis of novel solvents [51,61,62]. VEGA relies upon a k-nearest neighbors (KNN) algorithm to predict EHS properties based upon the structure of the input molecule and its database of experimental results [63]. VEGA model was run for each of the five properties studied for selected DES components in each appropriate projects for thoroughness and cross-checking validations. The persistence models were evaluated for soil, water, and air for thoroughness. For the

DES included in the EHS report, the pure components that comprise the solvent are analyzed as the DES readily dissociate in the presence of moisture and are not covalently bound. Thus, their fate in the environment would not be in the DES form but rather in the individual pure HBA and HBD forms. Furthermore, a cross validation of the results was performed through pure component safety data sheet (SDS) analysis. The National Fire Protection Association (NFPA) value rankings and the Occupational Safety and Health Administration (OSHA) Hazard Communication Standard (HCS) categorization are used from literature for validation of VEGA results when available.

2.2.2. COSMO Validation

Due to the novelty of the systems studied, little to no DES–difluoromethane system data was readily available to the authors. Thus, the approach for validating the COSMO system was to compare solubility data for difluoromethane in ionic liquid literature data, of which DES are considered analogues. This approach has been reportedly used in such novel systems where experimental data are unavailable, as is shown through the work of Abedin et al. [34]. The benchmarking data set consists of 42 molar solubility datapoints in various ionic liquids at various pressures at 298.15 k as reported by Shiflett et al. [35]. The ionic liquid components were generated using the same methods previously used, along with the solubility computations. These generated values were regressed with the experimental

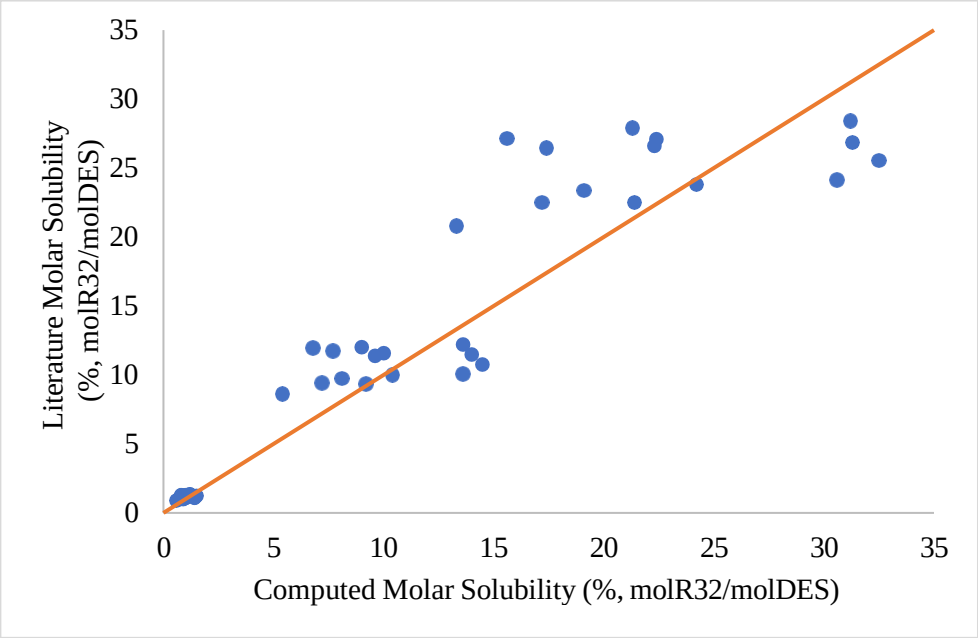

Figure 7: Experimental literature solubility data for difluoromethane in ionic liquids at varying pressures between 0.1 and 2.5 bar compared with computed values. The resulting error analysis produces an AARD% value of 25.7%, and a regressed R-squared value of 0.86.

values with a results R^2 value of 0.86. The same data set produced an absolute average relative deviation of 25.7% average absolute relative deviation (AARD). Figure 7 contains the resulting datapoints from a *y*-axis of experimental values, and an *x*-axis of COSMO predicted values from this work. While the single point error (AARD) is relatively high, the qualitative information predicted about these systems is well preserved as is evident from the high R-squared value. Thus, for the purpose of this study into the relative effectiveness of the solvents and energetic mechanisms driving them, COSMO is deemed an appropriate method of examination.

2.3. Results and Discussion

2.3.1. Evaluation of Novel HDES Solvent Combinations for R-32 Absorption

Table 3 contains ln activity coefficients for the top preforming DES combinations and R32 systems. Interestingly, all DES combinations provide ln activity coefficients below 1, suggesting non-ideal attractive forces. All compositions are kept at 1:1 molar ratio with a temperature of 25 °C and a pressure of 1 bar. The top four HBA in rank of lowest ln activity coefficients to highest were found to be tetrabutylammonium Bromide (N4Br) (−1.39), tetraoctylammonium Bromide (N8Br) (−1.39), benzyltriethylammonium chloride (BTACl) (−1.27), and methyltrioctylammonium bromide (MTOA) (−1.03). These HBA outperformed the terpenes, shorter chain quaternary ammonium salts, imidazoles, and phosphonium-based HBAs. These four HBA share a common trait of being the largest molecules. The results are logical as they contain significant amounts of carbon, which offers non-polar interaction sites. The results are in line with the sigma analysis. Other works have shown that longer chain quaternary ammonium salts have higher absorption capacities for non-polar gases vs. their shorter chain counterparts [130].

Table 3: ln activity coefficients for 1:1 ratio of top performing type 5 DES HBA (columns) and HBD (rows).

	N4Br	BTACl	N8Br	N81Br
PEG	-1.39	-1.28	-1.11	-1.04
Camphor	-1.34	-1.20	-1.07	-1.01
Lidocaine	-1.27	-1.16	-1.06	-1.00
Eucolyptol	-1.27	-1.11	-1.02	-0.94

The accompanied HBDs that produced the lowest ln activity coefficient with HBA are polyethylene glycol (PEG), camphor, eucalyptol, and lidocaine. Three of these are terpenes and one is glycol. These four HBD share the property of lacking polarity, which is favorable for a relatively non-polar molecule such as difluoromethane. The results are reasonable due to the electronic signatures of difluoromethane and the DES components. These types of DES components are utilized in non-polar absorption scenarios and aqueous extractions. The rest of the studies are performed with the 16 HBA–HBD combinations of these solvents.

2.3.2. Absorption Mechanism through Enthalpy and Sigma Analysis

Figure 8 contains the sigma profiles for the studied DES components following the primary *y*-axis. The *x*-axis is the sigma segment charge while the primary *y*-axis is the frequency of the segment on the

molecule. The secondary *Y*-axis is the chemical potential of difluoromethane when interacting with specific charged surfaces represented on the *x*-axis, which are represented as a dotted line. Negative chemical potential values correspond to energetically favorable interactions between difluoromethane, and a given surface charge. It is evident that difluoromethane prefers to interact with van der Waals and hydrogen bond accepting surfaces. The parabolic nature indicates repulsion from sufficiently negative or positively charged surfaces with a hydrophobic attribute [123]. The sigma profiles of the HBA and HBD all show large peaks in the non-polar region, with varying peak tail areas in the polarized segments (<-0.0078 e/A^2, >0.0078 e/A^2) [142]. This is expected due to the hydrophobic nature of type 5 DES which these components comprise. This compliments the difluoromethane interaction preferences, which explains the relatively low ln activity coefficient values witnessed for all solvent combinations as discussed earlier. However, the defining property for why N4Br, N8Br, BTACl, and MTOA outperformed the other HBA lies in the surface charge distributions. The four studied HBD (eucalyptol, polyethylene glycol, camphor, and lidocaine) are also included in Figure 8 and are represented as having remarkably similar sigma profiles to each other.

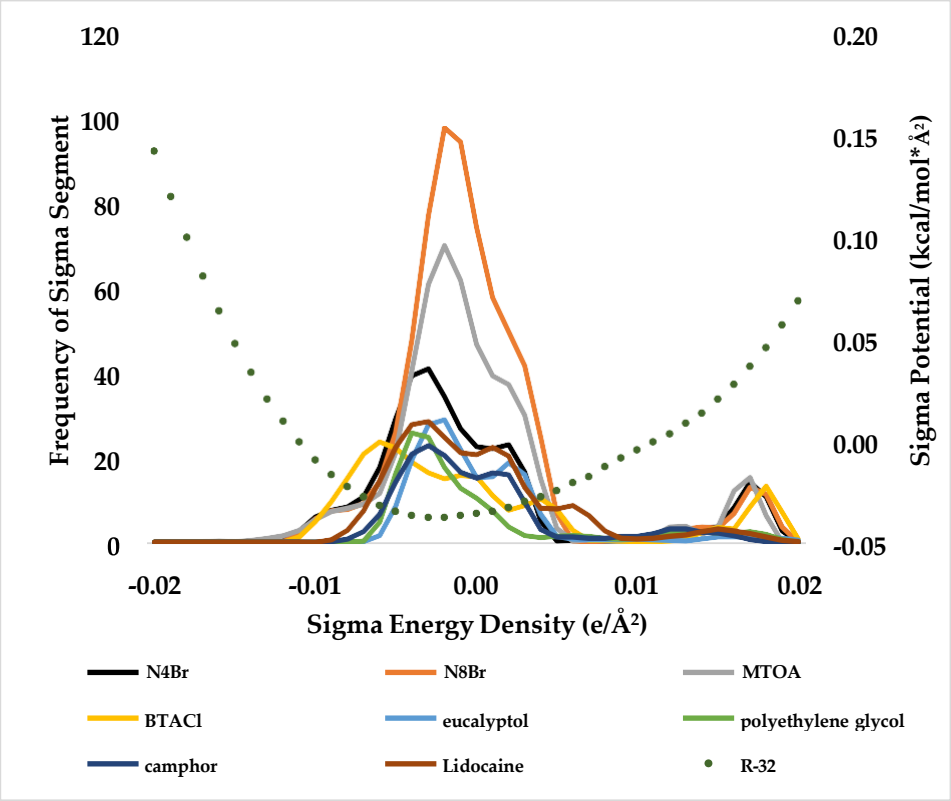

Figure 8: Sigma study with primary y axis representing sigma profile values of studied DES components, and secondary y-axis representing difluoromethane sigma potential plot.

Following the discovery from the sigma potential plot of difluoromethane, [TETA]Cl and TOPO were the worst performing of the HBA and contained the highest surface area percentage in the hydrogen bond donating region, which supplies a repulsive charge to difluoromethane. However, N4Br, N8Br, BTACl, MTOA, camphor, PEG, lidocaine, and eucalyptol all lack significant area in the hydrogen bond donating region (<6%), have the majority of their area in the non-polar

region (>80%), and some area in the favorable hydrogen bond accepting region (6% < x < 15%).

Table 4 contains the excess enthalpy of interaction computations for 16 combinations of solvents. This table contains H_{int}, H_{mf}, H_{hb}, and H_{vdw} values. As expected from the sigma analysis, the most energy is released through van der Waals interactions, with up to ten times the energetic release from favorable hydrogen bonding. The H_{vdw} values are all approximately −3 and the H_{HB} values are all between −0.3 and −0.5. All values across components represent a variance range of 15% between components in the same computation values, thus suggesting similar performance capacity between these solvents and difluoromethane despite the variation in DES components. The H_{mf} values are all 1.4 kJ/mol. This suggests that little steric hindrance and charge variance occurs between these DES–difluoromethane systems, overall contributing to negative H_{int} values. However, the H_{mf} values are more significant than the H_{HB}, overshadowing their contributions due to mismatched surface charges. This finding implies that there exists room for improvement in DES component selection, which may reduce the misfitting of molecular interaction sites. Overall, the PEG HBD paired with N4Br HBA produces the lowest H_{int}, even though the H_{mf} is moderate due to the significant H_{HB} and H_{vdw} interactions.

Table 4: Enthalpy of mixing analysis where H_{int} is the excess enthalpy of interaction, H_{mf} is the enthalpic contribution due to misfitting of sigma segments, H_{hb} is the enthalpic contribution from hydrogen bonding, and H_{vdw} is the enthalpic contribution from van der Waals interactions. All the enthalpies are presented as kJ/mol.

HBD	Property	N4Br (kJ/mol)	BTACl (kJ/mol)	N8Br (kJ/mol)	MTOA (kJ/mol)
PEG	H_{int}	−1.15158	−1.12681	−1.15158	−1.12756
PEG	H_{mf}	1.4377	1.44851	1.4377	1.42068
PEG	H_{hb}	−0.40207	−0.43892	−0.40207	−0.37627
PEG	H_{vdw}	−3.13471	−3.08391	−3.13471	−3.11947
Camphor	H_{int}	−1.12736	−1.10647	−1.15158	−1.11496
Camphor	H_{mf}	1.45191	1.45861	1.4377	1.40033
Camphor	H_{hb}	−0.39266	−0.42837	−0.40207	−0.33878
Camphor	H_{vdw}	−3.13412	−3.0842	−3.13471	−3.12401
Eucalyptol	H_{int}	−1.14948	−1.13061	−1.12736	−1.09226
Eucalyptol	H_{mf}	1.46866	1.47271	1.45191	1.41422
Eucalyptol	H_{hb}	−0.41278	−0.4479	−0.39266	−0.33038
Eucalyptol	H_{vdw}	−3.15286	−3.10292	−3.13412	−3.1236
Lidocaine	H_{int}	−1.12756	−1.1175	−1.14948	−1.11091
Lidocaine	H_{mf}	1.42068	1.4228	1.46866	1.42843
Lidocaine	H_{hb}	−0.37627	−0.40817	−0.41278	−0.3468
Lidocaine	H_{vdw}	−3.11947	−3.07964	−3.15286	−3.14005

2.3.3. Effects of Change in Composition of DES

Table 5 shows the results of the compositional analysis. Due to the nature of the ln activity coefficient procedure being performed at a composition of 1:1, the optimal ratio for affinitive interactions will be studied. The ln activity coefficient of difluoromethane was computed for each solvent combination in six different compositions: 1:0, 3:1, 2:1, 1:1, 1:2, and 1:3 being HBA:HBD. Nearly all DES eutectic compositions are found in the range from 1:1 to 1:3 HBA top HBD [75], [143][29,37]. Thus, the studied compositional ranges reflect this commonality. It is evident that the pure form of HBA has the lowest ln activity coefficients, which indicates a most favorable interaction with difluoromethane, and N4Br (−1.61) having the best of the four. However, the HBA have relatively high melting points compared to their DES form. To use the quaternary ammonium salts alone would require temperatures of approximately 100 °C for them to reach their melting points, which is counter conducive to gas solubility compared to room temperature absorption. Thus, the lowest possible concentration of HBD is recommended to create a room temperature solvent for difluoromethane uptake. Furthermore, the ranking of HBD follows PEG (−1.39), camphor (−1.34), lidocaine (−1.27), and eucalyptol (−1.27) for producing the lowest ln activity coefficients when paired with N4Br. This trend holds for pairings with all four HBA. This trend follows the findings of the sigma analysis where the ranked

components follow the favorable charge distributions that induce favorable difluoromethane interaction.

Table 5: Compositions study measured as ln activity coefficients for difluoromethane in varying molar DES HBA and HBD compositions ranging from pure components to 3:X.

HBD	Ratio	Pure	N4Br	N8Br	BTACl	MTOA
-	-	-	−1.61	−1.43	−1.61	−1.16
PEG	1:1	−0.71	−1.39	−1.39	−1.27	−1.03
PEG	1:2	-	−1.27	−1.27	−1.2	−0.97
PEG	1:3	-	−1.19	−1.19	−1.14	−0.93
PEG	2:1	-	−1.48	−1.33	−1.48	−1.08
PEG	3:1	-	−1.52	−1.36	−1.52	−1.10
Camphor	1:1	−0.44	−1.34	−1.34	−1.19	−0.99
Camphor	1:2	-	−1.18	−1.18	−1.08	−0.89
Camphor	1:3	-	−1.07	−1.07	−1.00	−0.83
Camphor	2:1	-	−1.45	−1.28	−1.45	−1.06
Camphor	3:1	-	−1.50	−1.31	−1.50	−1.09
Eucalyptol	1:1	−0.03	−1.27	−1.27	−1.11	−0.92
Eucalyptol	1:2	-	−1.07	−1.07	−0.95	−0.78
Eucalyptol	1:3	-	−0.93	−0.93	−0.85	−0.68
Eucalyptol	2:1	-	−1.41	−1.22	−1.41	−1.02
Eucalyptol	3:1	-	−1.47	−1.27	−1.47	−1.06
Lidocaine	1:1	−0.58	−1.27	−1.27	−1.16	−0.98
Lidocaine	1:2	-	−1.10	−1.10	−1.04	−0.89
Lidocaine	1:3	-	−1.00	−1.00	−0.96	−0.83
Lidocaine	2:1	-	−1.41	−1.25	−1.41	−1.05
Lidocaine	3:1	-	−1.46	−1.29	−1.46	−1.08

2.3.4. Effects of Varying System Pressure

Table 6 shows the results of the pressure analysis. Vapor liquid systems are typically operated at pressures higher than atmospheric to maximize gaseous solubility. As pressure increases, non-ideal interactions tend to have less of an overall effect on the studied systems as has been seen in other vapor liquid studies [130]. The significance of this pressure analysis is to determine how well the difluoromethane and DES system will respond to increases in pressure, and if the studied solvent combinations will behave differently. The solubility of difluoromethane was computed for each solvent combination at four different pressures; 1, 3, 6, and 9 bar. The baseline solubility is promising as the lowest is 18% mol solvent per mol difluoromethane at 25 °C and 1 bar for MTOA: Eucalyptol at a 1:1 molar ratio. With increase in pressure, solubility increases with values reaching up to 86% mol/mol solubility at 9 bar. The solubilities are consistent among the solvents with minor deviations due to the similarity of the surface charges. The trends are relatively linear between solubility and pressure. The solvents containing MTOA are shown to increase at a higher rate starting with the lowest solubilities and ending with the highest or equal. The lowest solubility for MTOA is with eucalyptol at 1 bar with 18.03 mol/mol. The highest for MTOA and the highest of the solvents is 86.2 mol/mol which is achieved at 9 bar for the three HBD combinations of PEG, camphor, and

eucalyptol. This result is likely described through hole theory, as MTOA is geometrically dissimilar from the others by being asymmetrical. This generally offers lower viscosities and pressure-assisted pore filling [30,38]. The HBA combinations for N4Br, N8Br, and BTACl all have similar solubilities, exhibiting deviations of no more than 10%. A 10% deviation is only witnessed at 1 bar, with decreasing discrepancy with an increase in pressure. The surface charge distribution is highest in the van der Waals and lowest in the hydrogen bond accepting region of the four studied HBA; this is likely the cause of this slight anomaly, as at higher pressures the polar interactions increase in significance, and the higher amount of van der Waals surfaces becomes a less dominating factor.

Table 6: Pressure study of the top 16 performing solubility of difluoromethane in DES is represented as mol/mol%. The system pressure is in bar.

HBD	Pressure (Bar)	N4Br	BTACl	N8Br	MTOA
Camphor	1	24.2	22.3	24.2	19.2
Camphor	3	49.8	48.3	49.8	43.9
Camphor	6	70.7	70.3	70.7	66.4
Camphor	9	85.8	85.6	84.7	86.2
Eucalyptol	1	22.9	20.9	22.9	18.0
Eucalyptol	3	47.8	46.2	47.8	41.8
Eucalyptol	6	68.9	68.6	68.9	64.2
Eucalyptol	9	86.0	85.6	84.5	86.2
Lidocaine	1	23.8	22.2	23.8	19.4
Lidocaine	3	50.2	48.8	50.2	44.8
Lidocaine	6	71.6	71.2	71.6	67.7
Lidocaine	9	83.7	83.1	81.4	84.0

2.3.5. EHS Analysis

In general, type 5 DES are considered as comprising “green” components that are environmentally benign. The four HBA and four HBD selected are evaluated for this merit through a search of the available safety data sheet (SDS) data from Fischer Scientific [136], [144]. The values that were unable to be determined were run through the VEGA KNN-based environmental health and safety (EHS) software. Table 7 contains the results of this study where the green (g) indicates a lower than moderate score of NFPA and/or OSHA rating, blue (b) indicates unreliable predictions due to missing data in VEGA and no available data found in the SDS database. Red (r) indicates moderate or higher NFPA and/or OSCHA rating for the property. The solvent components were studied rather than their combination, as DES readily dissociates in the presence of water in the environment. Of the values in the study, only one is red, being from MTOA as it possesses moderately acute toxicity. MTOA also contains two unavailable/unpredictable properties in regard to BCF and carcinogenicity. N4Br is indicated as safe in all areas except for soil persistence, BCF, and carcinogenicity for which there was no available data and thus it was unable to be reliably predicted. N8Br contained the least amount of information with all properties being unavailable, except mutagenicity and acute toxicity which were benign. Camphor and eucalyptol both show the absence of

negative properties except for air persistence, for which no data were available and unreliable predictions were made. PEG contained none of the adverse properties. BTACl contained none of the studied properties with the exception of BCF and carcinogenicity, which were undetermined. Due to the lack of significant harmful properties, the components studied have strong potential for use as environmentally safe alternatives to conventional systems. Thus, MTOA is not recommended as an HBA but the other 12 DES are candidates for this application. Difluoromethane is considered extremely flammable with an NFPA rating of 4, but is relatively non-toxic [145], [146]. The inclusion of difluoromethane into the working fluid may attribute this characteristic to the solution, and precautions should be undertaken accordingly.

Table 4: VEGA model for selected solvent components.

	Persistence Air	Persistence Water	Persistence Soil	Mutagenicity	Acute Toxicity	BCF	Carcinogenicity
N4Br	g	g	b	g	g	b	b
BTACl	g	g	g	g	g	b	b
N8Br	b	b	b	g	g	b	b
MTOA	g	g	g	g	r	b	b
PEG	g	g	g	g	g	g	g
Camphor	b	g	g	g	g	g	g
Eucalyptol	b	g	g	g	g	g	g
Lidocaine	b	b	g	g	g	g	g

2.4. Conclusions

Overall, 1298 Type 5 DES were inspected in a 1:1 ratio of HBA and HBD for favorable interactions with the HFC difluoromethane (R32). The results of this project were limited to the top 16 DES and analyzed further for pressure, composition, enthalpic, and EHS properties. The results indicate that the main mode of absorption within these DES with regard to difluoromethane is through van der Waals interactions. The solvents containing significant van der Waals interaction surfaces and some hydrogen bond accepting areas are deemed the most effective traits for the task. It was discovered through compositional analysis that the HBA in pure form had the highest solubility percentage for difluoromethane. However, because these chemicals have high melting points, it is recommended for the lowest possible ratio of HBD to be added to create a low temperature melting point for the absorption of difluoromethane. Through an increase in pressure, the solubility of difluoromethane increases. MTOA was shown to be the most pressure sensitive HBA of the four studied as it contained the lowest solubility at 1 bar (18 mol/mol%) and the highest at 9 bar (86.2 mol/mol%), likely due to the size of the quaternary salt being the least symmetrical of the four, following hole theory logic. By utilizing SDS and VEGA predictive software, an EHS analysis revealed a strong potential for the 16 DES to be environmentally safe, with MTOA being the only acutely toxic substance. These insights are provided to the scientific community as

evidence of the strong efficiency and safety potential of adopting DES into industrial and commercial usage for the absorption of difluoromethane.

Chapter 3
Carbon Capture from Biogas by Deep Eutectic Solvents: A COSMO Study to Evaluate the Effect of Impurities on Solubility and Selectivity

3.1. Introduction

Anaerobic digestion (AD) is the process of breaking down organic substances in anoxic conditions by bacteria [147]. Organic macro-molecules such as fats, carbohydrates, and proteins are digested into micro-molecules during AD, which results in a nutrient-rich solid for plants (fertilizer) and biogas [147]. This process occurs naturally in landfills, but also in a controlled environment in equipment called anaerobic digestors. The feedstock for AD are materials that are otherwise considered waste, such as agricultural waste, manure, organic waste from animal processing plants, food waste, and many others [22], [23]. The growing adoption of AD offers a new approach to these waste streams which supports a recycle economy that increases market efficiency and bolsters the renewable energy industry as the globe shifts towards green fuel.

During AD, several reactions occur, but the process can be categorized into four stages: hydrolysis, acidogenesis, acetogenesis, and methanogenesis. During hydrolysis, long-chain polymers like cellulose are hydrolyzed into fermentable forms like glucose. Acidogenesis and acetogenesis are characterized by the generation of hydrogen gas and

carbon dioxide from monomers and glucose. The final stage, methanogenesis, is the stage where most of the methane is produced. Apart from CH_4 and CO_2, several other impurities are formed dependent upon the feed, such as ammonia, hydrogen sulfide, water, nitrogen, and siloxanes. The presence of CO_2 and the impurities lower the overall energy content of the biogas and can cause premature failure of point-of-use equipment [25]. For these reasons, carbon capture and biogas upgrading are often required prior to biogas application. Currently, biogas upgrading is conventionally performed through amine-based ionic liquid absorption or water scrubbing [26]. Ionic liquid (IL) amine-based absorption is desirable due to the solvents having a high selectivity for CO_2 over CH_4, which can achieve ~99% CH_4 purity [26], [28], [29], [148]. However, the high viscosity, high cost, and toxicity of these solvents suggest the need for an alternative [26]. Water scrubbing has a high efficiency (~97% CH_4 purity achieved), but it has been associated with bacterial growth issues, massive water consumption, and its necessity for additional processes in series to remove feed impurities [26], [29]. Other processes have also been developed for CO_2 removal, such as solid sorbents. These solid-based sorbents are found to have a large range of CO_2 capacity that reach up to 80 weight percent but have high operating temperatures that exceed 500 °C [32], [33]. However, due to the low combustive properties of some impurities, low-temperature

solid adsorbents like zeolites are the only feasible option, which have significantly lower capacities [34], [35].

Deep eutectic solvents (DES) are a relatively new material that is being studied as a carbon capture media [149]–[151]. DES are made from a hydrogen bond donor (HBD) and a hydrogen bond acceptor (HBA) [149], [152]. The melting point of DES is decreased significantly compared to individual HBA and HBD due to charge delocalization from hydrogen bonding [71]. Studies have proven DES to exhibit desirable traits for use as a CO_2 absorbent, such as thermal stability, tunability, reversibility, and reasonable CO_2 solubility [35], [150], [153], with Zhang et al. [34] reporting a 1:1 mol CO_2 per mol solvent solubility ratio [154], Bi et al. [154] reporting a 0.25 g/g of CO_2 per solvent solubility, and Ren et al. [34] reporting 0.4 mol CO_2 per mol solvent solubility. The literature often uses experimental methods to develop CO_2 capture on DES. However, the use of computational software with highly accurate determinations may make the down-selection of DES easier. Therefore, conductor-like screening model for real solvents (COSMO-RS), which is a thermodynamic property prediction software that relies on the generation of sigma profiles rather than databases of functional group interactions, was used in this study. COSMO has been used by several authors to model CO_2 capture, such as Song et al. [155], who was able to screen a database containing thousands of HBD and HBA combinations for potential CO_2-capturing solvents. Of

the various DES, quaternary ammonium salts have garnered a significant amount of attention for their ability to solvate CO_2 [151], [156]. The accuracy of COSMO was also studied by Liu et al. [157] by testing hundreds of DES for CO_2 absorption, and they found a maximum of 10.3% error after tuning the program across the studied samples. Several studies have been performed on the solubility of CO_2 in DES [158], [159], however, to the best of the authors' knowledge, none was conducted on understanding how various impurities in biogas affect the carbon capture by DES. This knowledge is essential to design an absorption system for biogas upgrading since solubility and selectivity of a solvent can be adversely affected by contaminants, especially when accounting for accumulation during repeated use.

This study focuses on evaluating the affinity various DES have for selected contaminants and how their presence in various amounts affects the affinity for CO_2 in these solvents. This will be performed using COSMO by first modeling the DES and contaminants not found in the software library, then generating thermophysical properties of Henry's Law constants and activity. Selectivity of CO_2 over CH_4 and solubility of CO_2 changes in a selected group of DES were studied here for both infinite dilution and partial pressure at various temperature ranges. Finally, effects of impurities ranging from 0 to 5 mole % on CO_2 solubility in various DES were evaluated.

3.2. Materials and Methods

3.2.1. Composition of Biogas

The standard percent ranges of biogas composition used in this study have been listed in Table 8. The variance of the composition depends upon several factors surrounding the AD process, such as temperature, retention time, kinetics, and feed stock composition [160]. Table 8 shows the components studied with their respective abbreviations for the investigation and their industrial compositions.

Table 5: Pre-treatment biogas components and composition for studied molecules.

Molecule	Abbr.	Composition Volume %	PPM	Ref
Hydrogen Sulfide	H_2S	0–2	0–10,000	[161], [162]
Ammonia	NH_3	0–1	0–100	[161], [163]
Nitrogen	N_2	0–15	-	[161]
Water	H_2O	5–10	-	[162]
Propanone	Acetone	-	0–15	[164]
Octamethyltrisiloxane	Octa	-	0–41.35	[165]
Decamethylcyclopentasiloxan	Deca	-	0–5.17	[163]
Carbon Dioxide	CO_2	15–47	-	[161]
Methane	CH_4	35–70	-	[161]

3.2.2. Deep Eutectic Solvents

Table 9 lists the five common DES considered for this study, including choline chloride-urea, choline chloride-ethylene glycol, tetra butyl ammonium chloride-ethylene glycol, tetra butyl ammonium bromide-decanoic acid, and tetra octyl ammonium chloride-decanoic acid, along with their components and component mixing ratios. The solvents studied are termed quaternary ammonium salts due to the structure of the HBD. The quaternary ammonium salts are relatively cheap, safe for the environment, and naturally derived [149], [166], [167]. The specific solvents were chosen as an attempt to represent a large range of their class by means of carbon chain length of the quaternary ammonium salts and commonly paired HBDs.

Table 6: Selected deep eutectic solvents for biogas upgrading and their abbreviations.

DES	**Abbr.**	**HBA**	**HBD**	**Molar Ratio**	**Molar Mass (g/gmol)**
N_{8888}Br:Dec Acid	N8Br:DA	N_{8888}Br	Decanoic Acid	1:3	1019
N_{4444}Br:Dec Acid	N4Br:DA	N_{4444}Br	Decanoic Acid	1:3	839
N_{4444}Cl:EG	N4Cl:EG	N_{4444}Cl	Ethylene Glycol	1:3	464
ChCl:EG	ChCl:EG	ChCl	Ethylene Glycol	1:3	325
ChCl:Urea	ChCl:U	ChCl	Urea	1:2	259

3.2.3. COSMO Simulation

COSMO is a quantum modeling software that determines thermodynamic properties using density functional theory (DFT). To determine the thermodynamic properties, the HBAs and HBDs are modeled using TurboMoleX software. The impurities are selected from the COSMO library. HBAs and HBDs are then mathematically evaluated for their natural geometrical lowest energy state and conformers. COSMO was then used for all thermophysical property calculations. TurboMoleX® was used to generate all molecular sigma profiles, conformers, and data not already found in the included database. TZVP (tri-zeta-valence-polarized) settings were used with default numerical grid of m3 and BP86 functions. COSMOThermX® was used for all thermodynamic property calculations. These properties were used to calculate sigma profile of the molecules, where charge density is plotted with charge of the molecule. Here, the molecule is differentiated into charge density segments, with each segment representing areas with charge density ranging from −0.3 to +0.3 e/Å^2. The charge density segments are plotted to form the sigma profiles. The data from the sigma profiles are used to model microscopic molecular surface charge interactions between analytes, then a statistical thermodynamic procedure is carried out to derive macroscopic thermodynamic properties from the generated information [38]. The base values generated are chemical potentials of the systems' constituents, these are then applied to

thermodynamic calculations of Henry's Law coefficient and activity coefficients. Determination of the solubility and selectivity of the systems was carried out by COSMO-RS, whose results are based upon the chemical potential generated by COSMO-RS.

3.3. Results and Discussion

3.3.1. Sigma Profiles of DES's, Polar, and Non-Polar Molecules

A sigma profile is a distribution function that relates the surface area of a molecule to the charge density of the surface [168]. In this study, sigma profiles are used to understand the electrostatic interactions between DES and selected polar and nonpolar molecules. The sigma profiles explain the trends of solubility and selectivity for a DES-based extraction. To generate these profiles, COSMO creates incremental segments of the studied molecule, which are then organized based upon surface charge density. The area under these sigma profile curves gives the total surface area of the studied molecule. Peaks between ±0.0082 e/Å^2 charge density indicate that the molecule readily undergoes van der Waals interactions [142], [168]. Peaks outside of this range indicate hydrogen bonding as the preferred interaction due to polarity [142].

Sigma profiles are useful for determining how molecules will interact in a solvent-solute system. From a range of sigma profiles, appropriate

solvents may be identified for a given molecule based on how the charge densities between the two profiles align. A highly polar solvent that has significant charge density in the HBA region (−0.0082 e/Å^2) could be expected to have a high affinity for a solute that shows a significant charge density in the HBD region (+0.0082 e/Å^2). The same is true for two molecules that have significant charge densities in the non-polar region of the sigma profile (±0.0082 e/Å^2). This logic can be used to determine if an impurity will have a lesser or higher affinity than a solute, giving rise to competition for the solvents' binding sites.

In Figure 9, the sigma profiles of each DES are displayed. The order of the solvents from the most to the least polar and, therefore, most available for hydrogen bonding to least available, are as follows: ChCl:U > ChCl:EG > N4Cl:EG > N4Br:DA > N8Br:DA. The peaks between 0.015 and 0.002 e/Å^2 are from the halogens associated with each solvent. It is observed that by changing the HBD groups as with the tetrabutylammonium variants, the sigma structure is significantly altered, which lends to the notion of DES properties being highly tunable [149], [169].

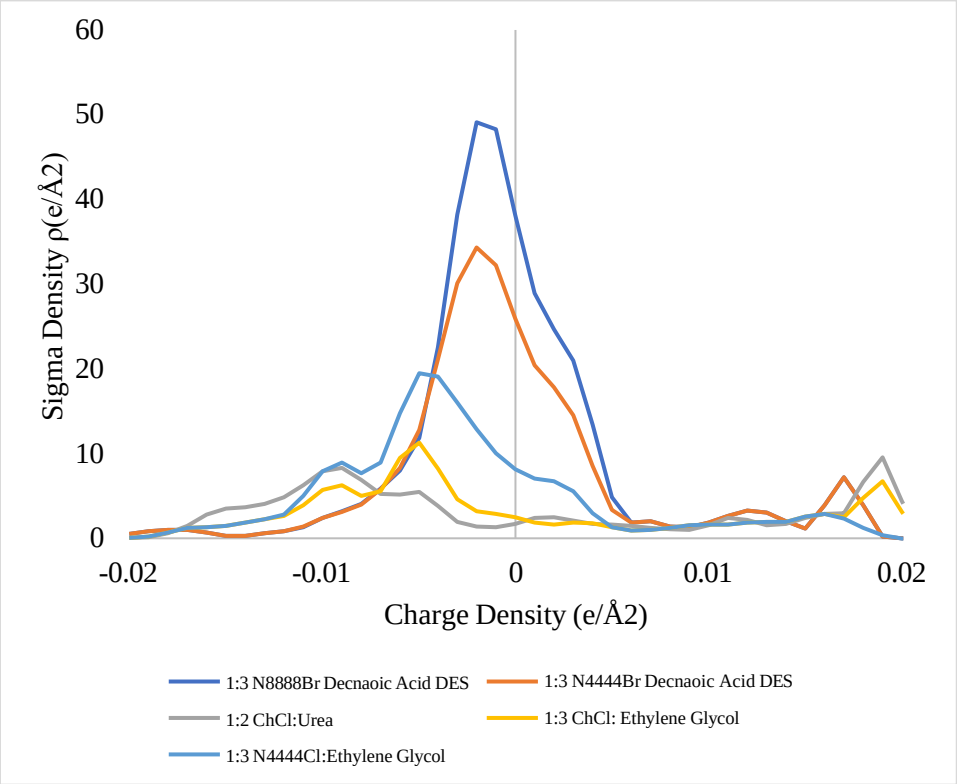

Figure 9: Sigma potential profiles of DES with respect to charge density.

Sigma profiles of non-polar gases can be seen in Figure 10. For the non-polar gases, the key difference in the sigma profiles of the molecules is the charge density distribution of CO_2 vs. N_2 vs. CH_4. N_2 and CH_4 have most of their area concentrated around the zero-x-axis compared to CO_2. CO_2 is considered a non-polar gas, since the distribution of the charges for CO_2 are weighted between ±0.0082 e/Å^2. However, CO_2 can be influenced by its environment to make it behave more like a polar molecule and participate in hydrogen bonding or behave more like a non-polar molecule and participate in van der Waals interactions. The potential for this behavior can be seen in the sigma profile as the charge density is concentrated

closely to the ±0.0082 e/Å^2 boundary. It is also understood that CO_2 contains two polar bonds, but the linear structure of the molecule creates a net-zero dipole moment. However, in a polar environment such as CO_2 in water, it behaves as an acid gas.

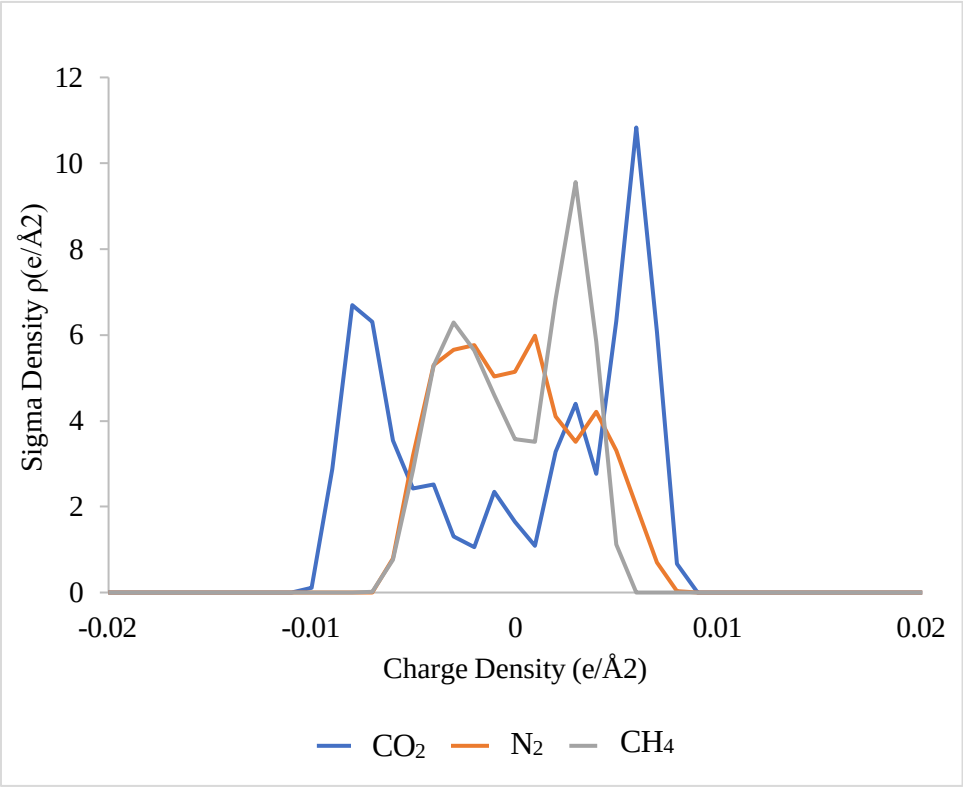

Figure 10: Sigma potential profiles of non-polar molecules with respect to charge density.

Regarding polar gases, only gases reported as impurities of biogas are selected for this study. There exist large variations in profiles among this group, as seen in figure 11. The most notable impurity is water, which reaches the farthest among the other gases on the charge density and is relatively symmetric, which concludes its adaptability in assuming the roles

as a Lewis acid or base. Acetone has a large peak near the 0 e/Å^2 yet behaves as a Lewis base due to the considerable peak beyond 0.01 e/Å^2. H_2S is relatively evenly dispersed along the x-axis, suggesting it can participate in both van der Waals interactions and hydrogen bonding depending upon its environment. SO_2 is heavily concentrated around the boundaries of ±0.0082 e/Å^2, and as such, would be expected to have lower solubility among the less polar DES. Ammonia is a weak base, and this is indicated in the large peaks near the HBA region (−0.0082 e/Å^2) but is capable of hydrogen donating interactions, as seen in the trailing area in the positive region of the plot as it extends to nearly 0.03 e/Å^2.

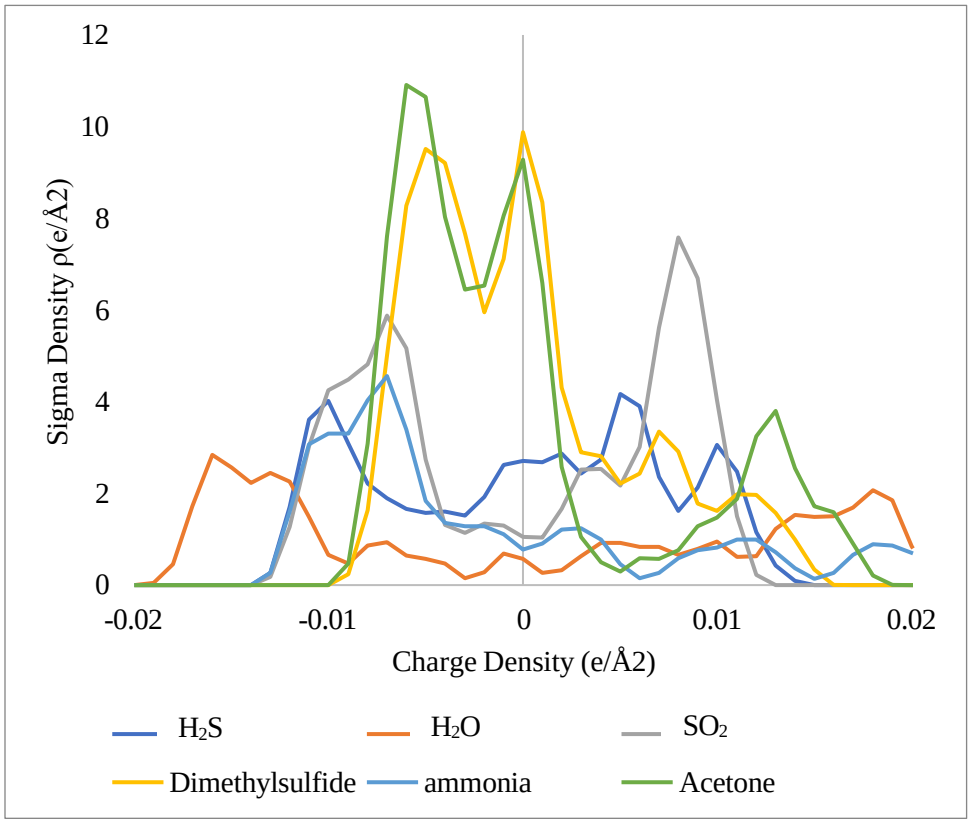

Figure 11: Sigma potential profiles of polar molecules with respect to charge density.

As discussed previously, CO_2 can be influenced by its environment to partake in hydrogen bonding or van der Waals interactions. Due to this and the generated sigma profiles, it stands to reason that a DES containing significant amounts of a polar or non-polar contaminant may change the level of solubility of CO_2 within that system. For example, when considering the relatively polar profile of ChCl:U, it could be reasoned that if it were to accumulate strong polar molecules like water then the effect of

hydrogen bond affinity for CO_2 would be enhanced. Thus, resulting in a higher selectivity for CO_2 than CH_4 in this particular solvent.

3.3.2. Selectivity for CO_2 over CH_4 by DES in Infinite Dilution

Considering the valuable product of biogas upgrading is methane, the selectivity of solvent to solvate is significant. The selectivity of CO_2 over CH_4 was first studied for various DES at infinite dilution by Henry's Law calculations and presented in Figure 12. Henry's Law constants are used to study the solubility of CO_2 vs. CH_4 for a pure DES regarding the first molecules of gas and how they selectively enter the DES and are only valid at low concentrations of gases in the DES. At room temperature and at infinite dilution, the largest selectivity of 4.7 can be observed in ChCl:U. Here, approximately 4.7 moles of CO_2 are expected to be absorbed per mole of CH_4. The least selective solvent in this model is N8Br:DA at approximately 1.75. The remaining solvents show a slight trend up from N8Br:DA. The data follows a rational trend of selectivity to size, with the smallest DES molecular constituents displaying the highest selectivity. However, this does not explain the dramatic increase in selectivity between ChCl:EG and ChCl:U, considering they are nearly the same mass (table 9) and considering the selectivity is molar-based. This behavior could be explained from sigma profiles. Figure 9 shows ChCl:U as being the most

likely to participate in hydrogen bonding of the five solvents and N8Br:DA as most likely to participate in van der Waals interactions. As previously mentioned, CO_2 can become polarized in a polar environment, which makes it much more likely to bind with ChCl:U than methane. In a relatively non-polar environment like N8Br:DA, both molecules will behave non-polar and bind closer to a 1:1 ratio. The values for simulated vs. experimental solubilities of CO_2 in ChCl:U at 5.6 MPa and 303.15 K are reported as 5.7 and 3.56 (mol/kg), respectively. The difference was reported to be caused by poorly optimized DES structures [120]. Xie et al. [28] and Ji et al. [170] report experimental solubilities of CO_2 in ChCl:U at 308.2 K and 0.651 and 0.678 p/MPa respectively, as 0.05 and 0.045 mole fraction, respectively. The solubility parameters were studied in this paper at a highest-pressure condition of 0.6 MPa and 25 °C, and for ChCl:U, the solubility of CO_2 at these conditions is 0.074. The discrepancies between experimental and calculated values could be attributed by the limitations of COSMO to fully model all solvation phenomena that occur, such as hole theory, induced polarity of solutes, and induced conformers of analytes. The selectivity appears to be mostly influenced by the polarity of the DES at room temperature. Similar observation was found in the literature, where Slupek et al. [30] compared the sigma profiles of their studied DES with solutes and determined that the overlapping regions between the two plots suggested interaction compatibility.

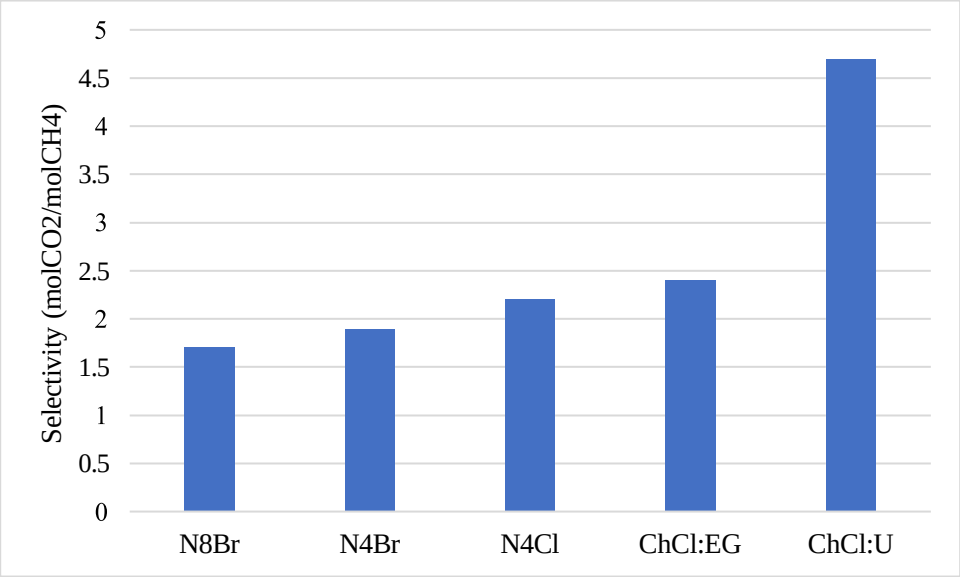

Figure 12: Selectivity of CO_2 vs. CH_4 at STP and infinite dilution calculated from Henry's Law coefficients for each DES.

The selectivity thus far has been discussed at 25 °C, however, temperature of the biogas could be as high as 55 °C depending on mesophilic or thermophilic microorganisms. Therefore, the effect of temperature on selectivity at infinite dilution is of practical interest. Figure 13 has shown the effect of temperature on Henry's Law constant, which is analogous to selectivity. Due to the unit of the Henry constant, the lower values are associated with higher solubility. With the increase of temperature, the Henry's Law constant increases. Interestingly, for the same HBA (e.g., ChCl), exceptional deviations in Henry's Law constant can be found for different HBD (e.g., urea versus ethylene glycol). This is probably due to the smaller HBA chain lengths that might have a naturally smaller affinity for CO_2 [169]. However, the induced polarity phenomena have a

stronger impact on the solubility outcome. This is due to CO_2 being naturally non-polar, as seen in Figure 10. Thus, the magnitude of the dipole moment of a solvent will determine the affinity CO_2 will have for it.

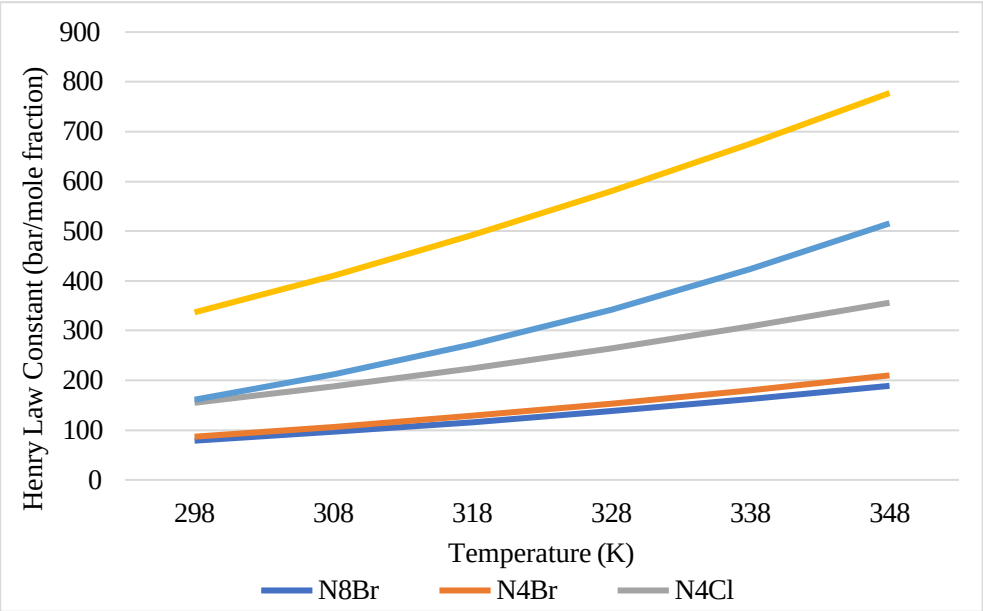

Figure 13: Effect of temperature on solubility of CO_2 at infinite dilution calculated with Henry's Law coefficients for each DES.

3.3.3. Effect of Pressure on Selectivity and Solubility of CO_2 in Various DES

Selectivity of CO_2 over CH_4 in various DES at infinite dilution provides valuable information on how polarity of DES and solute affect the selectivity. However, Henry's Law is only valid for infinite dilution, which might be misleading for carbon capture from biogas, as CO_2 concentration in biogas is often high. Therefore, Raoult's Law might provide more accurate information of the solubility and selectivity. In this study, modified Raoult's Law calculations are used to determine the maximum solubilities for a pure solvent by studying the last molecules to enter the system at any concentration. Understanding the effect pressure has on a system and how its constituents behave away from ideality is crucial to its design parameters. Figure 14 investigates the last molecules entering the system at equilibrium. It provides total saturation values for CO_2 on the left axis and selectivity of CO_2 vs. CH_4 on the right axis at varying partial pressures in 40% increments, since this falls within the composition range for both CO_2 and CH_4, as shown in table 8. The first observation in this Figure 14 is the increase in solubility of CO_2 with increased pressure, regardless of solvent. The next is the same trend being seen in Figure 12 with respect to the solvent ordering of selectivity. This trend becomes significantly more pronounced when the system is closer to saturation. For example, the selectivity of ChCl:U at 1 bar is nearly 25 in Figure 14 compared to the

Henry's Law calculations which were 4.7 in Figure 13. A possible explanation for this could be due to the solvent matrix becoming more of a polar environment as the holes fill with CO_2 and CH_4 has to squeeze into the smaller polarized spaces in order to occupy the solvent, which is not energetically favorable. The negative slopes of the selectivity analysis are due to the increase in pressure, as the molecules are forced into solvent, they become less selective. The more drastic change occurs within ChCl:U as the influence of polarity is overcome by the force of pressure, resulting in a non-linear relationship unlike the other less acidic solvents. The total capacity for CO_2 varies significantly between pressures, and the resulting trends of the bars suggest that the effect on the solvents also vary significantly. As discussed previously, the order of solvents in their ability to solvate CO_2 and the gaps in capacities are explained through alkyl-chain lengths [149], HBD selection, and the resulting polarity of these combinations with little effect from the halogens. The results here further confirm this by segregating the solvents into 3 visible groupings regarding solubility of CO_2 of N8Br:DA and N4Br:DA, N4Cl:EG and ChCl:U, and ChCl:EG. The most significant finding from this grouping is the relative effects on solubility between HBA chain length and associated HBD. N4Br:DA and N8Br:DA have relatively similar capacities for CO_2 that are significantly higher compared to N4Cl:EG. N4Br:DA finds a maximum ratio of approximately 1.9 over the CO_2 solubility of N4Cl:EG, where the

alkyl chain lengths are the same but the HBD are different. However, N8Br:DA only finds a maximum approximate ratio of 1.08 over the CO_2 solubility of N4Br:DA, which displays a difference in alkyl chain length but the same HBD.

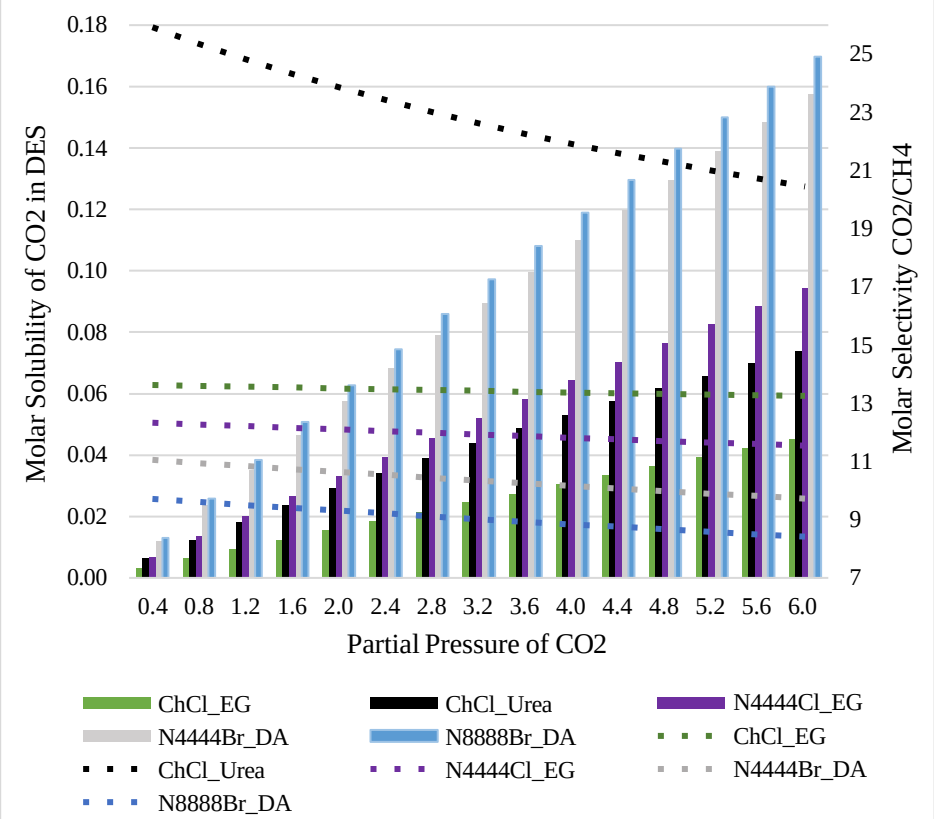

Figure 14: Effect of pressure on selectivity of CO_2 vs. CH_4 and solubility of CO2 at equilibrium and 25 °C for each DES. Y-axis 1 is the solubility and y-axis 2 is the selectivity. The dotted lines coincide with y-axis 2 and the bars coincide with y-axis 1.

Effect of selected impurities on CO_2 solubility of various DES at different temperatures under 3.6 bar pressure conditions are studied by

solubilities. Analysis was performed on each DES to determine how the presence of contaminants within the feed gas, captured by the solvent, would affect the absorptive capacity for CH_4 and CO_2. This was performed on a wide range of contaminants found in Table 8 over three temperatures (25, 37, and 55 °C) at ambient pressure and three mole fractions of contaminant within the solvent (1, 3, and 5 mol%). The solubilties were normalized to show the deviation from the maximum solubility of CO_2 and CH_4 at DES, with no contaminants.

Of the five DES, ChCl:U is the most affected to the presence of all the impurities within biogas, as can be seen in Table 10. With the increase of ammonia in biogas, the maximum solubility of CO_2 and CH_4 increase in ChCl:U. For instance, the values for CO_2 at 37 °C are 1.01 and 1.03 for ammonia in ChCl:U at 1 and 5 mol%, respectively. However, the presence of all other contaminants decrease the maximum solubility of both CO_2 and CH_4 in ChCl:U. All contaminants produce a change greater than 5% from the base case, with the octa and deca siloxane compounds inciting the greatest changes. This finding is significant, as Jiang et al. [171] report an average concentration of siloxanes in untreated biogas reaching up to 2000 mgm3mgm3. It is observed that change in temperature produces minimal effect on how the impurities in ChCl:U alter the maximum solubility of CO_2. Although, there is a significant change on the solubility of CO_2. For example, the presence of propanone at 5 mole percent in

CH_4 shows a deviation from the baseline of 1 as the values 0.89 and 0.92 for temperatures of 25 and 55 °C respectively, while the same conditions provide a range of 0.93 to 0.94 for CO_2.

Table 7: Normalized values for solubility of CO_2 at various mole percentages in ChCl:U and at varying temperatures. The values are normalized to fresh solvent solubilities of respective CO_2 and CH_4.

Temp (°C)	**25**			**37**			**55**		
Mol%	**1%**	**3%**	**5%**	**1%**	**3%**	**5%**	**1%**	**3%**	**5%**
H_2O	1.01	0.99	0.96	1.00	0.98	0.96	1.00	0.98	0.95
CO_2	-	-	-	-	-	-	-	-	-
CH_4	1.00	0.96	0.92	1.00	0.95	0.91	0.99	0.95	0.91
Octa	0.92	0.84	0.76	0.99	0.82	0.76	0.96	0.83	0.78
Deca	0.91	0.81	0.74	0.99	0.80	0.75	0.95	0.81	0.78
H_2S	1.01	0.98	0.95	1.00	0.98	0.95	1.00	0.97	0.95
NH_3	1.03	1.01	1.03	1.01	1.02	1.03	1.01	1.02	1.03
N_2	1.02	0.99	0.99	1.00	0.99	0.98	1.00	0.99	0.98
Acetone	1.01	0.97	0.94	1.00	0.96	0.93	1.00	0.96	0.93
SO_2	1.00	0.97	0.92	1.00	0.96	0.92	0.99	0.95	0.92

The other contaminants show asymmetry with a weighted area around the HBA region, whereas H_2O, H_2S, and SO_2 are significantly more symmetrical regarding sigma profiles. A notable difference between the two DES with these HBD groups is the response to the contaminants at varying concentrations. At lower concentrations of the contaminants (1 mol%), N4Cl:EG is much more affected in terms of maximum CO_2 and CH_4 solubility compared to its ChCl:EG counterpart, but the opposite is true at higher concentrations. For example, at 25 °C, the CO_2 maximum

solubility increases by 4% when octa makes up 1 mole percent of N4Cl:EG, however there is virtually no change when these same conditions are met for ChCl:EG as a value of 1 is reported. The trend found in ChCl:U between the temperature change and solubility change is not present in either of these DES.

Here, CH_4 solubility increases with the presence of octa and deca but CO_2 decreases with their presence. For these two DES, another similar trend follows regarding CO_2 and CH_4 solubility. The solubility varies little with contaminant mole percent, with nearly all changes being within 2%, with the exception of H_2O and ammonia for N8Br:DA and H_2O, ammonia, deca, and octa for N4Br:DA. At 1% contamination presence, the solubility of CO_2 in both DES start above 1 with higher solubility and decrease with increasing percentages of contaminant. Another trend to note is the slightly less negative effect the contaminants have upon N4Br:DA than N8Br:DA, whose main difference is their alkyl chain length.

3.4. Conclusions

The results of this study contain important preliminary data regarding the implementation of DES in biogas upgrading systems. The fundamental understanding of the solvents and their behavior under various temperatures, pressures, and influences from contaminants show that a complex web of variables exists that must be considered when choosing a DES for any application. It has been shown that the polarity of a solvent, its

size, and its constituents are factors contributing to solubility, but the main determinant is the HBD selection. The significance of the varied contaminant concentrations is providing a method to model the accumulation that occurs within recycled solvent, where not all contaminants will be purged through the regeneration process. This study is a glimpse into the potential lifetime of the solvent, and how each solvent will be suited for a specific feed gas composition. The results show that the DES are affected by these contaminants in varying degrees in order of most to least, as follows: ChCl:U, ChCl:EG, N4Cl:EG, N4Br:DA, and N8Br:DA. This trend is the same for polarity and the reverse of alkyl chain length, and also suggests the order in which the length of time the solvents will be able to operate before regeneration is necessary, from least to most. The pressure study suggests the ideal operating environment is closer to atmospheric pressure considering selectivity but not for solubility. The selectivity at ambient temperature and pressure (STP) and infinite dilution are 4.7, 2.4, 2.2, 2.0, and 1.7 mol CO_2/mol CH_4 for ChCl:U, ChCl:EG, N4Cl:EG, N4Br:DA, and N8Br:DA, respectively. However, the selectivity at STP and finite dilution conditions are 25.9, 13.6, 12.3, 11.1, and 9.7 mol CO_2/mol CH_4. For ChCl:U, the absorbance was decreased by the presence of deca at STP and 1, 3, and 5 mole % by 0.91, 0.81, and 0.74 respectively, from a normalized value of 1. The changes in the presence of CH_4 at STP and 1, 3, and 5 mole % are 1.00, 0.96, and 0.92, respectively.

These solvents have been shown to behave differently to each other when subjected to differing environmental factors such as temperature and pressure. All of these factors point to high tunability and complexity for these solvents.

Chapter 4
COSMO prediction of siloxane compounds absorption on type 3 and type 5 deep eutectic solvents

4.1. Introduction

Siloxane compounds often originated from silicon containing consumer products such as soaps, oils, personal care products, and pharmaceuticals [1]–[3]. When these and other silicon containing products are collected through wastewater treatment plant and landfill facilities, they are subjected to anaerobic digestion which produces siloxane compounds [4]–[6]. These siloxane compounds are present in gaseous streams at concentrations of 3–24 mg/m3 in landfill gasses, and up to 127 mg/Nm3 in wastewater treatment plants [7,8]. There are more than thirty siloxane compounds identified in literature, however, four common siloxane compounds are hexamethyldisiloxane (L2), octamethyltrisiloxane (L3), hexamethylcyclotrisiloxane (D3), and octamethylcyclotetrasiloxane (D4) [9]. These siloxane compounds have been classified as persistent, bio-accumulative, and toxic [10], [11], [12]. Literature indicated that siloxane compounds could be carcinogenic, endocrine disruptors, and immunosuppressants [13], [14], [15], [16], [17]. During combustion of siloxane compounds containing biogas and landfill gasses, silicone deposits on the turbines or engines are often observed, which cause adverse effects to the efficiency of the energy systems [4,7,18]. As a result, siloxane

compounds might need to be removed from gaseous streams through an additional upgrading process [19,20].

Several technologies that capture volatile organic compounds (VOCs) are often recommended for capturing siloxane compounds which include water scrubbing, chemical scrubbing, membrane separation, and pressure swing adsorption [172]–[175]. Among chemical absorbents, a handful of conventional solvents including monoethanolamine (MEA), dimethanolamine (DEA), methyldiethanolamine (MDEA), polyethyleneglycol dimethyl ethers, and methanol have been utilized in the industries [176]–[180]. However, a new class of green solvents called deep eutectic solvents (DES) have been increasingly explored for selective separation of trace contaminants or capture of harmful chemicals like siloxane compounds [130]. DES are multicomponent solvents of hydrogen bond donor (HBD) and hydrogen bond acceptor (HBA) which form a hydrogen bond complex. DES often results in a significant melting point depression compared to the pure HBA and pure HBD [116], [181]. The collection of known DES is currently divided into five types. Among them, type 3 and type 5 are considered the green due to the lack of metals and are comprised of two organic hydrogen bonding paired components HBD and HBA [117]. While type 3 DES are being polar in nature, type 5 DES are comprised of HBA and HBD that form less polar complexes which offers

the attribute of being hydrophobic, while maintaining the potential for environmental sustainability [75].

DES have been researched extensively regarding gases like CO_2, and sulfur containing acid gases with high selectivity and high solubility than traditional solvents like MEA, DEA, etc. [34], [118], [130]. However, siloxane compounds have received relatively little attention when it comes to DES-based absorption. Limited to small randomly selected DES are reported in the literature but with promising results. For instance, Slupek et al [119] analyzed type 3 DES formed with tetrapropylammonium bromide as the HBA and tetraethylene glycol as the HBD in a 1:3 ratio with L2, L3, and D4, at various temperatures and times, and reported absorbances up to 5000 g/L. They determined the likely reason for good solubility was due to hydrogen bonding of the DES with the oxygens in the siloxane chains. Meanwhile, Chelstowska et al [134] studied carvone based type 5 DES at various temperatures and times, and reported carboxylic acid HBD's showed higher absorption capabilities for siloxanes L2 and D3. Unlike Slupek et al. [119], the good solubility was proposed to be from Vander Waals interactions between DES and siloxane compounds. Villarim et al [135] also studied type 5 DES for D4 comprised of dodecanoic, decanoic, octanoic, and nonanoic acids, at varying temperatures, the results indicated that DES outperforming conventional solvents and Gibbs free energies at

30°C for D4 reaching below -20 kJ/mol for the DES, where conventional solvents reached as low as -13.1 kJ/mol.

From the limited literature, it can be found that DES may be effective at absorbing siloxane compounds. However, due to the overwhelming number of HBA and HBD combinations and compositions, an efficient computational approach can be employed to gain an understanding of pertinent DES characteristics and solvation potential of specific siloxane compounds. Conductor like Solvents for Molecular Screening for Real Solvents (COSMO-RS), is an ab-initio, non-empirical software tool kit which bases thermodynamic property predictions of molecules on density functional theory (DFT) computed energy profiles. Based on molecular structure and configuration, a charged sigma surface of a molecule is computed in COSMO-RS, which can be used to determine chemical potentials of solutes in pure and solvated forms [182]. The chemical potentials lead to computations of activity coefficient, partition co-efficient, and excess enthalpy. In the literature, COSMO-RS has been successfully used to predict VOC extraction by DES [155], [183], [184]. For instance, Song et al [155] and Qin et al [183] tested the accuracy of COSMO-RS with CO_2 absorption in various DES with a result R^2 value of 0.83-0.93 with over 70 datapoints [155]. However, to the best of the authors knowledge, no study for absorption of four selective siloxane compounds with the scope of type three and five DES at this scale has been reported.

The objective of this study was to determine the feasibility of type 3 and type 5 DES in absorption of siloxane compounds, and to clarify the discrepancy in literature for the energetic mechanism of solubilization for siloxanes in DES. A total of 151 type 3 and type 5 DES was gathered from literature and were evaluated in this study for four common siloxane compounds namely L2, L3, D3, and D4. Sigma surface, sigma profile, and sigma potentials were studied for the siloxane compounds to better understand their bonding characteristics. Activity coefficients were calculated for individual siloxane compounds in DES to evaluate absorptive capabilities. Excess enthalpy of mixing was computed to understand the mechanism of the absorption. Finally, the environmental health and safety (EHS) properties of the DES were examined for sustainability of the promising DES.

4.2. Studied siloxane compounds and DES

The four siloxane compounds studied were L2, L3, D3, and D4 which acted as representatives for the three main variations of the siloxane species: linear (L) and cyclic (D), methyl group quantity (hexyl-to-octyl) and siloxane chain length (di-to-tetra). A mixed database of 151 of known type 3 and type 5 DES were used in this study (available in table S1 along with compositions). This database was developed to include a wide range of HBA and HBD components from the type 3 and type 5 DES used in the literature. This specification was expected to allow the best chance for

finding sustainable solvents and to understand the energetic nature of solubilization among DES and siloxane compounds due to the variety of energy signatures available. These absorption phenomena were studied at 25 °C and 1 atm.

The objective of this study was to determine the feasibility of type 3 and type 5 DES in absorption of siloxane compounds, and to clarify the discrepancy in literature for the energetic mechanism of absorption for siloxane compounds in DES. A total of 151 type 3 and type 5 DES was gathered from literature and were evaluated in this study to absorb four common siloxane compounds namely L2, L3, D3, and D4. Sigma surface, sigma profile, and sigma potentials were studied for the siloxane compounds to better understand their bonding characteristics. Activity coefficients were calculated for individual siloxane compounds in DES to evaluate absorptive capabilities. Excess enthalpy of mixing was computed to understand the mechanism of the absorption. Finally, the environmental health and safety (EHS) properties of the DES were examined for sustainability of the promising DES.

$$\mu_s(\sigma) = -\frac{RT}{a_{eff}} \ln\left[\int p_s(\sigma') e^{\left(\frac{a_{eff}}{RT}(\mu_s(\sigma') - E_{misfit}(\sigma,\sigma') - E_{HB}(\sigma,\sigma'))\right)} d\sigma'\right] \quad (14)$$

where $\mu_s(\sigma)$ is the chemical potential as a function of sigma (σ). σ and σ' are two interacting surface segments between two molecules prime and non-prime. a_{eff} is the effective contact area. E_{misfit} is the energetic penalty for charge and steric misfits of the segments. E_{HB} is the energy

resulting from hydrogen bonding. $p_s(\sigma)$ is the distribution function. R is the gas constant and T is absorption temperature. These chemical potentials from equation 14 are further used as a basis for COSMO-RS calculations. Further description of the COSMO-RS software fundamentals may be found elsewhere [129]–[132]. Finally, the activity coefficients ($\ln\gamma$) are calculated through equation 15 in COSMOthermX which represent the affinity between solvent and solute and are strong indicators of solubility [121], [133].

$$\ln \gamma_{\underset{s}{i}} = \frac{(\mu^{i}_{s} - \mu^{i}_{p})}{RT} \quad (15)$$

COSMOthermX uses the chemical potentials (μ) to determine $\ln \gamma_s^i$ of siloxane compound (i) in DES (s) at infinite dilution. R is the gas constant, and T is the absorption temperature of the system which was kept at 25°C as similar studies report lower temperatures equate to better solubilities among DES and siloxanes [134], [135]. Equation 15 is used to convert $\ln \gamma_s^i$ into solubility capacity in section 6.1 [136].

Similar to the ln activity coefficient, Gibbs free energy of solvation (G_{solv}) is computed as a difference in chemical potentials. G_{solv} is the result from the difference of the chemical potential of the siloxane compound i in its pure phase μ^i_p and its chemical potential in the solvent phase μ^i_s at infinite dilution. Equation 16 describes the process.

$$G_{solv} = \mu_s^i - \mu_p^i \quad (16)$$

Along with activity coefficients, another powerful indicator of

solubility and interactions is the excess enthalpy of interaction (H_{int}) for the absorption [137]. Activity coefficient is limited as a study of affinity between chemicals through a measure of non-ideality, expressed through non-ideal interactions (hydrogen bonding). Where ln gamma draws its importance from its relation to Hildebrand solubility, excess enthalpy of interaction (H_{int}) is a temperature derivative of Gibbs free energy, allowing for a more precise study of the contributions from each interaction type (hydrogen bond and van der Waals bond) [138], [139]. These interaction types are represented through COSMOthermX parameters used to measure the total enthalpy of mixing as expressed in equation 17.

$$H_{int} = H_{mf} + H_{hb} + H_{vdw} \quad (17)$$

Where H_{mf} is the enthalpic penalty of a misfit factor which accounts for structural, steric hindrances, and charge misalignment [128]. H_{HB} is the enthalpic contribution from hydrogen bond interactions when mixing, and H_{vdw} is the Vander walls contribution [140].

Quantitative structure property relationships (QSPR) descriptors can be generated from sigma potential profiles reported in .cosmo files [141]. These moments (*M*) consist of σ polynomial function ($f_i(\sigma)$) which are reported in equation 18 and can be used in several property predictions in COSMOthermX like density and viscosity [131]. A siloxane specific moment (M_i) is computed through equation 19 from the σ profile (p(σ)) of the siloxane and $f_i(\sigma)$.

$$f_i(\sigma) = \sigma^i \; for \; i \geq 0 \; (18)$$

$$M_i^s = \int p(\sigma) f_i(\sigma) d\sigma \; (19)$$

Some of these moments have been correlated with the chemical's properties while others remain as simple regression parameters. The zeroth order moment (M_0^s, where i=0) is the total surface area of the siloxane "s", the first order moment (M_1^s, where i=1) is the total COSMO polarization charge on the surface of the given siloxane, the second moment (M_2^s, where i=2) is a vector of total COSMO polarization energy of the molecule, the third moment (M_3^s, where i=3) correlates to the measure of sigma profile symmetry, and the hydrogen bond donating and hydrogen bond accepting moments (M_{Hdon}^s and M_{Hacc}^s respectively) are measurements of the siloxanes ability to act as each, respectively [128].

4.3. Absorption conditions

The absorptions were studied at 25 °C and 1 atm except for methanol that is operated below −35 °C in industry, therefore, the calculations for methanol were run at −40 °C and 1 atm [57], [58]. The pressure was kept at 1 atm for all trials as the siloxanes have boiling points above 90 °C, thus resulting in incompressible systems at room temperature. A formal composition of Selexol was unable to be determined from literature, thus an equimolar mixture of its reported constituents (6 dimethyl ether, 8 dimethyl ether, and 9 dimethyl ether of polyethylene glycol ["DPEG Blend"]) was used [59].

4.4. Results and discussion

4.4.1. COSMO-RS validation

Compared to other computational thermodynamic predictive methods, COSMO-RS is entirely non-empirical, requiring only the molecular structure as an input for most property predictions. This makes COSMO-RS promising for exploring novel solvents like DES. A benchmark study has been performed here to determine if reasonable accuracy exists between DES and siloxane compounds. Due to the novelty of the absorption system, limited experimental values were available thus the benchmarking is based upon a dataset of 12 data points. Table 11 presents twelve computed data points from this work comparing with twelve experimental data points derived from the work of Villarim et al. [135]. The data is comprised of Gibbs solvation energies at varying temperatures, and enthalpy of mixing at 30 °C. The enthalpic mixing values are very accurate with an absolute average relative deviation (AARD) of ~0.31%. Although it is apparent that COSMO-RS underestimates the Gibbs solvation energies with an AARD of ~25%.

Table 8: Benchmark data for siloxane D4 in DES. Values are presented for enthalpy of mixing and Gibbs free energy of solvation. Enthalpy of mixing is reported for 30 °C while Gibbs free energy of solvation is reported for three different temperatures in kJ/mol. The resulting R^2 value for the two datasets (calculated and experimental) equates to 0.99 showing strong qualitative relationship. The calculated values are produced by COSMO-RS.

	HBD	Composition HBA:HBD	Enthalpy of mixing (kJ/mol)	Gibbs (kJ/mol) 30°C	Gibbs (kJ/mol) 45°C	Gibbs (kJ/mol) 60°C
Calculated	O acid	1:3	-40.21	-17.44	-15.31	-13.23
Calculated	N acid	1:3	-40.76	-17.67	-15.55	-13.47
Calculated	D acid	1:2	-41.00	-17.86	-15.74	-13.66
Experimental	O acid	1:3	-40.59	-20.47	-19.64	-18.48
Experimental	N acid	1:3	-39.38	-20.51	-19.63	-18.64
Experimental	D acid	1:2	-40.16	-20.33	-19.57	-18.36

4.4.2. Sigma surfaces, sigma profiles, and sigma potentials of siloxane compounds

Fig. 12 depicts the sigma surfaces of the siloxane compounds (L2, L3, D3, and D4) generated by TmoleX19. The colors represent a calculated charge gradient ranging from charge deficient to charge dense regions. The lack of significantly charge deficient regions (blue) suggests low hydrogen bond donating ability, the abundance of neutral (green) surface area

indicates a strong propensity towards Vander Waals interactions, and the presence of strong charge dense regions (red) indicate hydrogen bond accepting capability. The range of the sigma values on the surfaces are from −0.011 (e/Å^2) (blue) to 0.015 (e/Å^2) (red). It is evident through figure 15 that the red regions are associated with the oxygen and blue with the methyl groups. The silicone atoms are naturally positive and contribute to the electron deficient regions (blue). Sigma surface could indicate the behavior of these molecules regarding intermolecular interactions. One such judgement is the positioning of the red sites seen in figure 15 suggest steric hindrance will likely produce a dampening effect to the hydrogen bond accepting potential, which is a common takeaway from sigma surfaces [64]. The difficulty for other molecules to interact with the red regions in these sigma surfaces due to the methyl groups is quantitatively supported through computation of the QSAR determined hydrogen bond accepting moments of the siloxane molecules, as the sigma moments of two hexa-methyl siloxanes L2 and D3 (1.71, 1.83, respectively) are higher than their octa-methyl counterparts L3 and D4 at 1.25, and 1.19, respectively. These results suggest the amount of methyl groups on a siloxane compound are more determinate for hydrogen bonding capability than the linearity or siloxane chain length. Another qualitative determination may be made on the lack of sufficiently blue regions which would show affinity for hydrogen bond accepting sites on other molecules. This is confirmed quantitatively through

the hydrogen bond donating moment computation which is zero for all four siloxane compounds.

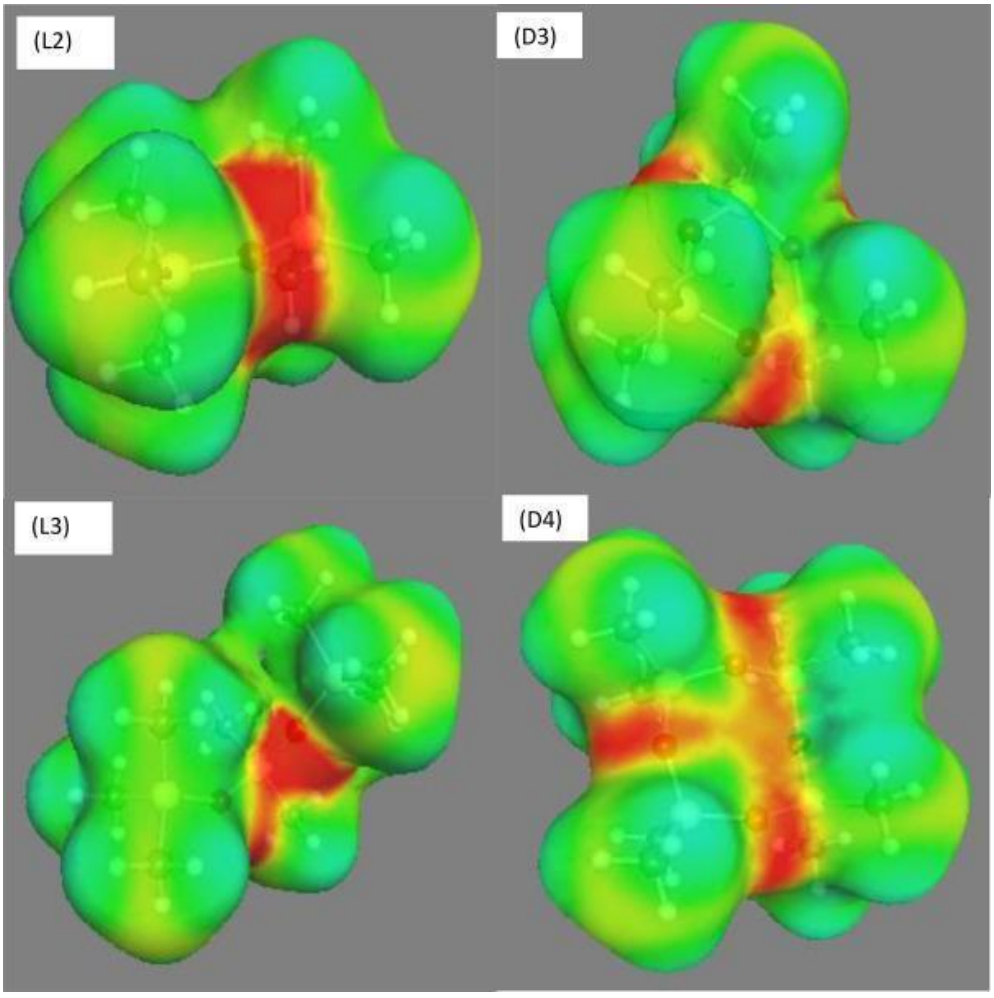

Figure 15: Sigma surfaces of siloxane compounds as computed by TmoleX19. Charge gradient is represented by the color scale of deficient = blue, neutral = green, and dense = red. Siloxanes represented are hexamethyldisiloxane (L2), octamethyltrisiloxane (L3), hexamethylcyclotrisiloxane (D3), and octamethylcyclotetrasiloxane (D4).

Figure 16 shows the sigma profiles of four siloxane compounds and HBA used in this study. A sigma profile offers quantitative information

about the surface charge attributes and distributions and can be considered a fingerprint of the molecule [65]. The x-axis is the associated surface charge in ($e/Å^2$), the y-axis is the frequency at which this charge segment can be found on the molecules surface or the amount of the respective color from sigma surfaces. Integration of these curves result in the total sigma surface area for each molecule present. Area between the range of -0.079 $e/Å^2$ and 0.079 $e/Å^2$ is relevant for Vander Waals interactions. Area outside of this central region is pertinent to hydrogen bonding and ionic interactions. As no ionic interactions are expected between DES and siloxane compounds, ionic interactions were omitted from the discussion. Negative sigma values outside of the Vander Waals region indicate hydrogen bond donating regions and positive sigma values higher than 0.079 $e/Å^2$ are representing hydrogen bond accepting regions. These histograms further support the conclusion that significant surface area of all siloxane compounds devoted to neutral charges resulting in Vander Waals interaction sites. Another note is the significantly less surface area the hexamethyl siloxanes L2 and D3 (162.38 and 222.46 g/gmol, respectively) are compared to the octamethyl siloxanes L3 and D4 (236.53 and 296.61 g/gmol, respectively). Table S2 contains the area distributions of these curves and shows more neutral surface area for the linear siloxanes L2 and L3 (94% and 93% respectively)

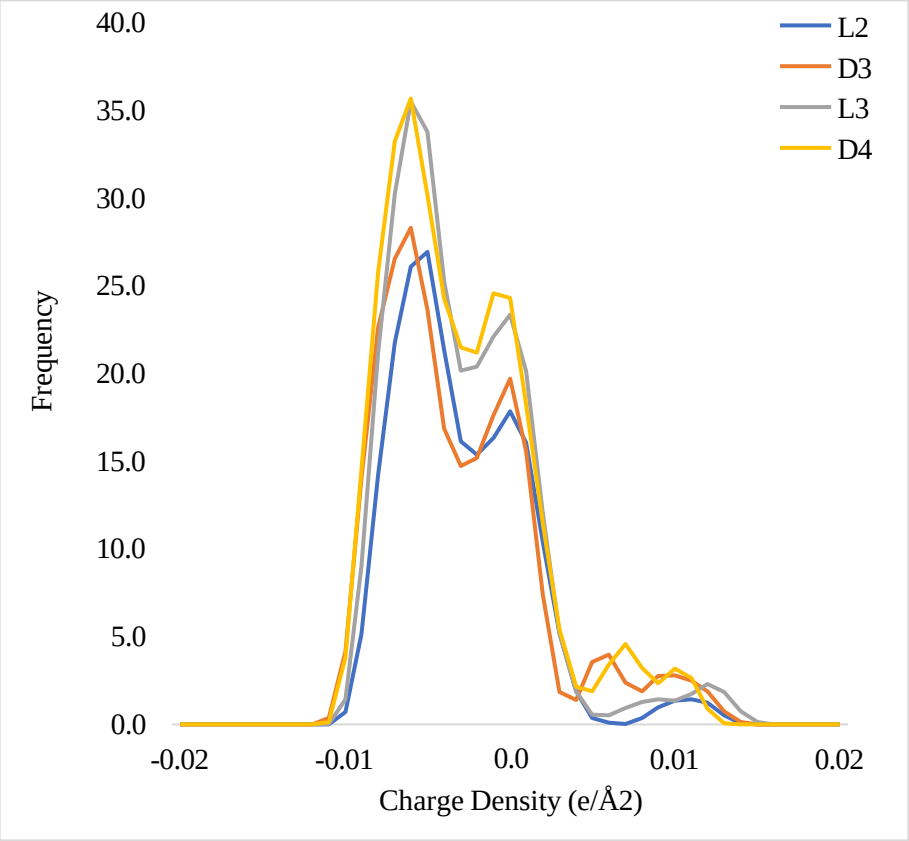

Figure 16: Sigma profiles of siloxanes as computed by TmoleX19 at B3LYP, BP-DEF2-TZVP level.

than the two cyclic siloxanes D3 and D4 (88% and 91%respectively). figure 18 shows the sigma potentials of the siloxane compounds. Figure 17 shows the sigma profiles of the DES components. Sigma profiles are visual representations of how each chemical will behave (y-axis) in the presence of a specifically charged surface (x-axis). As the y-axis is the predicted change in chemical potential from resting state to presence in the associated charged environment. The positive potentials indicate non-spontaneous interactions and vice versa. All of the siloxane compounds in Figure 14 are hydrophobic as indicated by the curve behavior around $x = 0$ as the

y-values are all negative, implying an affinity towards non-polar surfaces. This observation coincides with literature as siloxane compounds can be used to impart hydrophobic properties [66], [67]. These siloxane compounds are all repulsed by charge dense regions to similar degrees as the potentials for the curves at > 0.0078 e/Å^2 are all positive. The main difference is evident near the charge deficient environments (< −0.0078 e/Å^2) where the siloxane compound curves exhibit a mix of attractive and repulsive interactions. At strongly charge deficient regions (<−0.015 e/Å^2) the siloxane compounds are either strongly attracted (L2, L3, D3) or neutral (D4). However, as seen by figure 18 the HBA of the DES contain little if any surface charges in this region, making the relevant hydrogen bond donating zones limited to $-0.015\ e/Å^2 > x > -0.0078\ e/Å^2$. This region exhibits an order for the siloxane compounds from least to most repulsed of D3, L3, L2, D4. The order could be due to the complex surface area charge distributions and structuring. This region is indeed significant as any separations would be dependent upon it due to the uniformity of the other two regions. When considering suitable DES, the attribute of charge deficient regions will determine the degree of selectivity found between siloxane compounds and any product, whereas the presence of Vander Waals interaction sites and absence of charge dense regions will likely play

a considerable role in total solubility for siloxane compounds.

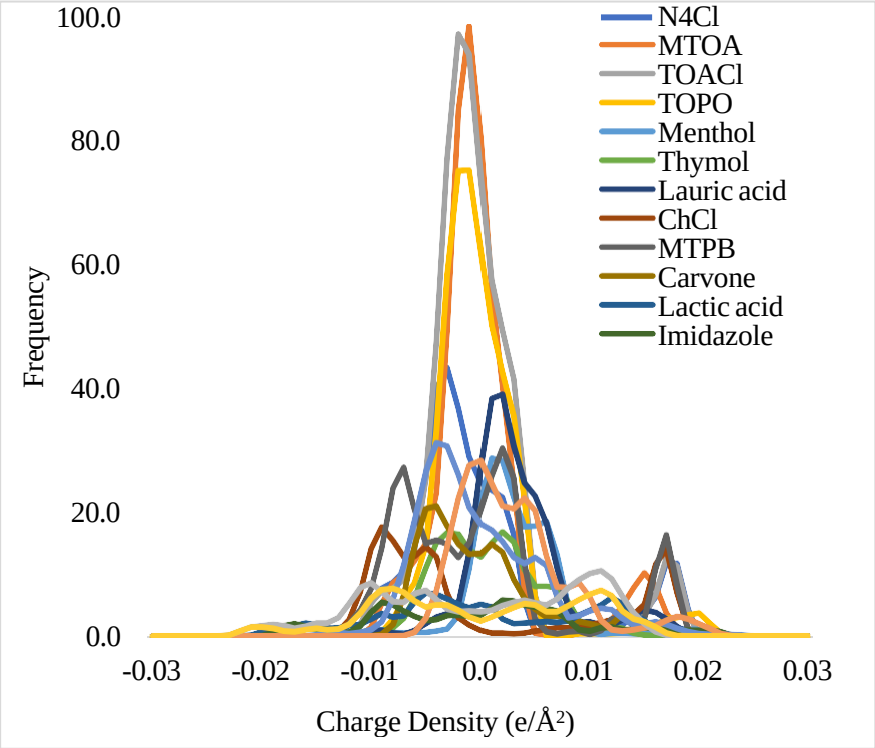

Figure 17: Sigma Profiles of HBA DES components

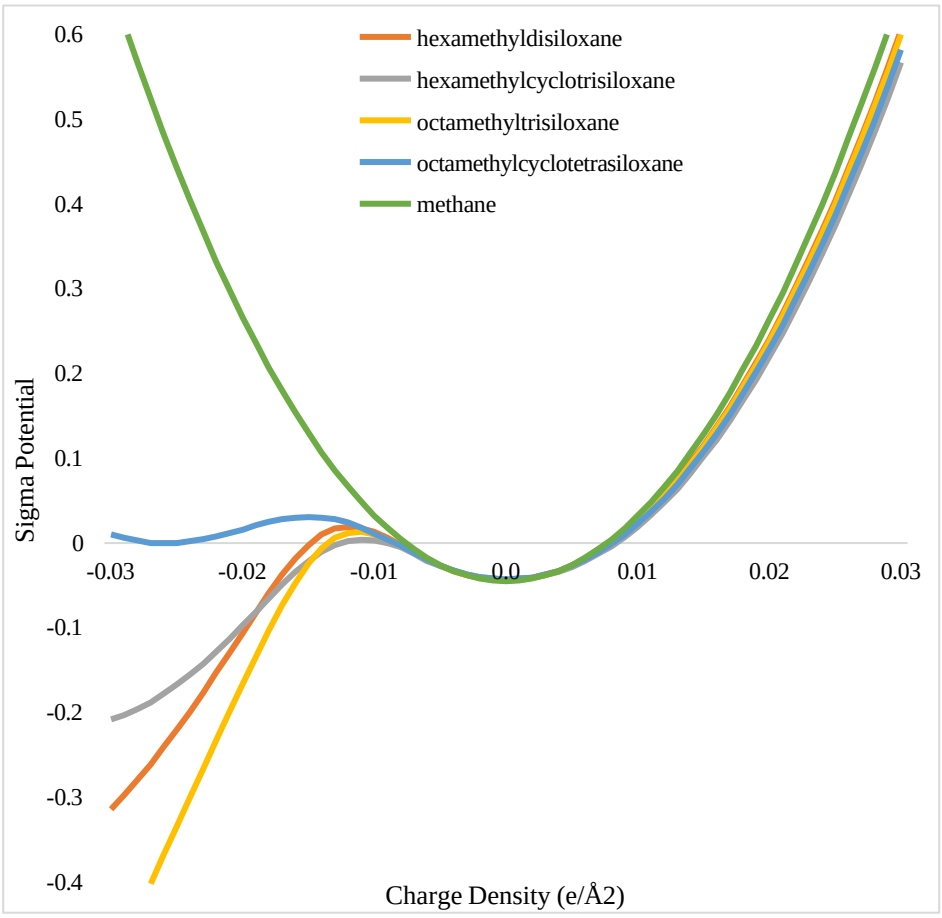

Figure 18: Solute potentials for siloxanes and methane.

4.4.3. Absorption of siloxane compounds on DES

The DES were measured by their solvating capability for the four siloxane compounds through thermodynamic properties, namely activity coefficients. Activity coefficients can be used in such predictive screening procedures as they are computationally inexpensive and robust indicators of relative solubility [68], [69], [71]. Direct correlations have been made for COSMO-RS derived infinite dilution ln activity coefficients and solubility of similar complex multi-component systems. One such correlation was recently made by Mood et al. [98], where several predicted properties were analyzed for correlation with lignin solubility in ionic liquids, where Infinite dilution ln activity coefficients proved the most reliable predictors. A similar tactic is used by Mohan et al. [185] in multiple works where the ln activity at infinite dilution is used to predict plastic solubility and/or conversions. The activity coefficients were calculated for each siloxane compound with respect to each DES at infinite dilution and reported in figure 19. Solvents 152–156 (MEA, DEA, MDEA, DPEG blend, and methanol) are conventional solvents which were included as a benchmarking for the prospective DES values of $\ln\gamma = 1$ indicate the interactions between the DES and siloxane compounds produce no significant deviations from ideal solubilization determined through Raoult's Law. Values of $\ln\gamma > +1$ indicate positive deviation or repulsive non-ideal effects, and $\ln\gamma < +1$ for attractive effects. Thus, anything above 1 is

considered ineligible for the application due to sufficiently repulsive interactions.

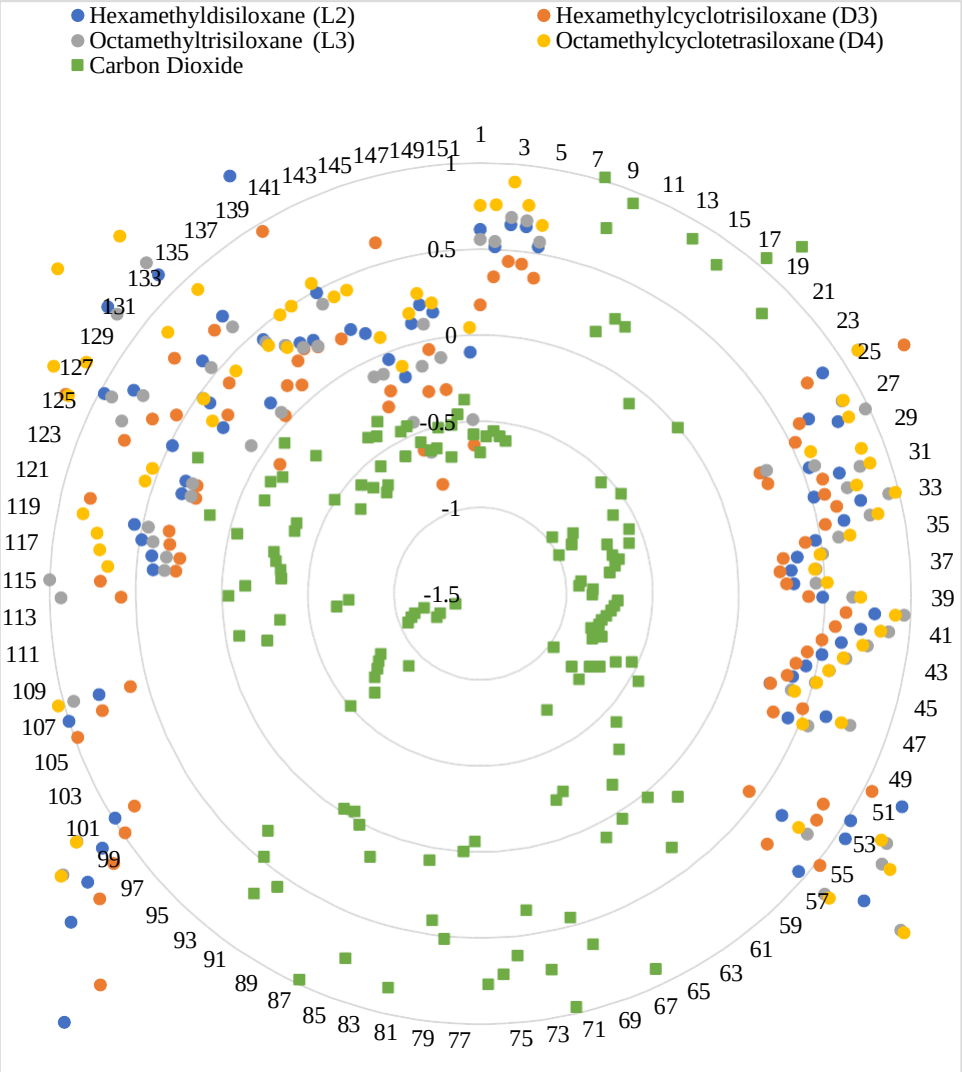

Figure 19: ln gamma values for siloxanes, CO_2, and CH_4 in 151 DES.

Solvents 6–23, and 57–98 are well above the cutoff of 1. This range includes all the type 3 DES (tetrabutylammonium bromide, atropine, choline chloride, methyltriphenyl phosphonium bromide, malic

acid, and citric acid based solvents) and four of the five conventional solvents (DEA, MEA, MDEA, and methanol), leaving only type 5 DES as potential candidates for siloxane compound absorptions. The reason for bias towards type 5 DES is likely due to the repulsive effects of non-neutral charged surfaces for the siloxane compounds as hydrophobicity for a solvent requires a significant weight in the volume of Vander Waals interaction sites. Of the represented type 5 DES, terpene and tetraoctyl-based solvents are consistently showing the lowest lnγ for the siloxanes whereas the shorter alkyl chain lengths (95–113) show less affinity. Moreover, thymol-based solvents stand out as the most affine for siloxane compounds. As for the difference in interaction potential witnessed between the type 5 DES it is likely attributed to the degree and distribution of the components regarding surface charged area available for proton donation and acceptance.

Siloxane D3 is shown to be best solvated by DES 144 (thymol: stearic acid, 4:1) as it consistently holds the lowest activity coefficient in any given solvent. It is apparent that siloxane D3 has the most charge dense interaction sites available of the four siloxane compounds. This, coupled with thymol containing the most charge deficient area distribution and the composition of the solvent as having four moles of thymol make a strong argument for the reason behind this result being due to the complimentary charge distributions. It is evident that the siloxane D3 is more readily

solubilized in the studied DES than the others, followed by L3. This observation is likely explained through the evidence in Fig. 14 which shows these siloxane compounds are the least repulsed by hydrogen bond donors present in DES. This is further confirmed through a Pearson correlation matrix value of −0.98 between ln activity coefficients of siloxane compounds in DES and the hydrogen bond accepting ability of the siloxane compounds. Furthermore, the work of Hełstowska et al. [38] shows of the 90 solvent combinations studied, acid based HBD's produced the highest affinity for siloxane compounds.

Other notable trend is the consistent placement of carbon dioxide as consistently more readily absorbed than the four siloxane compounds. This coincides with literature which repeatedly reports the exceptional solubilizing power DES's have for acid gases [36], [53]. This also means that through implementation of DES to capture siloxanes, additional stages may not be necessary to remove CO_2 as a co-contaminant.

4.4.4. Excess enthalpy of extraction of siloxane compounds in DES

Table 12 contains excess enthalpy values for the thymol-based solvents due to their superior performance. The solvent number is paired with each siloxane compound in the table. The enthalpy of mixing associated with hydrogen bonding (H_{HB}), Vander Waals (H_{vdw}) interactions, misfit factor (H_{mf}), and total enthalpic gain/release (+/- respectively) (H_{int}) is reported in

the Table 12 as calculated through COSMOthermX. Negative values correspond to favorable interactions as the resulting energetic state of the siloxane compound in DES is lower than the siloxane compound in pure form.

Table 12: enthalpy of mixing values for siloxanes L2, L3, D3, and D4 in thymol-based DES.

Solvent	**Siloxane**	H_{int} **(kcal/mol)**	H_{MF} **(kcal/mol)**	H_{HB} **(kcal/mol)**	H_{vdW} **(kcal/mol)**
140	L2	-6.49	1.8	-0.5	-10.99
140	D3	-7.54	2.5	-0.7	-12.47
140	L3	-8.22	2.41	-0.87	-14.34
140	D4	-9.31	2.82	-0.33	-15.77
141	L2	-7.26	1.63	-1.15	-10.93
141	D3	-8.72	2.28	-1.7	-12.44
141	L3	-9.6	2.19	-1.94	-14.37
141	D4	-10.1	2.61	-0.96	-15.72
142	L2	-7.36	1.49	-1.08	-10.97
142	D3	-8.75	2.16	-1.58	-12.46
142	L3	-9.67	2.01	-1.82	-14.39
142	D4	-10.22	2.43	-0.86	-15.76
143	L2	-7.41	1.57	-1.22	-10.96
143	D3	-8.95	2.22	-1.82	-12.48
143	L3	-9.85	2.12	-2.06	-14.42
143	D4	-10.33	2.54	-1.05	-15.78
144	L2	-7.45	1.6	-1.29	-10.96
144	D3	-9.06	2.23	-1.93	-12.49
144	L3	-9.95	2.15	-2.18	-14.44
144	D4	-10.4	2.57	-1.15	-15.79
147	L2	-6.72	1.64	-0.55	-11.02

147	D3	-7.81	2.33	-0.77	-12.5
147	L3	-8.56	2.21	-0.96	-14.38
147	D4	-9.59	2.61	-0.36	-15.81
148	L2	-7.18	1.5	-0.86	-11.02
148	D3	-8.57	2.13	-1.31	-12.53
148	L3	-9.33	2.02	-1.46	-14.44
148	D4	-10.19	2.42	-0.74	-15.84
149	L2	-5.65	2.28	-0.16	-10.99
149	D3	-6.69	2.89	-0.25	-12.46
149	L3	-6.97	3.02	-0.27	-14.3
149	D4	-8.53	3.4	-0.15	-15.75
151	L2	-7.46	1.53	-1.22	-10.97
151	D3	-8.99	2.18	-1.81	-12.5
151	L3	-9.91	2.07	-2.06	-14.44
151	D4	-10.39	2.48	-1.04	-15.8

All thymol-based type 5 DES reported in Table 12 have negative H_{int} which is expected as they were deemed highly favorable for solubilizing siloxane compounds. Furthermore, the degree of negativity follows that of the lnγ negativity results where solvent 144 (thymol: stearic acid, 4:1) and solvent 151 (thymol: hexadecanoic acid, 2:1) are determined to be the most affine for the siloxane compounds and solvent 149 (thymol: betaine, 3:1) is the least. While there is an agreement between general results between the two terms of lnγ and H_{int}, there is a discrepancy

regarding the ordering of the siloxane compounds themselves. For lnγ, it was seen that the ordering from most-to-least negative values were consistently ranked as D3 > L3 > L2 > D4. The general ranking for H_{int} is in reverse trend. The likely reason for the discrepancy is the accounting for Vander Waals interactions in H_{int} denoted as H_{vdw} and the reliance of hydrogen bonding for lnγ. Clearly the Vander Waals are significantly more impactful than the hydrogen bonds formed from siloxane-DES interactions by an order of magnitude. For instance, solvent 144 (thymol: stearic acid, 4:1) for siloxane D4 has H_{vdw} of −15.8 compared to H_{HB} of −1.15 kJ/mol. This observation is in line with previous observations, as there is significantly more neutrally charged surface than is present for hydrogen bonding in both the DES and all four siloxane compounds. Also as predicted previously, the positive values for H_{mf} overshadow the enthalpic release generated by H_{HB} as the methyl groups make reaching the negatively charged oxygen surfaces difficult. On this note the cyclical siloxanes have higher H_{mf} values as compared to linear but are significantly more exothermic due to H_{vdw} interactions occurring on larger surface areas attributed to the size of the cyclical vs linear compounds.

4.4.5. Toxicology assessment of DES suitable for siloxane compounds

Type 3 DES have been heralded for their nontoxic and environmentally benign properties. However, the DES studied include a

significant amount of type 5 DES. Consequently, an EHS has been conducted on the thymol-based solvents to assess them for sustainability. Thymol-based type 5 DES were chosen for VEGA EHS study due to their superior results. Table 13 contains the results of the EHS study. The columns are marked as EHS property and the rows as the DES components in pure form. EHS data is unavailable for DES compounds, therefore, individual HBA and HBD are selected for EHS study. The color scheme indicates whether a result is determined to contain the respective attribute and the confidence of the output from VEGA. Green indicates that the models generally agree that the concerning property is not associated with the chemical. Blue represents inconsistent predictions for which no determination could be made. Red is given to properties that have concerning properties attributed to the chemical. For a chemical to be attributed it must have at least a moderate risk associated with it regarding the property based upon conventional determination methods (NFPA > 2 or OSCH < 3). The results of the EHS study were checked for consistency through literature by means of safety data Sheets from Fischer Scientific [72] for available properties and is found that all components are considerably safe alternatives to conventional solvents [152–156]. The main discrepancies found between literature and VEGA model software predictions are for the toxicity models, for which the four predicted toxic substances of thymol, lauric, capric and hexadecenoic acids were found to

be nontoxic in literature (toxicity category of 3 or 4). For example, while considered corrosive thymol is reported as nontoxic, contrary to the results from the VEGA model as it contains an acute NFPA oral toxicity factor of 4 [73]. Therefore, all components are deemed nontoxic in the list of thymol based DES components presented.

Table 13: environmental health and safety report.

Component	Persistence Air	Persistence Water	Persistence Soil	Mutagenic	Toxic	BCF	Carcinogenic
Camphor	b	g	g	g	g	g	g
Capric acid	g	g	g	g	r	g	g
Lauric acid	g	b	g	g	r	g	b
Myristic acid	g	g	g	g	g	g	g
Stearic acid	g	g	g	g	g	g	g
Undecenoic acid	g	g	g	g	g	b	g
Borneol	g	g	g	g	g	g	g
Betaine	b	b	b	g	g	b	b
Hexadecanoic acid	g	g	g	g	r	g	g
Thymol	g	g	g	g	r	g	g

4.5. Conclusions

Type 3 and type 5 DES were analyzed for their potential to absorb siloxane compounds. Through sigma surface, sigma profiles, and sigma potentials of a total of 151 known DES, it was determined type 5 DES outperformed the type 3 solvents due to the steric hindrance of the hydrogen bond accepting sites of the siloxane compounds by the methyl groups they contain. With the information gained from activity coefficient and excess enthalpy of mixing, the discrepancy between literature as whether hydrogen bonding or Vander Waals interactions dominate in solubilizing siloxane compounds is answered as being Vander Waals with an enthalpic release of an order of magnitude higher than the hydrogen bonds. A performed EHS study concludes the high performing thymol-based DES as environmentally sustainable due to low toxicity, negligible persistence (in soil, water, and air), non-mutagenic properties, negligible BCF concerns, and non-carcinogenic attributes. These insights are presented to the scientific community as evidence that DES are suitable solvents for consideration in siloxane compounds.

Chapter 5
Computational exploration of Deep Eutectic Solvent utilization with CO_2, H_2, CO, and H_2S.

5.1. Introduction

Due to the climate crisis an increase in public pressure for renewable and sustainably sourced fuel and product sources are increasing in demand, such as syngas which is generated from biomass and waste materials [36]–[38];. Syngas is a mixture of hydrogen (H_2), carbon monoxide (CO), carbon dioxide (CO_2), and hydrogen sulfide (H_2S). Syngas may be utilized as a feedstock for the production of various chemicals and fuels [39], [40]. However, the presence of impurities like CO_2 and H_2S can decrease the efficiency and environmental friendliness of syngas utilization processes [41], [42].

Deep eutectic solvents (DESs) have gained considerable attention as promising candidates for various applications, including gas separation, due to their unique properties such as low volatility, non-flammability, and tunable physicochemical characteristics [186]–[188]. DESs are formed by mixing a hydrogen bond acceptor (HBA) and a hydrogen bond donor (HBD), resulting in a eutectic mixture with a lower melting point than its individual components [189]. The choice of HBA and HBD influence the physical and energetic properties of the resulting DES which enables the m to be tailored for specific applications [69], [158].

Many HBA and HBD combinations have been studied for their application in gas separation. The main groupings of DES components may be framed as acids, bases, phenols, and carbamides as HBDs, paired with ammonium salts, phosphonium salts, imidazoles, and phenolic HBAs [190]–[192]. While these solvents have been explored for CO_2 capture with excellent results, the studies are generally performed with a limited scope. Due to the vast library of potential DES combinations and molar ratios, the potential for their use has been understated due to restricted exploration.

Computational methods such as the Conductor-like Screening Model for Real Solvents (COSMO-RS) have been employed to predict the thermodynamic properties of DESs and guide their design for specific applications [96], [193], [194]. COSMO-RS has been successfully applied to study the solubility of various gases in DESs, including CO_2 and H_2S [55], [195], [196]. COSMO-RS has been used to investigate the influence of different HBA and HBD combinations on the thermodynamics of DES systems [121], [127]. These studies have demonstrated the potential of COSMO-RS as a valuable tool in identifying promising DESs for separation applications.

In addition to computational methods, machine learning techniques such as neural networks have been developed to predict the physicochemical properties of DESs. For instance, Yu et al. [99] developed a neural network model to predict the viscosity of various quaternary

ammonium-based DESs with high accuracy. This approach has been further validated by other researchers, who have successfully employed neural networks to predict viscosity in different DES systems [92], [197]. The integration of these machine learning techniques with computational methods like COSMO-RS can provide valuable insights into the design and optimization of DESs for syngas cleaning applications.

Environmental health and safety (EHS) analyses are necessary for determining the ramifications of introducing a chemical to a region or workers. The VEGA K-nearest neighbors (KNN) model has been utilized by various researchers to assess the potential hazards of DES and other chemicals [136], [155]. Through performing an EHS analysis, one is able to assess and compare the greenness of various chemicals in consideration for a process.

Aspen software has been utilized extensively in the chemical engineering realm as a tool to model process simulations. The models produced offer insights into performance of various unit components and solvents used in a multitude of separation problems [198]. Syngas has been extensively modelled successfully by various researchers [199]–[201]. DES have been modelled in aspen to compare the novel solvents performance such as in the work of Liu et al. [202] who modelled DES for extraction of m-cresol with high recovery of 0.9991. Aldawsari et al. [203] utilized Aspen to compare various DES with conventional solvents for natural gas

sweetening and found a 60% reduction in energy consumption for the novel solvents. However, while DES have been modelled in Aspen, there are few if any simulations of DES-syngas systems.

The objective of this study is to assess the thermodynamic potential and physical properties of DES in selectively separating syngas components such as CO, CO_2, H_2, and H_2S. Through utilization of thermodynamic predictive software COSMO-RS, Aspen, machine learning techniques, and EHS software (VEGA). The resulting work in this study is a bridge in the literature gap of a much-needed large scale evaluation of DES components and combinations to direct future researchers in their application.

5.2. Computational Methods: COSMO, TST-NN, VEGA

COSMO-RS was used to predict the infinite dilution activity coefficients ($\ln \gamma$) values of over a thousand DES to qualitatively screen them for their solubilization potential of lignin. Afterwards the DES were down selected for experimental evaluation and further studied computationally by COSMO-RS for sigma mapping to understand the solubilization mechanisms. The computational aspect was performed using the TURBOMOLE package (version 19.0.1, COSMOlogic, Leverkusen, Germany) which is comprised of TMoleX, COSMOconfX, and COSMOThermX. All computations for the screening procedure outlined in section 5 were performed at 30 °C and 1 bar as DES are considered room

temperature solvents [96]. All DFT calculations for these systems were performed at the Karlsruhe (Ahlrichs) def2-TZVP (default-2 Valence Triple-Zeta Polarization) basis set as recommended by TmoleX [129].

To better understand the interaction behaviors between deep eutectic solvent (DES) components and solute gases, sigma moment analysis using COSMO-RS was employed. In this context, sigma moments derived from sigma profiles in COSMO-RS provide insights into the interactions between DES components and solute gases, including H_2, CO, CO_2, and H_2S. The zero-order sigma moment represents the total surface area of the solute. The first-order moment is the polarization energy, or the negative of the total charge on the solute in the conductor continuum. The second-order sigma moment is highly correlated with the total COSMO polarization energy, indicating the overall ability of the solute to interact electrostatically with a polarizable continuum. A higher value suggests stronger electrostatic interactions between the solute gas and DES component, which can enhance gas absorption. The third-order sigma moment lacks a simple physical analogy but represents skewness or asymmetry of the sigma profile of the molecule. Additionally, there are two hydrogen-bond moments which quantify the ability of the molecule to interact as a hydrogen-bond and a hydrogen-bond donor. These parameters are particularly relevant for understanding hydrogen bonding interactions between solute gases and DES components.

5.2.1. TST-NN

The neural network used in this study was created by Wang et al. [25]. This team made a Transition State Theory-Inspired Neural Network (TST-NN) for estimating the viscosity of DES. The TST-NN is a machine learning model that uses the principles of transition state theory to predict the viscosity of various DES systems with high accuracy. Wang et al. constructed the neural network using a dataset of 2,229 experimentally measured literature-based viscosities for 183 DES. These DES are comprised of 47 HBA and 70 HBD. The viscosities input ranges from 1.3 to 85,000 mPa*s, temperatures of 278.15-378.15 K, and ratios between 1:19-49:1 (HBA:HBD).

The structure of the NN consists of three multilayer perceptrons (MLP). Two are for determining structural parameter information, and one takes all parameters to predict two specific viscosity equation parameters. Each MLP consists of two hidden layers comprised of 32 neurons each. The GELU function is used in place of RELU to allow for negative values. Through extensive training procedures the NN was found to have an ARD of 6.84% and an R^2 value of 0.9805.

5.2.2. VEGA

One identified advantage of deep eutectic solvents is their purported "greenness". As the list of DES compounds continues to grow, the

evaluation of environmental hazards must be continually examined. In this effort an EHS study was performed on the interested solvent components in this project. Much information is lacking in safety data sheet databases (SDS). As such "Virtual models for property Evaluation of chemicals within a Global Architecture" (VEGA) was used to predict the missing information. VEGA is a K-Nearest Neighbors (KNN) environmental health and safety (EHS) predictive model. It was used in the evaluation of persistence, bioconcentration factor (BCF), mutagenicity, carcinogenicity, and acute toxicity for selected DES components. VEGA is a collection of models that are based upon experimental results. The user simply inserts a molecular structure in the Simplified Molecular Input Line Entry System (SMILES) format. And the models chosen to evaluate the similarity of the input molecule's structure which provides a "reliability" metric. Along with this the models output whether the predicted value molecule contains the assessed attribute or not.

5.2.3. Aspen Plus V12

Aspen Plus V12 was utilized in this dissertation as a means of thermodynamically modelling process flow diagrams (PFDs). Due to the lack of experimentally derived empirical parameters for most DES combinations standard property methods could not be used. The utilized method for analyzing DES within Aspen Plus was COSMO-SAC. The DES was defined as a pseudo component with user defined inputs computed

from COSMO-RS or neural network in the form of viscosity, boiling point, density, vapor pressure, molecular weight, COSMO volume, and sigma profiles. This was also performed for CO_2 as this was not included in the Aspen database. Other molecules like CO, H_2, and H_2S existed in the complimentary COSMO-SAC database within Aspen. The conventional model representative of Selexol (DPEG) was taken from the on-board Aspen simulations as provided by the creators. These physical solvents were modelled under steady state, equilibrium assumptions and thus carried out for DES systems as well. Sensitivity analyses were performed for each necessary block and stream to determine reasonable system parameters by means of stage number, flow rates, pressures, temperature, and duty.

5.3. Results and Discussion

5.3.1. Benchmarking Study

Through the utilization of the COSMO-RS tool previously unattainable project scopes are made feasible. The flexibility of COSMO-RS over conventional group contribution methods and equation of state models lay within its apriori approach. This approach requires little to no experimental parameterizations regarding the molecules studied. This allows for the expedient generation of solvent-solute system interaction descriptors, especially helpful when attempting to screen a large quantity of solvents for further experimental evaluation. The determination of infinite

dilution activity coefficients (ln γ) DES-Syngas systems offer an understanding of relative solubility when screening multiple solvents.

Previous works have validated the use of COSMO-RS model against experimental literature for accurately predicting gas-liquid systems regarding DES with siloxanes and fluorinated compounds [96], [204]. liquid-liquid systems with platform chemicals and DES were validated in other work with similar methods as well [76]. In this study an attempt to validate the use of liquid-gas systems to accurately represent the thermodynamics of syngas components was made. The goal is to model DES-syngas systems through a focus of the main value/coproduct components of H_2, CO, CO_2, and H_2S.

This benchmark study evaluates both quantitative and qualitative abilities of COSMO-RS for DES-syngas through the evaluation of solubility and ln activity coefficients respectively utilizing literature based experimental data. 42 experimental literature values were used for DES-syngas systems at various temperatures and pressures, complimentary systems were simulated in COSMO-RS with the same methods outlined in section 6. The solubilities and ln activity coefficients were then generated for each system and plotted against the literature values as seen in figure 20. Linear regression was performed for experimental and computational representatives with R^2 values offering a goodness of fit measure and residual sum of squares (RSS) offering a measurement for prediction

accuracy. Overall excellent qualitative agreement is found between the relationships of experimental syngas solubility and computational Syngas components at infinite dilution activity coefficients with an R^2 value of 0.85 and an RSS value of 7.3.

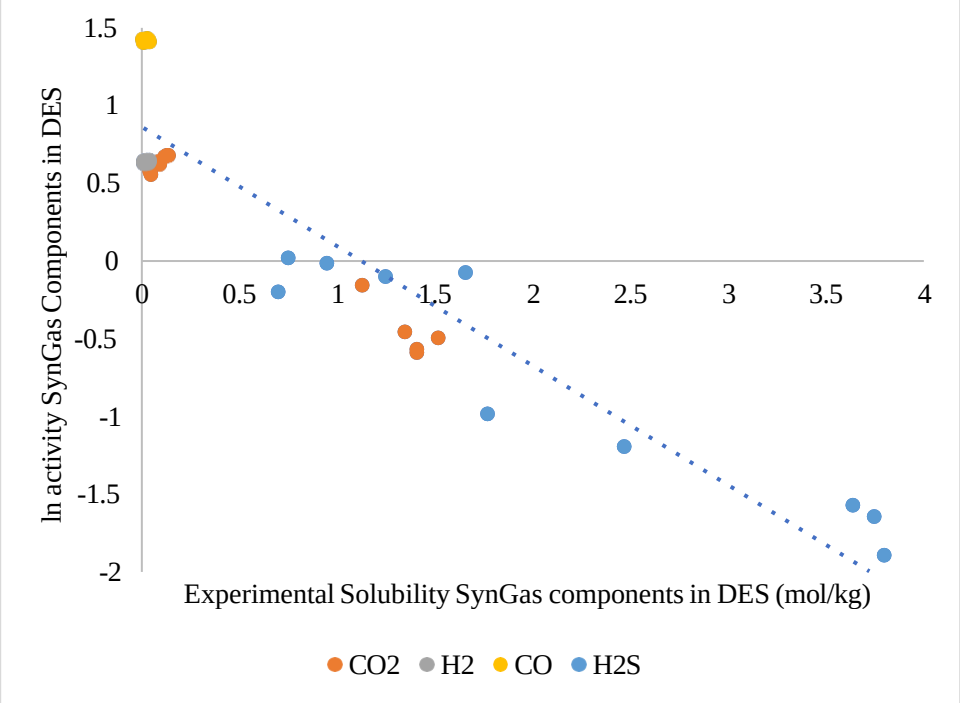

Figure 20: Benchmarking study for computed ln activity coefficients vs experimental solubilities exploring all four focused syngas components (CO2, H2, CO, H2S). The datapoints are at varying temperatures and pressures. The clear trend of increasing solubility correlated to decreasing ln activity coefficient instills confidence in the qualitative accuracy of the method.

The results here are in line with our previous works and those of Mood et al [205] who measured various indicators including ln activity coefficients generated by COSMO-RS to predict relative solubility of ionic

liquid (IL) systems. The findings here are presented as justification to continue with the proposed screening procedure outlined in section 6 to determine appropriate DES for syngas separations and to understand mechanisms of electrostatic interactions found in section 7.

5.3.2. Sigma Analysis

To understand the electrostatic mechanisms of absorption for syngas components H_2, H_2S, CO, and CO_2, a sigma potential analysis was performed. Through a sigma potential analysis of a molecule, insight into the types of intermolecular interactions one could expect against a range of surface charges is gained. During the COSMO-RS procedure an electronic shell is computed for the analyte which represents its electronegative surface area whose derivatized segments are referred to as “sigma” segments. The sigma profile of a molecule is an accounting of the entirety of its sigma segments while the sigma potential is the predicted chemical potential of a sigma profile interacting with the surface of a single consistent charge. Figure 21a depicts the sigma potentials of the analyte syngas components. The x-axis is the charge of a surface ranging from electropositive, to electronegative, with electroneutral existing between $\pm$ 0.0078 e/Å^2 [128].The y-axis represents the predicted chemical potential where negative values indicate spontaneous interactions. H_2, CO, and CO_2 are parabolic in nature with the vertex roughly centered in the electroneutral region of zero with negative chemical potentials indicating an affinity for

interacting with non-polar surfaces. These interactions are generally hydrophobic, π–π, cation–π, and CH–π type interactions [205]. An important distinction between the CO_2 curve vs CO and H_2 curves is the inclusion of -0.01 within its parabolic dip at/below y=0. CO_2 is going to favorably interact with electron deficient (< -0.0079 e/Å^2) surfaces where H_2 and CO will not, suggesting solvents with sufficient lightly electropositive (-0.01 to -0.079 e/Å^2) interaction sites will perform well for separations. Likewise, the flattening of the CO_2 parabola states the molecule will be less repulsed by more significant surface charges (>>-0.0079, 0.0079 e/Å^2 <<) that the value gases of H_2 and CO offering another mode of separation. H_2S breaks from uniformity as it is not parabolic in nature. This molecule is shown to possess the ability to favorably interact with electronegative (> 0.0079 e/Å^2) surfaces, neutral surfaces (-0.0079 > 0 < 0.0079 e/Å^2), and lightly electron deficient surfaces (-0.01 to -0.0079 e/Å^2) allowing for a more flexible solvent electrostatic profile to facilitate separation from the value products of H_2 and CO.

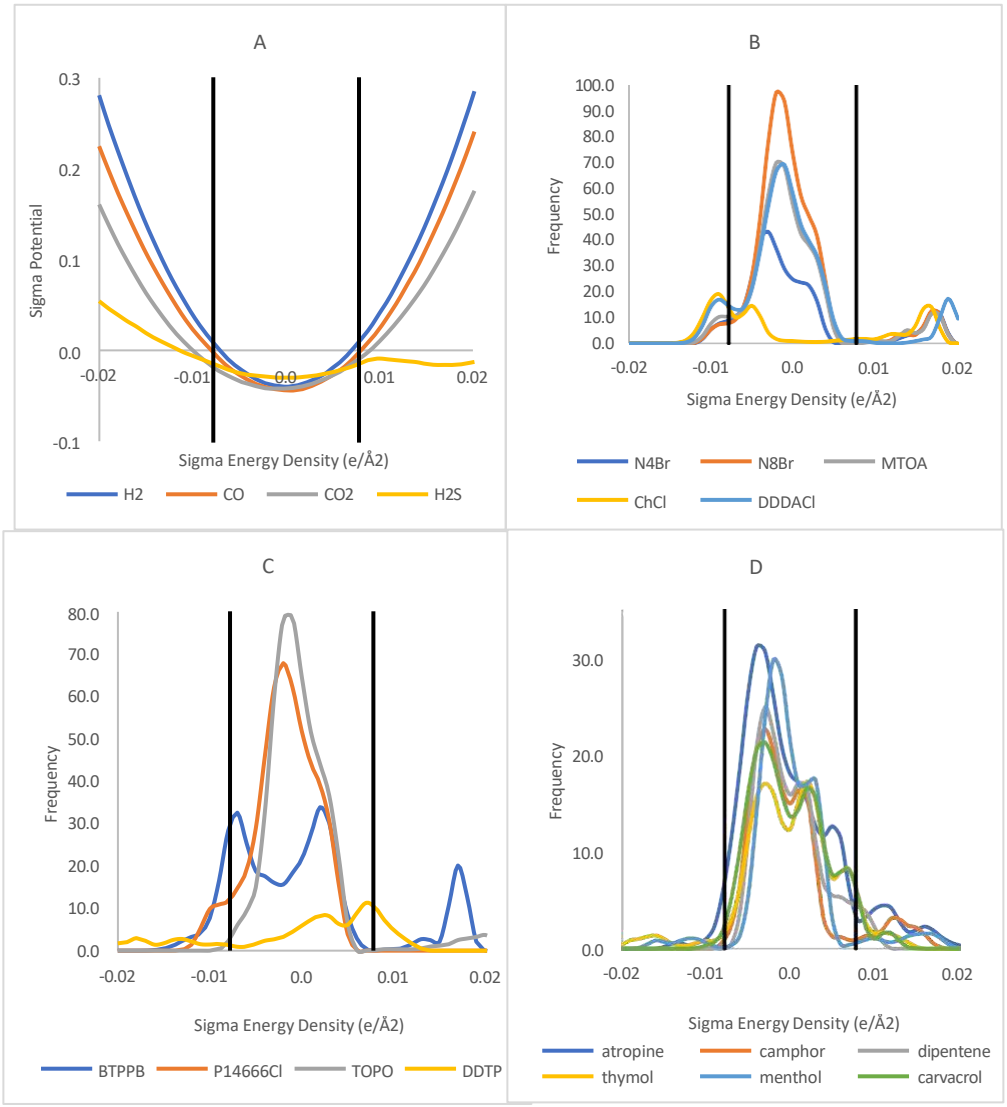

Figure 21 A,B,C, & D: Sigma potentials and profiles of studied absorbents and solvents. A) sigma potentials of H2, CO, CO2, and H2S. B) Sigma profiles of quaternary ammonium salt HBA. C) Sigma profiles of quaternary phosphonium salt HBA. D) Sigma profiles of terpenoic components.

The sigma profiles for the HBA studied in this project are displayed in figure 21b,c,d. Through previous works it was discovered the driving force of absorption by DES was primarily dependent upon the selected HBA while the HBD tweaked the physical properties of the solvent [96], [204]. This was discovered through thermodynamic analysis in the context of compositional studies. For this reason, the sigma analysis is focused upon the absorbents and studied HBA which are comprised of amines, phosphines, and phenolic compounds which are represented in figures 21b, c, and d respectively. Most of the discovered type 3 and type 5 DES are comprised of HBA from these three groups [75], [206]. These groups are represented in this work to provide a general understanding of potential solvent selection for the task.

Through analysis of the sigma profiles of these HBA it is evident all three groups (amine, phosphine, and phenolic) have most of their surface area composed of neutral interaction sites making them exceptional at absorption through Vander Waals interactions. The average neutral surface area ($-0.0079 > x < 0.0079$ e/Å^2) composition for each group is computed as at least 75% as reported in table 14 which shows the integrated surface areas per electrostatic zone for each group and individual HBA. This indicates a potential for affinity between all HBA types and all studied absorbents per the sigma potentials. The amide group on average contains significantly more hydrogen bond donating surface area at 13% compared

to phosphine (9%) and phenolics (2%). As evident in figure 21B, the bulk of the hydrogen bond donating surface interaction sites are between a sigma charge of -0.01 e/Å^2 and -0.0078 e/Å^2, which is expected to offer favorable interactions for CO_2 and H_2S while repulsing H_2 and CO. The phosphine and phenolic groups show more variability in hydrogen bond accepting surface area distribution which can be detrimental to the absorption and separation of the syngas components. In the hydrogen bond accepting region the sigma frequency for amine and phenolic compounds is expected to be entirely due to the associated ion which is sterically locked by the HBD's [207]. However, there are no ions associated with the phenolic HBA's whose surface areas average 6% in this region and are variably dispersed between 0.0079 e/Å^2 and 2 e/Å^2 which would be expected to offer an advantage in H_2S separation from H_2, CO, and CO_2.

Table 9: Normalized Integrated segments of sigma profiles of HBA broken into electron deficient, neutral, and electron dense surface areas available for intermolecular interactions.

Amides	N4Br	N8Br	MTOA	[TETA]Cl	ChCl	DDDACl	N10	Avg
Deficient %	0.04	0.02	0.04	0.09	0.28	0.07	0.39	0.13
Neutral %	0.83	0.91	0.88	0.77	0.42	0.85	0.57	0.75
Dense %	0.12	0.07	0.08	0.14	0.31	0.08	0.04	0.12
Phenols	atropine	camphor	dipentene	thymol	menthol	carvacrol	Average	
Deficient %	0.02	0.00	0.00	0.05	0.03	0.01	0.02	
Neutral %	0.89	0.90	0.97	0.91	0.91	0.96	0.92	
Dense %	0.09	0.09	0.03	0.05	0.06	0.03	0.06	
Phosphines	BTPPB	P14666Cl	TOPO	DDTP	Average			
Deficient %	0.09	0.05	0.00	0.21	0.09			
Neutral %	0.78	0.95	0.96	0.67	0.84			
Dense %	0.14	0.00	0.04	0.13	0.08			

5.3.3. Heat Maps

Type 3 and 5 DES are comprised of organic HBA's and HBD's. The eutectic depression is a result of the hydrogen network formed [208]. Thus, it has become a common practice to search for novel DES through combining known HBA's with known HBD's rather than treating them as exclusive

combinations [193], [194]. This approach offers significant insights into the mechanisms of absorption and offers the chance for a fundamental analysis of the types of HBA/HBD combinations most suitable for a given task. However, this quickly becomes infeasible on an experimental scale. For this reason, COSMO-RS was employed to analyze the thermodynamics of 990 DES component combinations for each syngas component H_2, H_2S, CO, and CO_2. The DES were all analyzed at a 1:1 (HBA: HBD) molar ratio for consistency and at 30 °C as DES are considered room temperature solvents.

Figure 22 depicts the heat map generated for ln activity coefficients of the DES and gas systems with the pseudo selectivity between CO_2 and CO in figure 23. A consistent trend developed from standard deviation analysis of the ln activity coefficient date matrices that encompassed all four syngas components. The average standard deviation among a single HBA and the range of HBD's was half (~20%) that of the average standard deviation among a single HBD with the whole range of HBA (> 40%). This is an indication that the HBA is the driving molecule for absorption for the four studied syngas components [209]. It should be noted that nearly all solvent combinations provided ln activity coefficient values below 1, suggesting some level of affinity for all 4 gases. This is expected as discussed in section 5.2 where the sigma potentials indicate favorable Vander Waals interactions would develop of which the HBA have in ample amounts. The types of HBA that were most suited to absorbing each gas

show deviations. For absorbing H_2, CO and CO_2 it is evident that long chain quaternary amine and phosphine groups (MTOA, N8Br, P14666Cl) dominate.

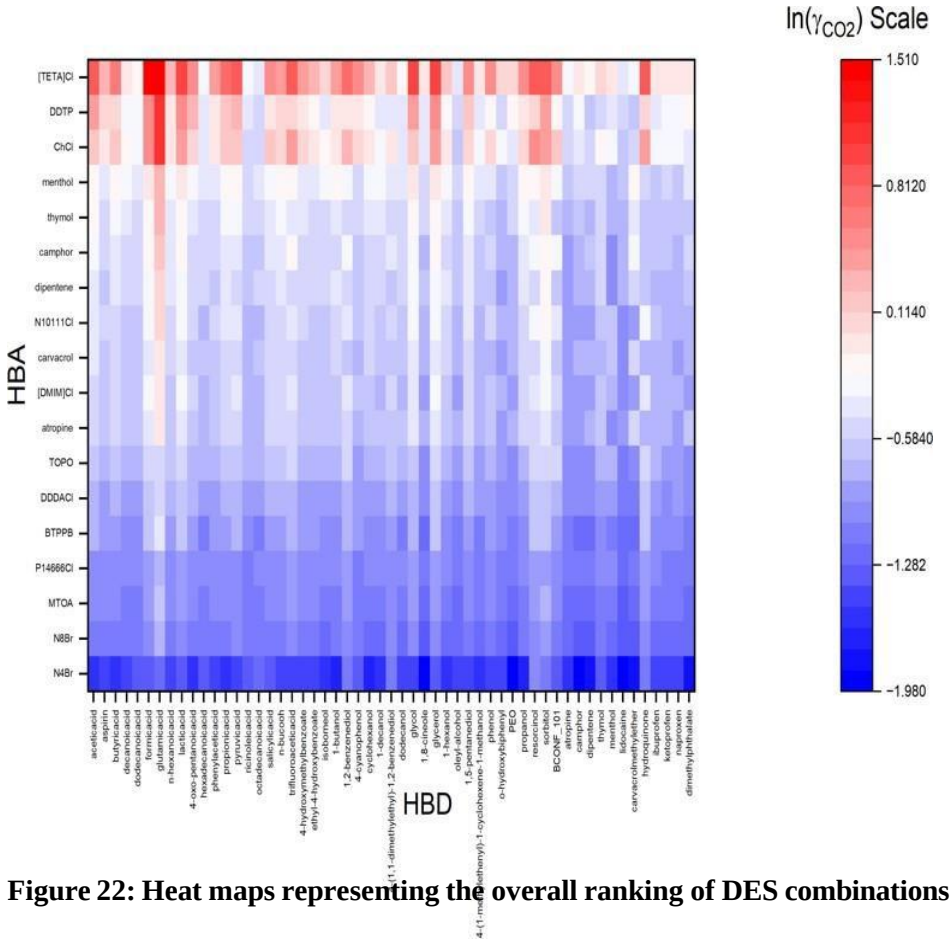

Figure 22: Heat maps representing the overall ranking of DES combinations with respect to CO_2 ln activities.

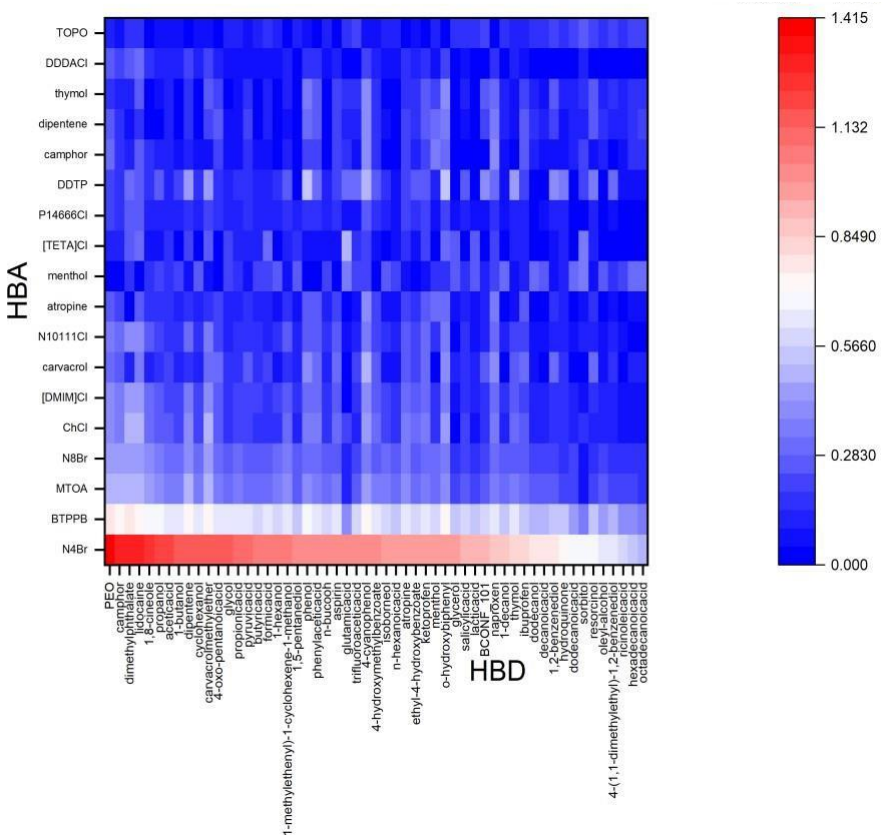

Figure 23: Heat maps representing the pseudo selectivities of CO_2 over H_2.

These results are supported by the work of Ali et al [210] whose experimental results in molar and mass based solubility suggest long chain HBA offer increased CO_2 mol/mol solubility specifically with MTOA (0.144) outpacing N4Br (0.116). The work also shows larger phosphine BTPPB (0.05 mol/mol) offering higher CO_2 solubilities than small chain quaternary ammonium salts like ChCl (0.03 mol/mol) which are reflected in the rankings of CO_2 heatmap study found in figure 22 [210]. One explanation for this finding is the increased surface area devoted to Vander

Waals interactions found in the longer chain HBA offering favorable interactions with the three gases per their sigma potential analyses. Yet the near overlapping of MTOA and N8Br curves with shorter chain HBA's like N4Br in the hydrogen bonding regions would lead one to expect more similarity. Further explanation can be found in kamlet-taft parameter studies like those of Teles et al [211] who show that with increase in tetra alkyl chain length, the potency of the hydrogens responsible for hydrogen bonding on the HBA changes. It is shown that with increased Vander Waals surface area, a decrease in hydrogen acidity takes place which in turn would offer less repulsivity to the three gases which are avoidant of such surfaces.

For absorbing H_2S an advantage is found in imidazoles ([DMIM]Cl) and long/mix chain quaternary amides and phosphines (BTPPB, N10111Cl, and DDDACl). These results are in line with the research by Wu et al [212] which indicates increased chain lengths on quaternary ammonia salts increases H_2S solubility. No other comparative studies were able to be found regarding phosphine or imidazole-based DES for H_2S absorption.

5.3.4. Compositional Study

Figure 24 contains results for a compositional study performed on N4Br based DES. The goal of this study is to determine how the change in molar composition would affect the selectivity for CO_2 over H_2 in a solvent system. The pseudo-selectivity of ln activity coefficient for CO_2 – ln

activity coefficient H_2 were computed for each solvent combination at molar compositions ranging 1:1 to 1:6 HBA:HBD.

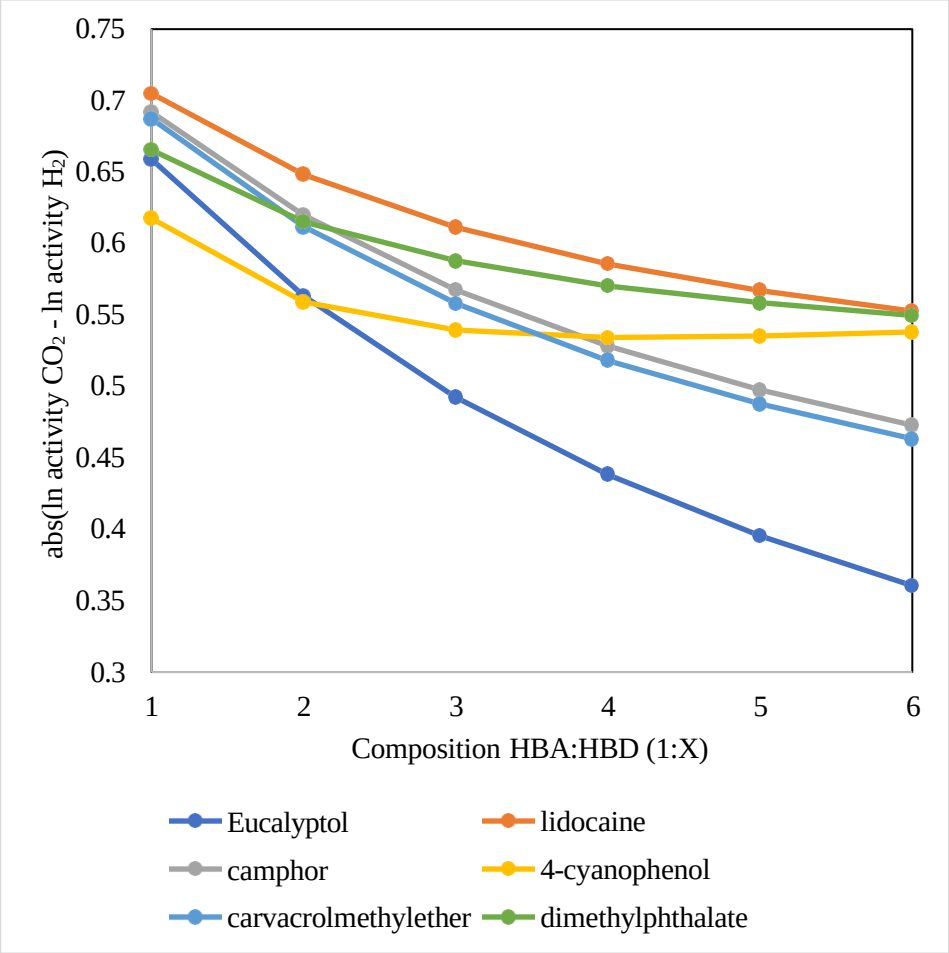

Figure 24: Compositional study of select DES whose HBA is N4Br.

Figure 24 showcases that the selectivity for CO_2 over H_2 is retained in solvents exhibiting higher polarizability as found in the HBD's lidocaine, 4-cyanophenol, and dimethylphthalate. The correlation was discovered through computing and comparing the dielectric energies of each HBD (using COSMO-RS) of which are below -13 kcal/mol for the previously

mentioned HBD and above -7.7 kcal/mol for the remaining 3: eucalyptol, camphor, and carvacrolmethylether.

This observation aligns with the hypothesis that polarizable solvents are more effective in selectively absorbing CO_2 compared to H_2. As the molar composition varies from 1:1 to 1:6, the polarizability of the solvent system increases in the DES with the stated 3 HBD, leading to stronger interactions between CO_2 and the solvents. The stabilized selectivity correlated to higher molecular polarizability results from the solvents' ability to reorient their electron clouds in response to the electric field generated by solute molecules [213], [214]. In contrast, the nonpolar nature of H_2 gas leads to weaker interactions with these solvents, thereby maintaining the selectivity for CO_2 absorption.

5.3.5. Viscosity

The viscosities of 6 DES were studied at varying compositions from 1:1 to 1:6 HBA:HBD at 30°C and 1 atm as seen in figure 25. It is recognized that not all represented DES compositions are liquid at room temperature which is evident from some values reaching upwards of 1600 mpa*s between compositions of 1:1 with significant decreases at 1:2 HBA:HBD. The results demonstrated that the N4Br-lidocaine DES consistently exhibited a significantly lower viscosity than the other DES at 30°C. This observation can be attributed to a combination of factors, including molecular structure, size, shape, and intermolecular forces.

Increases in hydrogen bond strength, number, and larger scale vdw interactions are major contributors to higher viscosities [215], [216]. Lidocaine is computed to have a hydrogen bond acceptor sigma moment (6.1) more than double that of camphor (2.5), and nearly eucalyptol (3.4) suggesting the hydrogen bond network formed between N4Br (an HBA) and lidocaine (also a common HBA) may result in a weaker hydrogen bonding network than that of N4Br and the more viscous DES. According to Osch et al [206] a DES with viscosity at or below 100 is the cutoff for industrial applications. This would exclude N4Br and camphor whose lowest viscosity is computed at 107 mPa*s at a 1:6 ratio.

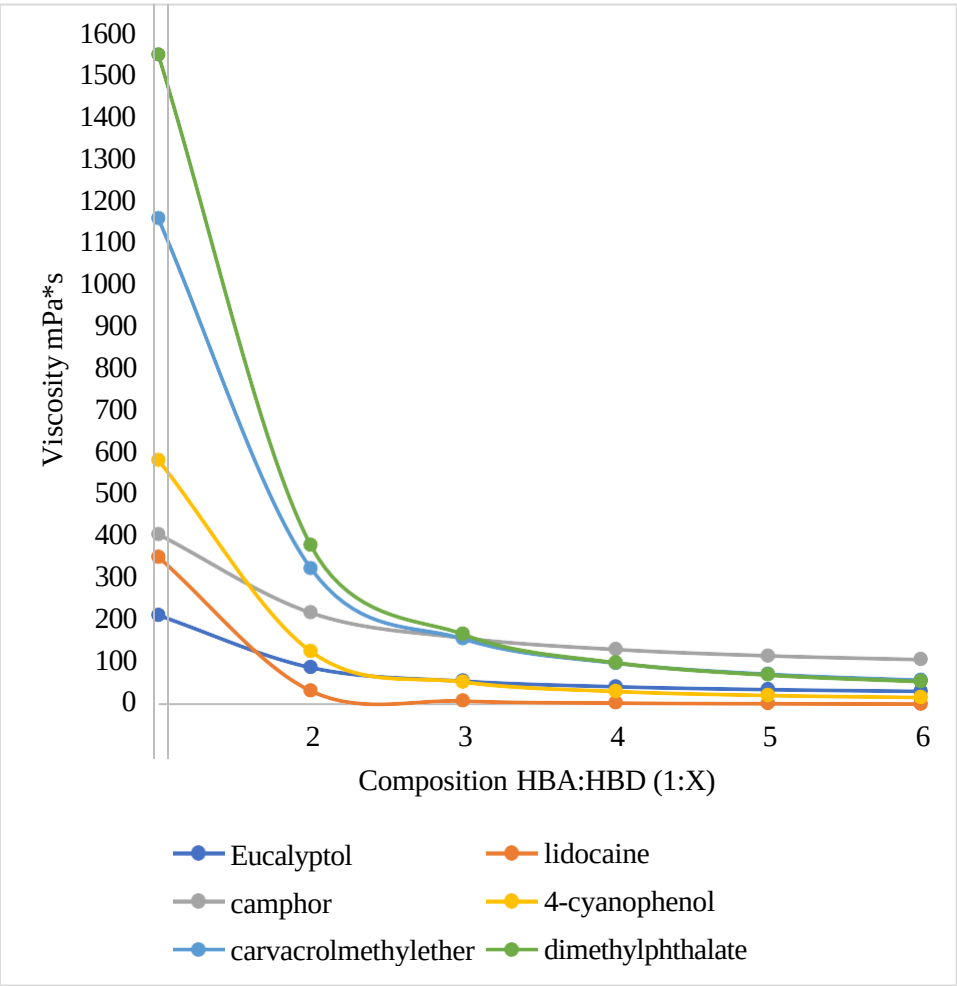

Figure 25: Viscosity study for select DES whose HBA is N4Br.

5.3.6. EHS Evaluation

Table 15 depicts the results of the EHS study performed for the select DES components. This section contains the results of the environmental health and safety (EHS) assessment for the deep eutectic solvents (DES) under investigation, namely N4Br, eucalyptol, lidocaine, camphor, 4-cyanophenol, carvacrolmethylether, and dimethyl ether. The EHS evaluation was carried out by examining seven key attributes:

persistence in air, persistence in water, persistence in soil, mutagenicity, acute toxicity, bioconcentration factor (BCF), and carcinogenicity. To obtain the necessary data for these attributes, safety data sheets (SDS) provided by Fischer Sci. [144] were utilized. However, as some information was missing from the SDS, an EHS k-nearest neighbors-based software called VEGA [143] was used to fill in the gaps.

Table 10: EHS study of DES

	Persistence Air	Persistence Water	Persistence Soil	Mutagenic	Toxic	BCF	Carcinogenic
N4Br	g	g	b	g	g	b	b
Eucalyptol	b	g	g	g	g	g	g
Lidocaine	b	b	g	g	g	g	g
Camphor	b	g	g	g	g	g	g
cyanophenol	b	g	g	g	g	g	g
carvacrol	b	g	b	g	g	g	g
dimp	b	g	g	g	g	g	g

Persistence in air, water, and soil are critical factors to consider when assessing the environmental impact of chemicals. These factors determine

the potential of a substance to accumulate and remain in different environmental compartments [217]. Some datapoints remain indeterminant due to lack of available published information for these molecules and ones similar enough to them to offer reliable fits to the models in VEGA. While neither resource explicitly finds any of the studied components to be persistent in air, there is no conclusive evidence that they are not, excpet N4Br. However it should be noted that a defining trait of DES is their low vapor pressures, signaling theoretically that this is not a likely issue [218], [219].

Mutagenicity is a measure of a substance's ability to cause genetic mutations. In our study, none of the examined DES showed any evidence of mutagenicity. Acute toxicity is another essential factor to consider when evaluating the safety of chemicals. The results of this study indicate that N4Br, eucalyptol, lidocaine, camphor, 4-cyanophenol, carvacrolmethylether, and dimethyl ether all possess low acute toxicity levels.

The bioconcentration factor (BCF) is a measure of the potential for a chemical to accumulate in living tissue. Eucalyptol, lidocaine, camphor, 4-cyanophenol, carvacrolmethylether, and dimethyl ether all displayed low BCF values. The exception is for N4Br which was unavailable in SDS literature and offered poor reliability measures in the VEGA model, which

means no determination may be made for this substance without further experimental investigation.

Carcinogenicity is a measure of a substance's potential to cause cancer. None of the examined DES were found to be carcinogenic though N4Br was not reliably modelled with the VEGA model and unavailable in SDS data, which means no determination may be made for this substance without further experimental investigation.

The EHS assessment of the investigated deep eutectic solvents revealed that they possess relatively low environmental and safety risks. Most of the solvents exhibited low persistence in various environmental media and low acute toxicity. None of the solvents were found to be mutagenic or carcinogenic. These findings suggest that the examined DES are promising candidates for further research as they will not adversely impact the environment or handlers.

5.3.7. Aspen analysis

With the resulting down selection of DES candidates an aspen model was generated to compare the separations capabilities against the conventional standard physical solvent DPEG. Figure 26 depicts the model PFD used in this work where the process begins with a radfrac absorption column with a product stream of either nearly pure H_2 or H_2 and CO mixture dependent upon solvent capabilities. The stream tables may be

found in Appendix D of this document. All absorber columns contained 10 stages. The varying pressures in each model can be found in table 11. Next the pressure is reduced to atmospheric as the bottoms of the absorber column passes through valve B4 and enters the flash separator for phase separation. The stream Flash-L is heated to the appropriate stripping temperature as it passes through Heatx-1 and enters the radfrac stripping column for solvent regeneration. Here there is a total condensation unit applied. The reboiler duty user input was iteratively solved for optimum operation. From here the stream Strip-B becomes cooled to absorber temperature by block Heatx-2 and pumped to absorber inlet pressure. In the simulations the mixer block was not required in the DES systems due to the low vapor pressures resulting in negligible solvent loss. The syngas entered the diagram at 72 kg/hr flowrate and a temperature of 30 °C.

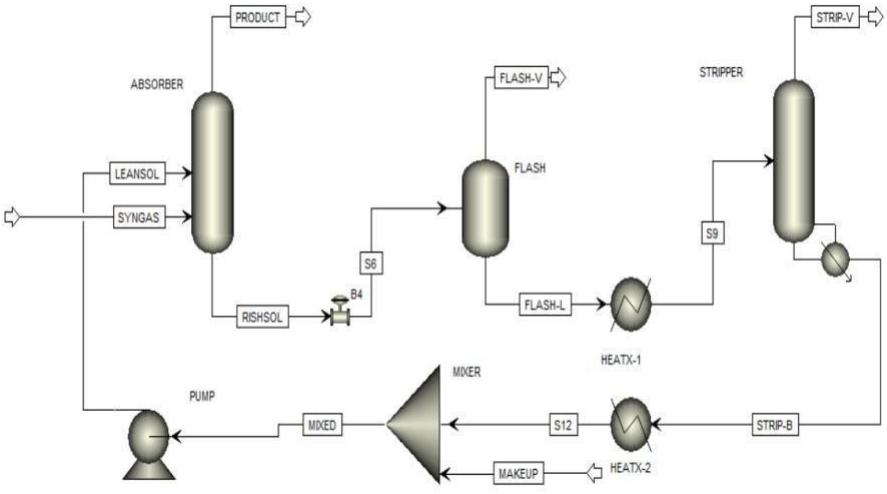

Figure 26: Model PFD for syngas separations.

In table 16 one may observe the initial molar fraction composition of the syngas feed stream, the molar fractions of the product streams from the absorber for each solvent case, and the recovery ratio of H_2 in the product stream vs feed rate, and absorber specific details. In a conventional system using DPEG the goal is to have a product stream with H_2 and CO only which is reflected by the results in table 16 [220]. However, when a DES increases in molar ratio as necessitated to reach the eutectic depression, the selectivity makeup changes. At 1:1 ratios the solvents studied were seen to behave similarly to DPEG for selectively disregarding CO and H_2. When increased in ratio and simulated in aspen the selectivity changed to selectively repulse H_2 only. This may be explained by the earlier mentioned phenomena of polarity shielding of the HBA by the added HBD's, resulting in a more favorable system for CO absorption. The singling out of H_2 can be seen to similar degrees in table 16 as all DES provide a significantly higher H_2 purity than DPEG. This effectively turns the system from two stage to single stage absorption which could be a major advantage.

Table 11: Absorber separations analysis for each studied solvent

molar fractions	Feed	Product DPEG	Product Eucalyptol (1:2)	Product 4-cyanophenol (1:3)	Product Lidocaine (1:2)
H_2	36	0.444	0.999	0.996	0.997
CO	46	0.556	0	0.003	0.003
CO_2	17	0.001	0	0.001	0
H_2S	1	0	0	0	0
Solvent	0	0	0	0	0
Solvent Feed Rate (kg/hr)	-	3000	1500	2200	2400
Absorber Pressure (bar)	-	18	11	14	10
Absorber Stage #	-	10	10	10	10
H_2 recovery	-	0.983	0.935	0.992	0.994

Table 17 contains data gathered from each of the four simulations conducted. The simulations are referenced by the HBD associated with the N4Br based DES. Each block may be found in figure25 for reference by name. It is clear that the conventional solvent DPEG requires significantly more energy than the eucalyptol and 4-cyanophenol based DES but is near to that of lidocaine. The ordering of energy requirement is directly associated with the amount of solvent flow required in the system to reach the desired product. Though the eucalyptol DES required less energy overall (616 kW) vs DPEG (902 kW), the total energy per unit of solvent is higher for DES recovery (314 kW) compared to the DPEG (293 kW). This finding is likely due to its high affinity for the solutes outlined by the COSMO-RS study. The stream tables for each simulation may be found in Appendix D.

Table 12: Energy comparison of Aspen models.

Energy Requirements (kW)	DPEG	Lidocaine	4-Cyanophenol	Eucalyptol
Pump	5	2	3	1
Flash	6	4	3	4
HeatX-1	132	22	23	28
HeatX-2	-467	-467	-379	-269
Stripper	293	398	346	314
Total (kW)	902	893	753	616

5.4. Conclusions

In total 4248 DES-absorbent ln activity datapoints were generated in the pursuit of understanding separations of H_2 and CO from CO_2 and H_2S gases in the context of syngas. This data provided insights in the form of understanding that HBA are the driving force of gas absorption among DES combinations, and that medium chain quaternary ammonium salts offer the best sensitivity between value and co-product gases in syngas. The compositional study performed revealed solvents with higher polarizability offer a sustained selectivity for CO_2 over H_2 gas with increases in HBD ratios. The increase in HBD ratios are found to be significantly important for industrial application through the viscosity study as higher amounts of HBD bring the viscosity to feasible operating values for all but N4Br and camphor. The EHS of each component showed no evidence of environmental or biological harm association maintaining that these DES are indeed “green”. The Aspen results indicate a significant decrease in overall energy demand for the DES based process when compared to the conventional physical absorbent DPEG.

Chapter 6
Conclusions

6.1. Concluding Remarks

This dissertation explores the cutting edge of DES application into GHG capture. The topics of R-32 absorption, re-parameterization of predictive software for exotic systems, and application of DES in biofuels upgrading have been thoroughly reviewed and discussed in answer to the literature gaps found and expressed in the titled section. The objectives of this study outlined in the "literature gap" section have been achieved through the chapters devoted to each goal. In place of testing a limited speciation of DES as most literature on the subject, a significant dataset was generated for each task with some databases reaching over 1000 DES in mostly novel combinations. Where most conventional organic solvents fail, the thermodynamic analysis suggests DES indeed have favorable absorptive properties for the fluorinated compound R-32. This finding suggests an alternative to cryovac distillation commonly used for these systems mainly in the form of ammonium-based DES. It has been found that DES-R32 systems produce viable thermodynamics for absorption and contain complex energy interaction structures. It has been shown that exotic

systems like DES-R134a which are not suitable for general COSMO-RS study may be modelled with good accuracy after re-parameterization.

DES have been repeatedly studied in literature in the application of biogas but neglected in scope and detail. This was remedied through an analysis of how various contaminants affect the absorption systems of DES. Here it was found that the notoriously difficult to capture siloxane contaminants disrupt the effectiveness of ChCl:U to effectively absorb GHGs. It was also found that absorption and selectivity of GHGs can be modified extensively through changing DES components. The contaminants most detrimental to GHG uptake in DES in the application of biogas were further studied for their absorption mechanisms in DES to either selectively uptake or avoid them in a separation's environment. Finally, the syngas system components were studied in the context of finding suitable DES candidates for separations and modelled PFDs were generated to promising results. These PFDs were compared to the conventional physical absorbent DPEG with very promising energy requirement comparisons.

Overall, it has been shown repeatedly in this dissertation that DES offer a banquet of tunable features which lend to application in a limitless range of tasks. Due to this, the current limitations imposed by current research in terms of scope is especially short sighted and impeding to the adoption of these novel solvents where they may be most suited. The

adoption of modern computational approaches and their betterments have made the large-scale analysis of such novel solvent species possible as methodized in this dissertation.

6.2. Future Recommendations

Future works should utilize the methods developed and outlined in this work to assist in the selection of DES candidates for any given task. It would be especially beneficial to catalogue and quantize the effect system variables of DES have on given solutes to serve as tangible guidelines for DES selections for given tasks. This may be done as an extension of the work done here by using the data generated in combination with literature and newly created data with statistical analyses. Specifically, using ANOVA and correlation matrices one may derive significant insights into how QSPR parameters and physical properties of DES components contrive systematic DES properties in the form of absorption specific attributes like kamlet-taft parameters and sigma profile distributions. Utilizing this would result in efficient and targeted approaches to determining initial DES datasets for down-selection procedures.

Though energy comparisons have been performed for Syngas type systems, it would be highly beneficial to perform life cycle assessments, energy analysis, techno-economic analyses with conventional comparisons in these applications and beyond. Furthered still through experimental validations. The nearest work would be to perform experimental analyses of mass transfer properties of DES for improved PFD analysis. Ideally the work would extend to neural networks which predict mass transfer

coefficients of DES for use in more accurate computational experiments and assessments as previously listed.

A continuing expansion of the DES database and their experimentally derived EHS attributes should be strongly considered as many properties of these solvents remain unknown. Knowledge of these aspects of DES are critical to their adoption as worker and environmental safety is of great concern to the modern engineer. Thus, any future work should consider the implications of applying these solvents and their components.

References

[1] U. Nations, “What Is Climate Change?,” United Nations. Accessed: Jul. 26, 2023. [Online]. Available: https://www.un.org/en/climatechange/what-is-climate-change

[2] S. Fawzy, A. I. Osman, J. Doran, and D. W. Rooney, “Strategies for mitigation of climate change: a review,” *Environ. Chem. Lett.*, vol. 18, no. 6, pp. 2069–2094, Nov. 2020, doi: 10.1007/s10311-020-01059-w.

[3] O. US EPA, “Basics of Climate Change.” Accessed: Jul. 27, 2023. [Online]. Available: https://www.epa.gov/climatechange-science/basics-climate-change

[4] “Climate change widespread, rapid, and intensifying – IPCC — IPCC.” Accessed: Jul. 26, 2023. [Online]. Available: https://www.ipcc.ch/2021/08/09/ar6-wg1-20210809-pr/

[5] “What is climate change? A really simple guide,” *BBC News*, Sep. 23, 2013. Accessed: Jul. 26, 2023. [Online]. Available: https://www.bbc.com/news/science-environment-24021772

[6] “What Is Climate Change?,” NASA Climate Kids. Accessed: Jul. 26, 2023. [Online]. Available: https://climatekids.nasa.gov/climate-change-meaning/

[7] “Home,” Climate Change: Vital Signs of the Planet. Accessed: Jul. 28, 2023. [Online]. Available: https://climate.nasa.gov/

[8] R. Jackson, “The Effects of Climate Change,” Climate Change: Vital Signs of the Planet. Accessed: Jul. 28, 2023. [Online]. Available: https://climate.nasa.gov/effects

[9] “The Paris Agreement | UNFCCC.” Accessed: Jul. 28, 2023. [Online]. Available: https://unfccc.int/process-and-meetings/the-paris-agreement

[10] O. US EPA, “Clean Air Act Text.” Accessed: Jul. 28, 2023. [Online]. Available: https://www.epa.gov/clean-air-act-overview/clean-air-act-text

[11] “The Montreal Protocol on Substances That Deplete the Ozone Layer - United States Department of State.” Accessed: Jul. 28, 2023. [Online]. Available: https://www.state.gov/key-topics-office-of-environmental-quality-and-transboundary-issues/the-montreal-protocol-on-substances-that-deplete-the-ozone-layer/

[12] O. US EPA, “Overview of Greenhouse Gases.” Accessed: Oct. 19, 2022. [Online]. Available: https://www.epa.gov/ghgemissions/overview-greenhouse-gases

[13] “How much carbon dioxide does the United States and the World emit each year from energy sources? | U.S. Geological Survey.” Accessed: Aug. 13, 2023. [Online]. Available: https://www.usgs.gov/faqs/how-much-carbon-dioxide-does-united-states-and-world-emit-each-year-energy-sources

[14] Review of the regulation on fluorinated greenhouse gases | Think Tank | European Parliament." Accessed: Jul. 28, 2023. [Online]. Available: Absorbents," *Energy Fuels*, vol. 30, no. 6, pp. 5052–5064, Jun. 2016, doi: 10.1021/acs.energyfuels.6b00364
[15] "Sources of Greenhouse Gas Emissions | US EPA." Accessed: Aug. 13, 2023. [Online]. Available: https://www.epa.gov/ghgemissions/sources-greenhouse-gas-emissions
[16] "An introduction to biogas and biomethane – Outlook for biogas and biomethane: Prospects for organic growth – Analysis," IEA. Accessed: Aug. 13, 2023. [Online]. Available: https://www.iea.org/reports/outlook-for-biogas-and-biomethane-prospects-for-organic-growth/an-introduction-to-biogas-and-biomethane
[17] A. Paykani, H. Chehrmonavari, A. Tsolakis, T. Alger, W. F. Northrop, and R. D. Reitz, "Synthesis gas as a fuel for internal combustion engines in transportation," *Prog. Energy Combust. Sci.*, vol. 90, p. 100995, May 2022, doi: 10.1016/j.pecs.2022.100995.
[18] "Current California GHG Emission Inventory Data | California Air Resources Board." Accessed: Sep. 10, 2023. [Online]. Available: https://ww2.arb.ca.gov/ghg-inventory-data
[19] "Fact Sheet | Biogas: Converting Waste to Energy | White Papers | EESI." Accessed: Aug. 13, 2023. [Online]. Available: https://www.eesi.org/papers/view/fact-sheet-biogasconverting-waste-to-energy
[20] Q. Zhang, J. Hu, and D.-J. Lee, "Biogas from anaerobic digestion processes: Research updates," *Renew. Energy*, vol. 98, pp. 108–119, Dec. 2016, doi: 10.1016/j.renene.2016.02.029.
[21] A. Khalid, M. Arshad, M. Anjum, T. Mahmood, and L. Dawson, "The anaerobic digestion of solid organic waste," *Waste Manag.*, vol. 31, no. 8, pp. 1737–1744, Aug. 2011, doi: 10.1016/j.wasman.2011.03.021.
[22] C. Mao, Y. Feng, X. Wang, and G. Ren, "Review on research achievements of biogas from anaerobic digestion," *Renew. Sustain. Energy Rev.*, vol. 45, pp. 540–555, May 2015, doi: 10.1016/j.rser.2015.02.032.
[23] J. B. Holm-Nielsen, T. Al Seadi, and P. Oleskowicz-Popiel, "The future of anaerobic digestion and biogas utilization," *Bioresour. Technol.*, vol. 100, no. 22, pp. 5478–5484, Nov. 2009, doi: 10.1016/j.biortech.2008.12.046.
[24] O. US EPA, "How Does Anaerobic Digestion Work?" Accessed: Sep. 10, 2023. [Online]. Available: https://www.epa.gov/agstar/how-does-anaerobic-digestion-work
[25] R. Santiago, C. Moya, and J. Palomar, "Siloxanes capture by ionic liquids: Solvent selection and process evaluation," *Chem. Eng. J.*, vol. 401, p. 126078, Dec. 2020, doi: 10.1016/j.cej.2020.126078.
[26] Y. Xu, Y. Huang, B. Wu, X. Zhang, and S. Zhang, "Biogas upgrading technologies: Energetic analysis and environmental impact assessment," *Chin. J. Chem. Eng.*, vol. 23, no. 1, pp. 247–254, Jan. 2015, doi: 10.1016/j.cjche.2014.09.048.

[27] P. García-Gutiérrez *et al.*, "Techno-Economic Feasibility of Selective CO_2 Capture Processes from Biogas Streams Using Ionic Liquids as Physical Absorbents," *Energy Fuels*, vol. 30, no. 6, pp. 5052–5064, Jun. 2016, doi: 10.1021/acs.energyfuels.6b00364.
[28] Y. Xie *et al.*, "Techno-economic evaluation of biogas upgrading using ionic liquids in comparison with industrially used technology in Scandinavian anaerobic digestion plants," *Appl. Energy*, vol. 227, pp. 742–750, Oct. 2018, doi: 10.1016/j.apenergy.2017.07.067.
[29] E. Ryckebosch, M. Drouillon, and H. Vervaeren, "Techniques for transformation of biogas to biomethane," *Biomass Bioenergy*, vol. 35, no. 5, pp. 1633–1645, May 2011, doi: 10.1016/j.biombioe.2011.02.033.
[30] E. Słupek, P. Makoś, and J. Gębicki, "Theoretical and economic evaluation of low-cost deep eutectic solvents for effective biogas upgrading to bio-methane," *Energies*, vol. 13, no. 13, 01 2020, doi: 10.3390/en13133379.
[31] T. P. Thuy Pham, C.-W. Cho, and Y.-S. Yun, "Environmental fate and toxicity of ionic liquids: A review," *Water Res.*, vol. 44, no. 2, pp. 352–372, Jan. 2010, doi: 10.1016/j.watres.2009.09.030.
[32] L. K. G. Bhatta, S. Subramanyam, M. D. Chengala, S. Olivera, and K. Venkatesh, "Progress in hydrotalcite like compounds and metal-based oxides for CO2 capture: a review," *J. Clean. Prod.*, vol. 103, pp. 171–196, Sep. 2015, doi: 10.1016/j.jclepro.2014.12.059.
[33] B. Dou *et al.*, "Solid sorbents for in-situ CO2 removal during sorption-enhanced steam reforming process: A review," *Renew. Sustain. Energy Rev.*, vol. 53, pp. 536–546, Jan. 2016, doi: 10.1016/j.rser.2015.08.068.
[34] Y. Bi, Z. Hu, X. Lin, N. Ahmad, J. Xu, and X. Xu, "Efficient CO2 capture by a novel deep eutectic solvent through facile, one-pot synthesis with low energy consumption and feasible regeneration," *Sci. Total Environ.*, vol. 705, p. 135798, Feb. 2020, doi: 10.1016/j.scitotenv.2019.135798.
[35] K. R. Siongco, R. B. Leron, and M.-H. Li, "Densities, refractive indices, and viscosities of N,N-diethylethanol ammonium chloride–glycerol or –ethylene glycol deep eutectic solvents and their aqueous solutions," *J. Chem. Thermodyn.*, vol. 65, pp. 65–72, Oct. 2013, doi: 10.1016/j.jct.2013.05.041.
[36] M. Taheri, R. Zhu, G. Yu, and Z. Lei, "Ionic liquid screening for CO2 capture and H2S removal from gases: The syngas purification case," *Chem. Eng. Sci.*, vol. 230, p. 116199, Feb. 2021, doi: 10.1016/j.ces.2020.116199.
[37] B. Ayodele, S. I. Mustapa, T. A. R. Tuan Abdullah, and S. F. Salleh, "A Mini-Review on Hydrogen-Rich Syngas Production by Thermo-Catalytic and Bioconversion of Biomass and Its Environmental Implications," *Front. Energy Res.*, vol. 7, 2019, Accessed: Jun. 13, 2023. [Online]. Available: https://www.frontiersin.org/articles/10.3389/fenrg.2019.00118
[38] D. Saebea, P. Ruengrit, A. Arpornwichanop, and Y. Patcharavorachot, "Gasification of plastic waste for synthesis gas production," *Energy Rep.*, vol. 6, pp. 202–207, Feb. 2020, doi: 10.1016/j.egyr.2019.08.043.

[39] “Syngas Production, Properties, and Its Importance | IntechOpen.” Accessed: Jun. 13, 2023. [Online]. Available: https://www.intechopen.com/chapters/69842

[40] T. Xu, X. Wang, B. Xiao, H. Zhao, and W. Liu, “Optimisation of syngas production from a novel two-step chemical looping reforming process using Fe-dolomite as oxygen carriers,” *Fuel Process. Technol.*, vol. 228, p. 107169, Apr. 2022, doi: 10.1016/j.fuproc.2022.107169.

[41] A. A. Werkneh, “Biogas impurities: environmental and health implications, removal technologies and future perspectives,” *Heliyon*, vol. 8, no. 10, p. e10929, Oct. 2022, doi: 10.1016/j.heliyon.2022.e10929.

[42] A. Rückel, J. Hannemann, C. Maierhofer, A. Fuchs, and D. Weuster-Botz, “Studies on Syngas Fermentation With Clostridium carboxidivorans in Stirred-Tank Reactors With Defined Gas Impurities,” *Front. Microbiol.*, vol. 12, 2021, Accessed: Jun. 13, 2023. [Online]. Available: https://www.frontiersin.org/articles/10.3389/fmicb.2021.655390

[43] “5.1. Gasification Introduction,” netl.doe.gov. Accessed: Sep. 10, 2023. [Online]. Available: https://netl.doe.gov/research/Coal/energy-systems/gasification/gasifipedia/intro-to-gasification

[44] “Hydrogen Fueling Overview | Clean Vehicle Rebate Project.” Accessed: Aug. 10, 2023. [Online]. Available: https://cleanvehiclerebate.org/en/ev/technology/fueling/hydrogen

[45] “Executive summary – Global Hydrogen Review 2021 – Analysis,” IEA. Accessed: Aug. 10, 2023. [Online]. Available: https://www.iea.org/reports/global-hydrogen-review-2021/executive-summary

[46] M. Nordio, S. A. Wassie, M. Van Sint Annaland, D. A. Pacheco Tanaka, J. L. Viviente Sole, and F. Gallucci, “Techno-economic evaluation on a hybrid technology for low hydrogen concentration separation and purification from natural gas grid,” *Int. J. Hydrog. Energy*, vol. 46, no. 45, pp. 23417–23435, Jul. 2021, doi: 10.1016/j.ijhydene.2020.05.009.

[47] “Gas Prices Explained.” Accessed: Aug. 10, 2023. [Online]. Available: https://www.api.org/oil-and-natural-gas/energy-primers/gas-prices-explained

[48] M. Ozkan, R. Custelcean, and Guest Editors, “The status and prospects of materials for carbon capture technologies,” *MRS Bull.*, vol. 47, no. 4, pp. 390–394, Apr. 2022, doi: 10.1557/s43577-022-00364-9.

[49] “CO2 Capture in the Sustainable Wheat-Derived Activated Microporous Carbon Compartments | Scientific Reports.” Accessed: Aug. 17, 2023. [Online]. Available: https://www.nature.com/articles/srep34590

[50] C. A. Trickett, A. Helal, B. A. Al-Maythalony, Z. H. Yamani, K. E. Cordova, and O. M. Yaghi, “The chemistry of metal–organic frameworks for CO2 capture, regeneration and conversion,” *Nat. Rev. Mater.*, vol. 2, no. 8, Art. no. 8, Jul. 2017, doi: 10.1038/natrevmats.2017.45.

[51] F. R. H. Abdeen, M. Mel, M. S. Jami, S. I. Ihsan, and A. F. Ismail, “A review of chemical absorption of carbon dioxide for biogas upgrading,” *Chin. J. Chem. Eng.*, vol. 24, no. 6, pp. 693–702, Jun. 2016, doi: 10.1016/j.cjche.2016.05.006.

[52] S. Kammerer, I. Borho, J. Jung, and M. S. Schmidt, “Review: CO2 capturing methods of the last two decades,” *Int. J. Environ. Sci. Technol.*, vol. 20, no. 7, pp. 8087–8104, Jul. 2023, doi: 10.1007/s13762-022-04680-0.

[53] B. Aghel, S. Behaein, S. Wongwises, and M. S. Shadloo, “A review of recent progress in biogas upgrading: With emphasis on carbon capture,” *Biomass Bioenergy*, vol. 160, p. 106422, May 2022, doi: 10.1016/j.biombioe.2022.106422.

[54] A. I. Papadopoulos *et al.*, “Computer-aided molecular design and selection of CO 2 capture solvents based on thermodynamics, reactivity and sustainability,” *Mol. Syst. Des. Eng.*, vol. 1, no. 3, pp. 313–334, 2016, doi: 10.1039/C6ME00049E.

[55] T. Quaid and M. T. Reza, “Carbon Capture from Biogas by Deep Eutectic Solvents: A COSMO Study to Evaluate the Effect of Impurities on Solubility and Selectivity,” *Clean Technol.*, vol. 3, no. 2, Art. no. 2, Jun. 2021, doi: 10.3390/cleantechnol3020029.

[56] P. Cozma, C. Ghinea, I. Mămăligă, W. Wukovits, A. Friedl, and M. Gavrilescu, “Environmental Impact Assessment of High Pressure Water Scrubbing Biogas Upgrading Technology,” *CLEAN – Soil Air Water*, vol. 41, no. 9, pp. 917–927, 2013, doi: 10.1002/clen.201200303.

[57] F. Bauer, T. Persson, C. Hulteberg, and D. Tamm, “Biogas upgrading – technology overview, comparison and perspectives for the future,” *Biofuels Bioprod. Biorefining*, vol. 7, no. 5, pp. 499–511, 2013, doi: 10.1002/bbb.1423.

[58] X. Yu *et al.*, “Trends in Research and Development for CO2 Capture and Sequestration,” *ACS Omega*, vol. 8, no. 13, pp. 11643–11664, Mar. 2023, doi: 10.1021/acsomega.2c05070.

[59] C. Ma, C. Liu, X. Lu, and X. Ji, “Techno-economic analysis and performance comparison of aqueous deep eutectic solvent and other physical absorbents for biogas upgrading,” *Appl. Energy*, vol. 225, pp. 437–447, Sep. 2018, doi: 10.1016/j.apenergy.2018.04.112.

[60] “Introduction: Ionic Liquids,” *Chem. Rev.*, vol. 117, no. 10, pp. 6633–6635, May 2017, doi: 10.1021/acs.chemrev.7b00246.

[61] M. Aghaie, N. Rezaei, and S. Zendehboudi, “A systematic review on CO2 capture with ionic liquids: Current status and future prospects,” *Renew. Sustain. Energy Rev.*, vol. 96, pp. 502–525, Nov. 2018, doi: 10.1016/j.rser.2018.07.004.

[62] K. Ghandi, “A Review of Ionic Liquids, Their Limits and Applications,” *Green Sustain. Chem.*, vol. 2014, Jan. 2014, doi: 10.4236/gsc.2014.41008.

[63] M. Perumal and D. Jayaraman, “Amine-Ionic Liquid Blends in CO2 Capture Process for Sustainable Energy and Environment,” *Energy Environ.*, vol. 34, no. 3, pp. 517–532, May 2023, doi: 10.1177/0958305X211070782.

[64] B. Zacchello, E. Oko, M. Wang, and A. Fethi, “Process simulation and analysis of carbon capture with an aqueous mixture of ionic liquid and monoethanolamine solvent,” *Int. J. Coal Sci. Technol.*, vol. 4, no. 1, pp. 25–32, Mar. 2017, doi: 10.1007/s40789-016-0150-1.

[65] Y. Huang, X. Zhang, X. Zhang, H. Dong, and S. Zhang, “Thermodynamic Modeling and Assessment of Ionic Liquid-Based CO2 Capture Processes,” *Ind. Eng. Chem. Res.*, vol. 53, no. 29, pp. 11805–11817, Jul. 2014, doi: 10.1021/ie501538e.

[66] S. K. Shukla, S. G. Khokarale, T. Q. Bui, and J.-P. T. Mikkola, “Ionic Liquids: Potential Materials for Carbon Dioxide Capture and Utilization,” *Front. Mater.*, vol. 6, 2019, Accessed: Aug. 15, 2023. [Online]. Available: https://www.frontiersin.org/articles/10.3389/fmats.2019.00042

[67] W. Faisal Elmobarak, F. Almomani, M. Tawalbeh, A. Al-Othman, R. Martis, and K. Rasool, “Current status of CO2 capture with ionic liquids: Development and progress,” *Fuel*, vol. 344, p. 128102, Jul. 2023, doi: 10.1016/j.fuel.2023.128102.

[68] R. Svigelj, N. Dossi, C. Grazioli, and R. Toniolo, “Deep Eutectic Solvents (DESs) and Their Application in Biosensor Development,” *Sensors*, vol. 21, no. 13, p. 4263, Jun. 2021, doi: 10.3390/s21134263.

[69] B. B. Hansen *et al.*, “Deep Eutectic Solvents: A Review of Fundamentals and Applications,” *Chem. Rev.*, vol. 121, no. 3, pp. 1232–1285, Feb. 2021, doi: 10.1021/acs.chemrev.0c00385.

[70] A. P. Abbott, G. Capper, D. L. Davies, R. K. Rasheed, and V. Tambyrajah, “Novel solvent properties of choline chloride/urea mixtures,” *Chem. Commun.*, no. 1, pp. 70–71, Jan. 2003, doi: 10.1039/B210714G.

[71] E. L. Smith, A. P. Abbott, and K. S. Ryder, “Deep Eutectic Solvents (DESs) and Their Applications,” *Chem. Rev.*, vol. 114, no. 21, pp. 11060–11082, Nov. 2014, doi: 10.1021/cr300162p.

[72] “Tunable and functional deep eutectic solvents for lignocellulose valorization | Nature Communications.” Accessed: Oct. 19, 2022. [Online]. Available: https://www.nature.com/articles/s41467-021-25117-1

[73] P. Makoś-Chełstowska, M. Kaykhaii, J. Płotka-Wasylka, and M. de la Guardia, “Magnetic deep eutectic solvents – Fundamentals and applications,” *J. Mol. Liq.*, vol. 365, p. 120158, Nov. 2022, doi: 10.1016/j.molliq.2022.120158.

[74] A. R. Zarei, M. Nedaei, and S. A. Ghorbanian, “Ferrofluid of magnetic clay and menthol based deep eutectic solvent: Application in directly suspended droplet microextraction for enrichment of some emerging contaminant explosives in water and soil samples,” *J. Chromatogr. A*, vol. 1553, pp. 32–42, Jun. 2018, doi: 10.1016/j.chroma.2018.04.023.

[75] D. J. G. P. van Osch, C. H. J. T. Dietz, S. E. E. Warrag, and M. C. Kroon, “The Curious Case of Hydrophobic Deep Eutectic Solvents: A Story on the Discovery, Design, and Applications,” *ACS Sustain. Chem. Eng.*, vol. 8, no. 29, pp. 10591–10612, Jul. 2020, doi: 10.1021/acssuschemeng.0c00559.

[76] T. Quaid and T. Reza, “COSMO-RS predictive screening of type 5 hydrophobic deep eutectic solvents for selective platform chemicals absorption,” *J. Mol. Liq.*, vol. 382, p. 121918, Jul. 2023, doi: 10.1016/j.molliq.2023.121918.

[77] S. Khandelwal, Y. K. Tailor, and M. Kumar, “Deep eutectic solvents (DESs) as eco-friendly and sustainable solvent/catalyst systems in organic transformations,” *J. Mol. Liq.*, vol. 215, pp. 345–386, Mar. 2016, doi: 10.1016/j.molliq.2015.12.015.

[78] A. K. Halder and M. N. D. S. Cordeiro, “Probing the Environmental Toxicity of Deep Eutectic Solvents and Their Components: An In Silico Modeling Approach,” *ACS Sustain. Chem. Eng.*, vol. 7, no. 12, pp. 10649–10660, Jun. 2019, doi: 10.1021/acssuschemeng.9b01306.

[79] A. Shishov, A. Bulatov, M. Locatelli, S. Carradori, and V. Andruch, “Application of deep eutectic solvents in analytical chemistry. A review,” *Microchem. J.*, vol. 135, pp. 33–38, Nov. 2017, doi: 10.1016/j.microc.2017.07.015.

[80] P. Kalhor and K. Ghandi, “Deep Eutectic Solvents for Pretreatment, Extraction, and Catalysis of Biomass and Food Waste,” *Molecules*, vol. 24, no. 22, Art. no. 22, Jan. 2019, doi: 10.3390/molecules24224012.

[81] Y. Nahar and S. C. Thickett, “Greener, Faster, Stronger: The Benefits of Deep Eutectic Solvents in Polymer and Materials Science,” *Polymers*, vol. 13, no. 3, Art. no. 3, Jan. 2021, doi: 10.3390/polym13030447.

[82] S. P. Ijardar, V. Singh, and R. L. Gardas, “Revisiting the Physicochemical Properties and Applications of Deep Eutectic Solvents,” *Molecules*, vol. 27, no. 4, Art. no. 4, Jan. 2022, doi: 10.3390/molecules27041368.

[83] I. Cichowska-Kopczyńska, B. Nowosielski, and D. Warmińska, “Deep Eutectic Solvents: Properties and Applications in CO2 Separation,” *Molecules*, vol. 28, no. 14, Art. no. 14, Jan. 2023, doi: 10.3390/molecules28145293.

[84] H. Bowen *et al.*, “Application of deep eutectic solvents in protein extraction and purification,” *Front. Chem.*, vol. 10, 2022, Accessed: Aug. 13, 2023. [Online]. Available: https://www.frontiersin.org/articles/10.3389/fchem.2022.912411

[85] A. Paiva, R. Craveiro, I. Aroso, M. Martins, R. L. Reis, and A. R. C. Duarte, “Natural Deep Eutectic Solvents – Solvents for the 21st Century,” *ACS Sustain. Chem. Eng.*, vol. 2, no. 5, pp. 1063–1071, May 2014, doi: 10.1021/sc500096j.

[86] Y. Liu *et al.*, “Ionic liquids/deep eutectic solvents for CO2 capture: Reviewing and evaluating,” *Green Energy Environ.*, vol. 6, no. 3, pp. 314–328, Jun. 2021, doi: 10.1016/j.gee.2020.11.024.

[87] P. J. Castro *et al.*, “Absorption of Fluorinated Greenhouse Gases in Deep Eutectic Solvents,” *Ind. Eng. Chem. Res.*, vol. 59, no. 29, pp. 13246–13259, Jul. 2020, doi: 10.1021/acs.iecr.0c01893.

[88] Y. Gu, Y. Hou, S. Ren, Y. Sun, and W. Wu, “Hydrophobic Functional Deep Eutectic Solvents Used for Efficient and Reversible Capture of CO2,” *ACS Omega*, vol. 5, no. 12, pp. 6809–6816, Mar. 2020, doi: 10.1021/acsomega.

[89] X.-J. Hou, L.-Y. Yu, Y.-X. Wang, K.-J. Wu, and C.-H. He, "Comprehensive Prediction of Densities for Deep Eutectic Solvents: A New Bonding-Group Interaction Contribution Scheme," *Ind. Eng. Chem. Res.*, vol. 60, no. 35, pp. 13127–13139, Sep. 2021, doi: 10.1021/acs.iecr.1c02260.
[90] T. Lemaoui *et al.*, "Predicting the Surface Tension of Deep Eutectic Solvents Using Artificial Neural Networks," *ACS Omega*, vol. 7, no. 36, pp. 32194–32207, Sep. 2022, doi: 10.1021/acsomega.2c03458.
[91] T. Lemaoui *et al.*, "Prediction of Electrical Conductivity of Deep Eutectic Solvents Using COSMO-RS Sigma Profiles as Molecular Descriptors: A Quantitative Structure–Property Relationship Study," *Ind. Eng. Chem. Res.*, vol. 59, no. 29, pp. 13343–13354, Jul. 2020, doi: 10.1021/acs.iecr.0c02542.
[92] T. Lemaoui *et al.*, "Predicting the density and viscosity of hydrophobic eutectic solvents: towards the development of sustainable solvents," *Green Chem.*, vol. 22, no. 23, pp. 8511–8530, Dec. 2020, doi: 10.1039/D0GC03077E.
[93] X. Kang, C. Liu, S. Zeng, Z. Zhao, J. Qian, and Y. Zhao, "Prediction of Henry's law constant of CO2 in ionic liquids based on SEP and Sσ-profile molecular descriptors," *J. Mol. Liq.*, vol. 262, pp. 139–147, Jul. 2018, doi: 10.1016/j.molliq.2018.04.026.
[94] N. Nkosi, K. Tumba, and S. Ramsuroop, "Activity coefficients at infinite dilution of various organic solutes in the deep eutectic solvent (tetramethylammonium chloride + 1,6 hexanediol in the 1:1 molar ratio)," *South Afr. J. Chem. Eng.*, vol. 27, pp. 7–15, Jan. 2019, doi: 10.1016/j.sajce.2018.11.003.
[95] R. Haghbakhsh, S. Raeissi, and A. R. C. Duarte, "Group contribution and atomic contribution models for the prediction of various physical properties of deep eutectic solvents," *Sci. Rep.*, vol. 11, no. 1, Art. no. 1, Mar. 2021, doi: 10.1038/s41598-021-85824-z.
[96] T. Quaid and T. Reza, "COSMO prediction of siloxane compounds absorption on type 3 and type 5 deep eutectic solvents," *Chem. Eng. J. Adv.*, vol. 14, p. 100489, May 2023, doi: 10.1016/j.ceja.2023.100489.
[97] A. Boublia *et al.*, "Molecular-based artificial neural network for predicting the electrical conductivity of deep eutectic solvents," *J. Mol. Liq.*, vol. 366, p. 120225, Nov. 2022, doi: 10.1016/j.molliq.2022.120225.
[98] M. Mohan, O. Demerdash, B. A. Simmons, J. C. Smith, M. K. Kidder, and S. Singh, "Accurate prediction of carbon dioxide capture by deep eutectic solvents using quantum chemistry and a neural network," *Green Chem.*, vol. 25, no. 9, pp. 3475–3492, 2023, doi: 10.1039/D2GC04425K.
[99] L.-Y. Yu, G.-P. Ren, X.-J. Hou, K.-J. Wu, and Y. He, "Transition State Theory-Inspired Neural Network for Estimating the Viscosity of Deep Eutectic Solvents," *ACS Cent. Sci.*, vol. 8, no. 7, pp. 983–995, Jul. 2022, doi: 10.1021/acscentsci.2c00157.
[100] S. Linke, K. McBride, and K. Sundmacher, "Systematic Green Solvent Selection for the Hydroformylation of Long-Chain Alkenes," *ACS Sustain. Chem Eng.*, vol. 8, no. 29, pp. 10795–10811, Jul. 2020, doi: 10.1021/acssuschemeng.0c02611.

[101] ncoze, “SEPAWA Innovation Award,” Dassault Systèmes blog. Accessed: Aug. 16, 2023. [Online]. Available: https://blog.3ds.com/brands/biovia/sepawa-innovation-award/
[102] J. E. Sosa *et al.*, “Adsorption of fluorinated greenhouse gases on activated carbons: evaluation of their potential for gas separation,” *J. Chem. Technol. Biotechnol.*, vol. 95, no. 7, pp. 1892–1905, 2020, doi: 10.1002/jctb.6371.
[103] C. Moya, D. Hospital-Benito, R. Santiago, J. Lemus, and J. Palomar, “Prediction of CO2 chemical absorption isotherms for ionic liquid design by DFT/COSMO-RS calculations,” *Chem. Eng. J. Adv.*, vol. 4, p. 100038, Dec. 2020, doi: 10.1016/j.ceja.2020.100038.
[104] N. Islam, H. Warsi Khan, A. A. Gari, M. Yusuf, and K. Irshad, “Screening of ionic liquids as sustainable greener solvents for the capture of greenhouse gases using COSMO-RS approach: Computational study,” *Fuel*, vol. 330, p. 125540, Dec. 2022, doi: 10.1016/j.fuel.2022.125540.
[105] O. US EPA, “Fluorinated Greenhouse Gas Emissions and Supplies Reported to the GHGRP.” Accessed: Oct. 09, 2022. [Online]. Available: https://www.epa.gov/ghgreporting/fluorinated-greenhouse-gas-emissions-and-supplies-reported-ghgrp
[106] “Fluorocarbon Refrigerants and their Syntheses: Past to Present | Chemical Reviews.” Accessed: Oct. 09, 2022. [Online]. Available: https://pubs.acs.org/doi/full/10.1021/acs.chemrev.9b00719?casa_token=as5gGhmVI0YAAAAA%3Ae_Dt0YfBX4Gv-mTRctdDnlrXpwewaRvD _ 7u6Z2nhiAf1SFXr8MGxNKO3SqYe5fcSbrkcX2QZv6b12uK
[107] M. O. McLinden and M. L. Huber, “(R)Evolution of Refrigerants,” *J. Chem. Eng. Data*, vol. 65, no. 9, pp. 4176–4193, Sep. 2020, doi: 10.1021/acs.jced.0c00338.
[108] O. US EPA, “Ozone-Depleting Substances.” Accessed: Dec. 02, 2022. [Online]. Available: https://www.epa.gov/ozone-layer-protection/ozone-depleting-substances
[109] O. US EPA, “Overview of Greenhouse Gases.” Accessed: Oct. 09, 2022. [Online]. Available: https://www.epa.gov/ghgemissions/overview-greenhouse-gases
[110] “What Are Hydrofluorocarbons? - EIA US.” Accessed: Oct. 09, 2022. [Online]. Available: https://us.eia.org/campaigns/climate/what-are-hydrofluorocarbons/
[111] “Refrigerant R32 as lower GWP working fluid in residential air conditioning systems in Europe and the USA - ScienceDirect.” Accessed: Dec. 02, 2022. [Online]. Available: https://www.sciencedirect.com/science/article/abs/pii/S1364032117308559
[112] F. Pardo, G. Zarca, and A. Urtiaga, “Separation of Refrigerant Gas Mixtures Containing R32, R134a, and R1234yf through Poly(ether-block-amide) Membranes,” *ACS Sustain. Chem. Eng.*, vol. 8, no. 6, pp. 2548–2556, Feb. 2020, doi: 10.1021/acssuschemeng.9b07195.

[113] X. Liu, N. Lv, C. Su, and M. He, “Solubilities of R32, R245fa, R227ea and R236fa in a phosphonium-based ionic liquid,” *J. Mol. Liq.*, vol. 218, pp. 525–530, Jun. 2016, doi: 10.1016/j.molliq.2016.02.041.
[114] X. Liu, N. Lv, C. Su, and M. He, “Solubilities of R32, R245fa, R227ea and R236fa in a phosphonium-based ionic liquid,” *J. Mol. Liq.*, vol. 218, pp. 525–530, Jun. 2016, doi: 10.1016/j.molliq.2016.02.041.
[115] S. Asensio-Delgado, M. Viar, F. Pardo, G. Zarca, and A. Urtiaga, “Gas solubility and diffusivity of hydrofluorocarbons and hydrofluoroolefins in cyanide-based ionic liquids for the separation of refrigerant mixtures,” *Fluid Phase Equilibria*, vol. 549, p. 113210, Dec. 2021, doi: 10.1016/j.fluid.2021.113210.
[116] S. Asensio-Delgado, F. Pardo, G. Zarca, and A. Urtiaga, “Absorption separation of fluorinated refrigerant gases with ionic liquids: Equilibrium, mass transport, and process design,” *Sep. Purif. Technol.*, vol. 276, p. 119363, Dec. 2021, doi: 10.1016/j.seppur.2021.119363.
[117] M. A. R. Martins, S. P. Pinho, and J. A. P. Coutinho, “Insights into the Nature of Eutectic and Deep Eutectic Mixtures,” *J. Solut. Chem.*, vol. 48, no. 7, pp. 962–982, Jul. 2019, doi: 10.1007/s10953-018-0793-1.
[118] “SciELO - Brazil - Use of Natural Deep Eutectic Solvents for Polymerization and Polymer Reactions Use of Natural Deep Eutectic Solvents for Polymerization and Polymer Reactions.” Accessed: Aug. 08, 2022. [Online]. Available: https://www.scielo.br/j/jbchs/a/fSYnzjCc6Tg5b5KvY3F7NMJ/?lang=en
[119] H. Ren, S. Lian, X. Wang, Y. Zhang, and E. Duan, “Exploiting the hydrophilic role of natural deep eutectic solvents for greening CO2 capture,” *J. Clean. Prod.*, vol. 193, pp. 802–810, Aug. 2018, doi: 10.1016/j.jclepro.2018.05.051.
[120] E. Słupek, P. Makoś-Chełstowska, and J. Gębicki, “Removal of Siloxanes from Model Biogas by Means of Deep Eutectic Solvents in Absorption Process,” *Materials*, vol. 14, no. 2, Jan. 2021, doi: 10.3390/ma14020241.
[121] O. Alioui, Y. Benguerba, and I. M. Alnashef, “Investigation of the CO2-solubility in deep eutectic solvents using COSMO-RS and molecular dynamics methods,” *J. Mol. Liq.*, vol. 307, p. 113005, Jun. 2020, doi: 10.1016/j.molliq.2020.113005.
[122] P. Arenas, I. Suárez, and B. Coto, “Combination of molecular dynamics simulation, COSMO-RS, and experimental study to understand extraction of naphthenic acid,” *Sep. Purif. Technol.*, vol. 280, p. 119810, Jan. 2022, doi: 10.1016/j.seppur.2021.119810.
[123] F. Eckert and A. Klamt, “Fast solvent screening via quantum chemistry: COSMO-RS approach,” *AIChE J.*, vol. 48, no. 2, pp. 369–385, 2002, doi: 10.1002/aic.690480220.
[124] A. Klamt, *COSMO-RS From Quantum Chemistry to Fluid Phase Thermodynamics and Drug Design*. Elsevier B.V., 2005. [Online]. Available: https://www.elsevier.com/books/cosmo-rs/klamt/978-0-444-51994-8

[125] J. L. Anderson and K. D. Clark, “Ionic liquids as tunable materials in (bio)analytical chemistry,” *Anal. Bioanal. Chem.*, vol. 410, no. 19, pp. 4565–4566, Jul. 2018, doi: 10.1007/s00216-018-1125-4.
[126] T. L. Greaves, A. Weerawardena, C. Fong, I. Krodkiewska, and C. J. Drummond, “Protic Ionic Liquids: Solvents with Tunable Phase Behavior and Physicochemical Properties,” *J. Phys. Chem. B*, vol. 110, no. 45, pp. 22479–22487, Nov. 2006, doi: 10.1021/jp0634048.
[127] G. Gonfa, M. A. Bustam, A. M. Sharif, N. Mohamad, and S. Ullah, “Tuning ionic liquids for natural gas dehydration using COSMO-RS methodology,” *J. Nat. Gas Sci. Eng.*, vol. 27, pp. 1141–1148, Nov. 2015, doi: 10.1016/j.jngse.2015.09.062.
[128] T. Jeliński and P. Cysewski, “Application of a computational model of natural deep eutectic solvents utilizing the COSMO-RS approach for screening of solvents with high solubility of rutin,” *J. Mol. Model.*, vol. 24, no. 7, 01 2018, doi: 10.1007/s00894-018-3700-1.
[129] A. Klamt, *From Quantum Chemistry to Fluid Phase Thermodynamics and Drug Design.* Elsevier. [Online]. Available: vbk://Nv6N2OsaRD8E81A_v2rDwsUUDzfOeb9-Zta_8LcUe_0
[130] “TURBOMOLE Documentation & How To,” TURBOMOLE. Accessed: Jun. 26, 2022. [Online]. Available: https://www.turbomole.org/turbomole/turbomole-documentation/
[131] T. Quaid and M. T. Reza, “Carbon Capture from Biogas by Deep Eutectic Solvents: A COSMO Study to Evaluate the Effect of Impurities on Solubility and Selectivity,” *Clean Technol.*, vol. 3, no. 2, Art. no. 2, Jun. 2021, doi: 10.3390/cleantechnol3020029.
[132] K. Wichmann, “COSMOthermX User Guide,” p. 131.
[133] “BIOVIA COSMOconf, BIOVIA COSMO-RS - Dassault Systèmes®.” Accessed: Aug. 21, 2022. [Online]. Available: https://www.3ds.com/products-services/biovia/products/molecular-modeling-simulation/solvation-chemistry/biovia-cosmoconf/
[134] E. Zurob *et al.*, “Design of natural deep eutectic solvents for the ultrasound-assisted extraction of hydroxytyrosol from olive leaves supported by COSMO-RS,” *Sep. Purif. Technol.*, vol. 248, p. 117054, Oct. 2020, doi: 10.1016/j.seppur.2020.117054.
[135] P. Makoś-Chełstowska, E. Słupek, A. Kramarz, and J. Gębicki, “New Carvone-Based Deep Eutectic Solvents for Siloxanes Capture from Biogas,” *Int. J. Mol. Sci.*, vol. 22, no. 17, Art. no. 17, Jan. 2021, doi: 10.3390/ijms22179551.
[136] P. Villarim, E. Genty, J. Zemmouri, and S. Fourmentin, “Deep eutectic solvents and conventional solvents as VOC absorbents for biogas upgrading: A comparative study,” *Chem. Eng. J.*, vol. 446, p. 136875, Oct. 2022, doi: 10.1016/j.cej.2022.136875.
[137] J. Cheng, H. Qin, H. Cheng, Z. Song, Z. Qi, and K. Sundmacher, “Rational Screening of Deep Eutectic Solvents for the Direct Extraction of α-Tocopherol from Deodorized Distillates,” *ACS Sustain. Chem. Eng.*, vol. 10, no. 25, pp. 8216–8227, Jun. 2022, doi: 10.1021/acssuschemeng.2c01992. K.

[138] A. Kurnia and J. A. P. Coutinho, “Overview of the Excess Enthalpies of the Binary Mixtures Composed of Molecular Solvents and Ionic Liquids and Their Modeling Using COSMO-RS,” *Ind. Eng. Chem. Res.*, vol. 52, no. 38, pp. 13862–13874, Sep. 2013, doi: 10.1021/ie4017682.
[139] K. Paduszyński and M. Królikowska, “Interactions between molecular solutes and task-specific ionic liquid: Measurements of infinite dilution activity coefficients and modeling,” *J. Mol. Liq.*, vol. 221, pp. 235–244, Sep. 2016, doi: 10.1016/j.molliq.2016.05.063.
[140] Y. Chu and X. He, “MoDoop: An Automated Computational Approach for COSMO-RS Prediction of Biopolymer Solubilities in Ionic Liquids,” *ACS Omega*, vol. 4, no. 1, pp. 2337–2343, Jan. 2019, doi: 10.1021/acsomega.8b03255.
[141] A. Klamt and F. Eckert, “COSMO-RS: a novel and efficient method for the a priori prediction of thermophysical data of liquids,” *Fluid Phase Equilibria*, vol. 172, no. 1, pp. 43–72, Jul. 2000, doi: 10.1016/S0378-3812(00)00357-5.
[142] “Sigma Moments — COSMO-RS 2022.1 documentation.” Accessed: Aug. 23, 2022. [Online]. Available: https://www.scm.com/doc/COSMO-RS/advanced_scripts/Sigma_moments.html
[143] K. McGaughy and M. T. Reza, “Liquid–Liquid Extraction of Furfural from Water by Hydrophobic Deep Eutectic Solvents: Improvement of Density Function Theory Modeling with Experimental Validations,” *ACS Omega*, vol. 5, no. 35, pp. 22305–22313, Sep. 2020, doi: 10.1021/acsomega.0c02665.
[144] “VEGA HUB – Virtual models for property Evaluation of chemicals within a Global Architecture.” Accessed: Dec. 02, 2022. [Online]. Available: https://www.vegahub.eu/
[145] “SDS Search.” Accessed: Jun. 14, 2023. [Online]. Available: https://www.fishersci.com/us/en/catalog/search/sdshome.html
[146] J. Esteban, A. J. Vorholt, and W. Leitner, “An overview of the biphasic dehydration of sugars to 5-hydroxymethylfurfural and furfural: a rational selection of solvents using COSMO-RS and selection guides,” *Green Chem.*, vol. 22, no. 7, pp. 2097–2128, 2020, doi: 10.1039/C9GC04208C.
[147] “Airgas.” Accessed: Dec. 23, 2022. [Online]. Available: https://www.airgas.com/search/nonproduct?text=R32&tabId=sds
[148] Q. Zhang, J. Hu, and D.-J. Lee, “Biogas from anaerobic digestion processes: Research updates,” *Renew. Energy*, vol. 98, pp. 108–119, Dec. 2016, doi: 10.1016/j.renene.2016.02.029.
[149] P. García-Gutiérrez *et al.*, “Techno-Economic Feasibility of Selective CO2 Capture Processes from Biogas Streams Using Ionic Liquids as Physical Absorbents,” *Energy Fuels*, vol. 30, no. 6, pp. 5052–5064, Jun. 2016, doi: 10.1021/acs.energyfuels.6b00364.
[150] S. Sarmad, D. Nikjoo, and J.-P. Mikkola, “Amine functionalized deep eutectic solvent for CO2 capture: Measurements and modeling,” *J. Mol. Liq.*, vol. 309, p. 113159, Jul. 2020, doi: 10.1016/j.molliq.2020.113159.

[151] H. Ghaedi, M. Ayoub, S. Sufian, A. M. Shariff, S. M. Hailegiorgis, and S. N. Khan, “CO2 capture with the help of Phosphonium-based deep eutectic solvents,” *J. Mol. Liq.*, vol. 243, pp. 564–571, Oct. 2017, doi: 10.1016/j.molliq.2017.08.046.

[152] R. B. Leron and M.-H. Li, “Solubility of carbon dioxide in a choline chloride–ethylene glycol based deep eutectic solvent,” *Thermochim. Acta*, vol. 551, pp. 14–19, Jan. 2013, doi: 10.1016/j.tca.2012.09.041.

[153] A. P. Abbott, G. Capper, D. L. Davies, R. K. Rasheed, and V. Tambyrajah, “Novel solvent properties of choline chloride/urea mixtures,” *Chem. Commun.*, vol. 0, no. 1, pp. 70–71, 2003, doi: 10.1039/B210714G.

[154] J. D. Figueroa, T. Fout, S. Plasynski, H. McIlvried, and R. D. Srivastava, “Advances in CO2 capture technology—The U.S. Department of Energy’s Carbon Sequestration Program,” *Int. J. Greenh. Gas Control*, vol. 2, no. 1, pp. 9–20, Jan. 2008, doi: 10.1016/S1750-5836(07)00094-1.

[155] N. Zhang, Z. Huang, H. Zhang, J. Ma, B. Jiang, and L. Zhang, “Highly Efficient and Reversible CO 2 Capture by Task-Specific Deep Eutectic Solvents,” *Ind. Eng. Chem. Res.*, vol. 58, no. 29, pp. 13321–13329, Jul. 2019, doi: 10.1021/acs.iecr.9b02041.

[156] Z. Song *et al.*, “Systematic Screening of Deep Eutectic Solvents as Sustainable Separation Media Exemplified by the CO2 Capture Process,” *ACS Sustain. Chem. Eng.*, vol. 8, no. 23, pp. 8741–8751, Jun. 2020, doi: 10.1021/acssuschemeng.0c02490.

[157] K. McGaughy and M. T. Reza, “Systems Analysis of SO2-CO2 Co-Capture from a Post-Combustion Coal-Fired Power Plant in Deep Eutectic Solvents,” *Energies*, vol. 13, no. 2, Art. no. 2, Jan. 2020, doi: 10.3390/en13020438.

[158] Y. Liu *et al.*, “Screening Deep Eutectic Solvents for CO2 Capture With COSMO-RS,” *Front. Chem.*, vol. 8, 2020, doi: 10.3389/fchem.2020.00082.

[159] “Deep Eutectic Solvents Formed between Choline Chloride and Carboxylic Acids: Versatile Alternatives to Ionic Liquids | Journal of the American Chemical Society.” Accessed: Mar. 15, 2021. [Online]. Available: https://pubs-acs-org.portal.lib.fit.edu/doi/10.1021/ja048266j

[160] “Experimental Study of the Solubility of CO2 in Novel Amine Based Deep Eutectic Solvents,” *Energy Procedia*, vol. 105, pp. 1394–1400, May 2017, doi: 10.1016/j.egypro.2017.03.519.

[161] A. Anukam, A. Mohammadi, M. Naqvi, and K. Granström, “A Review of the Chemistry of Anaerobic Digestion: Methods of Accelerating and Optimizing Process Efficiency,” *Processes*, vol. 7, no. 8, Art. no. 8, Aug. 2019, doi: 10.3390/pr7080504.

[162] M. Hagen, E. Polman, J. K. Jensen, A. Myken, O. Joensson, and A. Dahl, “Adding gas from biomass to the gas grid,” Jul. 2001, Accessed: Mar. 14, 2021. [Online]. Available: https://www.osti.gov/etdeweb/biblio/20235595

[163] M. R. Al Mamun and S. Torii, “Enhancement of Methane Concentration by Removing Contaminants from Biogas Mixtures Using Combined Method of Absorption and Adsorption,” *Int. J. Chem. Eng.*, vol. 2017, p. e7906859, Mar. 2017, doi: 10.1155/2017/7906859.

[164] P. Nyamukamba, P. Mukumba, E. S. Chikukwa, and G. Makaka, “Biogas Upgrading Approaches with Special Focus on Siloxane Removal—A Review,” *Energies*, vol. 13, no. 22, Art. no. 22, Jan. 2020, doi: 10.3390/en13226088.
[165] Y. Zhang *et al.*, “Characterization of Volatile Organic Compound (VOC) Emissions from Swine Manure Biogas Digestate Storage,” *Atmosphere*, vol. 10, no. 7, Art. no. 7, Jul. 2019, doi: 10.3390/atmos10070411.
[166] M. Shen, Y. Zhang, D. Hu, J. Fan, and G. Zeng, “A review on removal of siloxanes from biogas: with a special focus on volatile methylsiloxanes,” *Environ. Sci. Pollut. Res.*, vol. 25, no. 31, pp. 30847–30862, Nov. 2018, doi: 10.1007/s11356-018-3000-4.
[167] Y.-H. Hsu, R. B. Leron, and M.-H. Li, “Solubility of carbon dioxide in aqueous mixtures of (reline+monoethanolamine) at T=(313.2 to 353.2)K,” *J. Chem. Thermodyn.*, vol. 72, pp. 94–99, May 2014, doi: 10.1016/j.jct.2014.01.011.
[168] T. Zhekenov, N. Toksanbayev, Z. Kazakbayeva, D. Shah, and F. S. Mjalli, “Formation of type III Deep Eutectic Solvents and effect of water on their intermolecular interactions,” *Fluid Phase Equilibria*, vol. 441, pp. 43–48, Jun. 2017, doi: 10.1016/j.fluid.2017.01.022.
[169] H. Palmelund, M. P. Andersson, C. J. Asgreen, B. J. Boyd, J. Rantanen, and K. Löbmann, “Tailor-made solvents for pharmaceutical use? Experimental and computational approach for determining solubility in deep eutectic solvents (DES),” *Int. J. Pharm. X*, vol. 1, p. 100034, Dec. 2019, doi: 10.1016/j.ijpx.2019.100034.
[170] G. García, S. Aparicio, R. Ullah, and M. Atilhan, “Deep Eutectic Solvents: Physicochemical Properties and Gas Separation Applications,” *Energy Fuels*, vol. 29, no. 4, pp. 2616–2644, Apr. 2015, doi: 10.1021/ef5028873.
[171] J. Cao, M. Yang, F. Cao, J. Wang, and E. Su, “Well-Designed Hydrophobic Deep Eutectic Solvents As Green and Efficient Media for the Extraction of Artemisinin from Artemisia annua Leaves,” *ACS Sustain. Chem. Eng.*, vol. 5, no. 4, pp. 3270–3278, Apr. 2017, doi: 10.1021/acssuschemeng.6b03092.
[172] T. Jiang *et al.*, “Siloxane D4 adsorption by mesoporous aluminosilicates,” *Chem. Eng. J.*, vol. 289, pp. 356–364, Apr. 2016, doi: 10.1016/j.cej.2015.12.094.
[173] K. Starr, X. Gabarrell, G. Villalba, L. Talens, and L. Lombardi, “Life cycle assessment of biogas upgrading technologies,” *Waste Manag.*, vol. 32, no. 5, pp. 991–999, May 2012, doi: 10.1016/j.wasman.2011.12.016.
[174] Niesner J., Jecha D., and Stehlik P., “Biogas upgrading techniques: state of art review in european region,” *Chem. Eng. Trans.*, vol. 35, pp. 517–522, Sep. 2013, doi: 10.3303/CET1335086.
[175] M. Struk, I. Kushkevych, and M. Vítězová, “Biogas upgrading methods: recent advancements and emerging technologies,” *Rev. Environ. Sci. Biotechnol.*, vol. 19, no. 3, pp. 651–671, Sep. 2020, doi: 10.1007/s11157-020-09539-9.

[176] A. I. Adnan, M. Y. Ong, S. Nomanbhay, K. W. Chew, and P. L. Show, "Technologies for Biogas Upgrading to Biomethane: A Review," *Bioengineering*, vol. 6, no. 4, Art. no. 4, Dec. 2019, doi: 10.3390/bioengineering6040092.

[177] L. Zhu, G. W. Schade, and C. J. Nielsen, "Real-time monitoring of emissions from monoethanolamine-based industrial scale carbon capture facilities," *Environ. Sci. Technol.*, vol. 47, no. 24, pp. 14306–14314, Dec. 2013, doi: 10.1021/es4035045.

[178] L. Brickett, "CARBON DIOXIDE CAPTURE HANDBOOK." U.S. DEPARTMENT OF ENERGY, Aug. 2015. [Online]. Available: chrome-extension://efaidnbmnnnibpcajpcglclefindmkaj/https://www.netl.doe.gov/sites/default/files/netl-file/Carbon-Dioxide-Capture-Handbook-2015.pdf

[179] Merched Azzi, Dennys Angove, Narendra Dave, Stuart Day, Thong Do, Paul Feron, Sunil Sharma, Moetaz Attalla, Mohammad Abu Zahra, "Emissions to the Atmosphere from Amine-Based Post Combustion CO2 Capture Plant– Regulatory Aspects." OGST Journal, 2014.

[180] A. Carranza-Abaid, R. R. Wanderley, H. K. Knuutila, and J. P. Jakobsen, "Analysis and selection of optimal solvent-based technologies for biogas upgrading," *Fuel*, vol. 303, p. 121327, Nov. 2021, doi: 10.1016/j.fuel.2021.121327.

[181] R. Sadegh-Vaziri, M. Amovic, R. Ljunggren, and K. Engvall, "A Medium-Scale 50 MWfuel Biomass Gasification Based Bio-SNG Plant: A Developed Gas Cleaning Process," *Energies*, vol. 8, no. 6, Art. no. 6, Jun. 2015, doi: 10.3390/en8065287.

[182] A. P. Abbott, G. Capper, D. L. Davies, R. K. Rasheed, and V. Tambyrajah, "Novel solvent properties of choline chloride/urea mixtures," *Chem. Commun.*, no. 1, pp. 70–71, Jan. 2003, doi: 10.1039/B210714G.

[183] A. Klamt, "Conductor-like Screening Model for Real Solvents: A New Approach to the Quantitative Calculation of Solvation Phenomena," *J. Phys. Chem.*, vol. 99, no. 7, pp. 2224–2235, Feb. 1995, doi: 10.1021/j100007a062.

[184] H. Qin, Z. Song, H. Cheng, L. Deng, and Z. Qi, "Physical absorption of carbon dioxide in imidazole-PTSA based deep eutectic solvents," *J. Mol. Liq.*, vol. 326, p. 115292, Mar. 2021, doi: 10.1016/j.molliq.2021.115292.

[185] Y. Zhang, X. Ji, and X. Lu, "Choline-based deep eutectic solvents for CO2 separation: Review and thermodynamic analysis," *Renew. Sustain. Energy Rev.*, vol. 97, pp. 436–455, Dec. 2018, doi: 10.1016/j.rser.2018.08.007.

[186] M. Mohan, V. V. Goud, and T. Banerjee, "Solubility of glucose, xylose, fructose and galactose in ionic liquids: Experimental and theoretical studies using a continuum solvation model," *Fluid Phase Equilibria*, vol. 395, pp. 33–43, Jun. 2015, doi: 10.1016/j.fluid.2015.03.020.

[187] A. P. Abbott, G. Capper, D. L. Davies, H. L. Munro, R. K. Rasheed, and V. Tambyrajah, "Preparation of novel, moisture-stable, Lewis-acidic ionic liquids containing quaternary ammonium salts with functional side chains," *Chem. Commun.*, no. 19, pp. 2010–2011, Oct. 2001, doi: 10.1039/B106357J.

[188] T. El Achkar, H. Greige-Gerges, and S. Fourmentin, “Basics and properties of deep eutectic solvents: a review,” *Environ. Chem. Lett.*, vol. 19, no. 4, pp. 3397–3408, Aug. 2021, doi: 10.1007/s10311-021-01225-8.

[189] K. A. Omar and R. Sadeghi, “Physicochemical properties of deep eutectic solvents: A review,” *J. Mol. Liq.*, vol. 360, p. 119524, Aug. 2022, doi: 10.1016/j.molliq.2022.119524.

[190] Y. Dai, J. van Spronsen, G.-J. Witkamp, R. Verpoorte, and Y. H. Choi, “Natural deep eutectic solvents as new potential media for green technology,” *Anal. Chim. Acta*, vol. 766, pp. 61–68, Mar. 2013, doi: 10.1016/j.aca.2012.12.019.

[191] A. Alhadid, J. Safarov, L. Mokrushina, K. Müller, and M. Minceva, “Carbon Dioxide Solubility in Nonionic Deep Eutectic Solvents Containing Phenolic Alcohols,” *Front. Chem.*, vol. 10, 2022, Accessed: Jun. 13, 2023. [Online]. Available: https://www.frontiersin.org/articles/10.3389/fchem.2022.864663

[192] Y. Wang, S. Ren, Y. Hou, and W. Wu, “Capture of Acidic Gases from Flue Gas by Deep Eutectic Solvents,” *Processes*, vol. 9, no. 8, Art. no. 8, Aug. 2021, doi: 10.3390/pr9081268.

[193] F. P. Pelaquim, A. M. Barbosa Neto, I. A. L. Dalmolin, and M. C. da Costa, “Gas Solubility Using Deep Eutectic Solvents: Review and Analysis,” *Ind. Eng. Chem. Res.*, vol. 60, no. 24, pp. 8607–8620, Jun. 2021, doi: 10.1021/acs.iecr.1c00947.

[194] J. P. Wojeicchowski, A. M. Ferreira, D. O. Abranches, M. R. Mafra, and J. A. P. Coutinho, “Using COSMO-RS in the Design of Deep Eutectic Solvents for the Extraction of Antioxidants from Rosemary,” *ACS Sustain. Chem. Eng.*, vol. 8, no. 32, pp. 12132–12141, Aug. 2020, doi: 10.1021/acssuschemeng.0c03553.

[195] M. Panić, V. Gunjević, K. Radošević, M. C. Bubalo, K. K. Ganić, and I. R. Redovniković, “COSMOtherm as an Effective Tool for Selection of Deep Eutectic Solvents Based Ready-To-Use Extracts from Graševina Grape Pomace,” *Molecules*, vol. 26, no. 4722, p. 4722, Aug. 2021, doi: 10.3390/molecules26164722.

[196] O. Alioui, Y. Benguerba, and I. M. Alnashef, “Investigation of the CO2-solubility in deep eutectic solvents using COSMO-RS and molecular dynamics methods,” *J. Mol. Liq.*, vol. 307, p. 113005, Jun. 2020, doi: 10.1016/j.molliq.2020.113005.

[197] H. Cheng, C. Liu, J. Zhang, L. Chen, B. Zhang, and Z. Qi, “Screening deep eutectic solvents for extractive desulfurization of fuel based on COSMO-RS model,” *Chem. Eng. Process. - Process Intensif.*, vol. 125, pp. 246–252, Mar. 2018, doi: 10.1016/j.cep.2018.02.006.

[198] X. Xu, J. Range, G. Gygli, and J. Pleiss, “Analysis of Thermophysical Properties of Deep Eutectic Solvents by Data Integration,” *J. Chem. Eng. Data*, vol. 65, no. 3, pp. 1172–1179, Mar. 2020, doi: 10.1021/acs.jced.9b00555.

[199] J. Castro, J. Leaver, and S. Pang, "Simulation and Techno-Economic Assessment of Hydrogen Production from Biomass Gasification-Based Processes: A Review," *Energ. 19961073*, vol. 15, no. 22, p. 8455, Nov. 2022, doi: 10.3390/en15228455.

[200] I. L. Motta, N. T. Miranda, R. Maciel Filho, and M. R. Wolf Maciel, "Sugarcane bagasse gasification: Simulation and analysis of different operating parameters, fluidizing media, and gasifier types," *Biomass Bioenergy*, vol. 122, pp. 433–445, Mar. 2019, doi: 10.1016/j.biombioe.2019.01.051.

[201] Y. Cao, Q. Wang, J. Du, and J. Chen, "Oxygen-enriched air gasification of biomass materials for high-quality syngas production," *Energy Convers. Manag.*, vol. 199, p. 111628, Nov. 2019, doi: 10.1016/j.enconman.2019.05.054.

[202] D. K. Singh and J. V. Tirkey, "Modeling and multi-objective optimization of variable air gasification performance parameters using Syzygium cumini biomass by integrating ASPEN Plus with Response surface methodology (RSM)," *Int. J. Hydrog. Energy*, vol. 46, no. 36, pp. 18816–18831, May 2021, doi: 10.1016/j.ijhydene.2021.03.054.

[203] Q. Liu and X. Zhang, "Multiscale Screening of Deep Eutectic Solvents for Efficient Extraction of m-Cresol from Model Coal Tar," *ACS Omega*, vol. 7, no. 38, pp. 34485–34494, Sep. 2022, doi: 10.1021/acsomega.2c04234.

[204] J. N. Aldawsari, I. A. Adeyemi, A. Bessadok-Jemai, E. Ali, I. M. AlNashef, and M. K. Hadj-Kali, "Polyethylene glycol-based deep eutectic solvents as a novel agent for natural gas sweetening," *PLoS ONE*, vol. 15, no. 9, p. e0239493, Sep. 2020, doi: 10.1371/journal.pone.0239493.

[205] T. Quaid and M. T. Reza, "Mechanistic Understanding on Difluoromethane Absorption Thermodynamics on Novel Deep Eutectic Solvents by COSMO-Based Molecular Simulation," *Appl. Sci.*, vol. 13, no. 10, Art. no. 10, Jan. 2023, doi: 10.3390/app13106182.

[206] M. Mohan, J. D. Keasling, B. A. Simmons, and S. Singh, "In silico COSMO-RS predictive screening of ionic liquids for the dissolution of plastic," *Green Chem.*, vol. 24, no. 10, pp. 4140–4152, 2022, doi: 10.1039/D1GC03464B.

[207] D. J. G. P. van Osch *et al.*, "A Search for Natural Hydrophobic Deep Eutectic Solvents Based on Natural Components," *ACS Sustain. Chem. Eng.*, vol. 7, no. 3, pp. 2933–2942, Feb. 2019, doi: 10.1021/acssuschemeng.8b03520.

[208] E. O. Fetisov *et al.*, "First-Principles Molecular Dynamics Study of a Deep Eutectic Solvent: Choline Chloride/Urea and Its Mixture with Water," *J. Phys. Chem. B*, vol. 122, no. 3, pp. 1245–1254, Jan. 2018, doi: 10.1021/acs.jpcb.7b10422.

[209] H. Wang, S. Liu, Y. Zhao, J. Wang, and Z. Yu, "Insights into the Hydrogen Bond Interactions in Deep Eutectic Solvents Composed of Choline Chloride and Polyols," *ACS Sustain. Chem. Eng.*, vol. 7, no. 8, pp. 7760–7767, Apr. 2019, doi: 10.1021/acssuschemeng.8b06676.

[210] H. Cheng and Z. Qi, “Applications of deep eutectic solvents for hard-to-separate liquid systems,” *Sep. Purif. Technol.*, vol. 274, p. 119027, Nov. 2021, doi: 10.1016/j.seppur.2021.119027.
[211] E. Ali *et al.*, “Solubility of CO2 in deep eutectic solvents: Experiments and modelling using the Peng–Robinson equation of state,” *Chem. Eng. Res. Des.*, vol. 92, no. 10, pp. 1898–1906, Oct. 2014, doi: 10.1016/j.cherd.2014.02.004.
[212] A. R. R. Teles, E. V. Capela, R. S. Carmo, J. A. P. Coutinho, A. J. D. Silvestre, and M. G. Freire, “Solvatochromic parameters of deep eutectic solvents formed by ammonium-based salts and carboxylic acids,” *Fluid Phase Equilibria*, vol. 448, pp. 15–21, Sep. 2017, doi: 10.1016/j.fluid.2017.04.020.
[213] H. Wu, M. Shen, X. Chen, G. Yu, A. A. Abdeltawab, and S. M. Yakout, “New absorbents for hydrogen sulfide: Deep eutectic solvents of tetrabutylammonium bromide/carboxylic acids and choline chloride/carboxylic acids,” *Sep. Purif. Technol.*, vol. 224, pp. 281–289, Oct. 2019, doi: 10.1016/j.seppur.2019.04.082.
[214] M. Ramdin, T. W. de Loos, and T. J. H. Vlugt, “State-of-the-Art of CO2 Capture with Ionic Liquids,” *Ind. Eng. Chem. Res.*, vol. 51, no. 24, pp. 8149–8177, Jun. 2012, doi: 10.1021/ie3003705.
[215] J. Y. Shin, S. A. Yamada, and M. D. Fayer, “Dynamics of a Room Temperature Ionic Liquid in Supported Ionic Liquid Membranes vs the Bulk Liquid: 2D IR and Polarized IR Pump–Probe Experiments,” *J. Am. Chem. Soc.*, vol. 139, no. 1, pp. 311–323, Jan. 2017, doi: 10.1021/jacs.6b10695.
[216] R. Sekharan, M. Chandira, R. S.C., S. Tamilvanan, CT. Vijayakumar, and B. S. Venkateswarlu, “pH, Viscosity of Hydrophobic Based Natural Deep Eutectic Solvents and the Effect of Curcumin Solubility in it,” *Biointerface Res. Appl. Chem.*, vol. 11, no. 6, pp. 14620–14633, 2021.
[217] Amos K. Dwamena, “Recent Advances in Hydrophobic Deep Eutectic Solvents for Extraction,” *Separations*, vol. 6, no. 1, pp. 9–9, Feb. 2019, doi: 10.3390/separations6010009.
[218] R. P. Schwarzenbach, T. Egli, T. B. Hofstetter, U. von Gunten, and B. Wehrli, “Global Water Pollution and Human Health,” *Annu. Rev. Environ. Resour.*, vol. 35, no. 1, pp. 109–136, 2010, doi: 10.1146/annurev-environ-100809-125342.
[219] N. M. Stephens and E. A. Smith, “Structure of Deep Eutectic Solvents (DESs): What We Know, What We Want to Know, and Why We Need to Know It,” *Langmuir ACS J. Surf. Colloids*, vol. 38, no. 46, pp. 14017–14024, Nov. 2022, doi: 10.1021/acs.langmuir.2c02116.

[220] K. Xin, I. Roghair, F. Gallucci, and M. van Sint Annaland, “Total vapor pressure of hydrophobic deep eutectic solvents: Experiments and modelling,” *J. Mol. Liq.*, vol. 325, p. 115227, Mar. 2021, doi: 10.1016/j.molliq.2020.115227.

[221] Z. Kapetaki, P. Brandani, S. Brandani, and H. Ahn, “Process simulation of a dual-stage Selexol process for 95% carbon capture efficiency at an integrated gasification combined cycle power plant,” *Int. J. Greenh. Gas Control*, vol. 39, pp. 17–26, Aug. 2015, doi: 10.1016/j.ijggc.2015.04.015.

[222] L. F. Lepre, D. Andre, S. Denis-Quanquin, A. Gautier, A. A. H. Pádua, and M. Costa Gomes, “Ionic Liquids Can Enable the Recycling of Fluorinated Greenhouse Gases,” *ACS Sustain. Chem. Eng.*, vol. 7, no. 19, pp. 16900–16906, Oct. 2019, doi: 10.1021/acssuschemeng.9b04214.

[223] D. Jovell *et al.*, “Insight on the Solubility of R134a in Fluorinated Ionic Liquids and Deep Eutectic Solvents,” *J. Chem. Eng. Data*, vol. 65, no. 10, pp. 4956–4969, Oct. 2020, doi: 10.1021/acs.jced.0c00588.

[224] J. E. Sosa *et al.*, “Design of Ionic Liquids for Fluorinated Gas Absorption: COSMO-RS Selection and Solubility Experiments,” *Environ. Sci. Technol.*, vol. 56, no. 9, pp. 5898–5909, May 2022, doi: 10.1021/acs.est.2c00051.

[225] Amirhossein Saali, H. Sakhaeinia, and M. Shokouhi, “Modeling the Solubility of Carbon Dioxide and 1,1,1,2-Tetrafluoroethane in Ionic Liquids Using the van der Waals and Generic Redlich–Kwong Equations of State,” *Theor. Found. Chem. Eng.*, vol. 55, no. 1, pp. 129–139, Jan. 2021, doi: 10.1134/S0040579521010127.

7. Appendix A: COSMO-RS Re-Parameterization Using Global Constants

When confronted with general organic systems COSMO-RS performs well in terms of accuracy for thermodynamic predictions. This is expected as the general parameters guiding the perceived intermolecular interactions were tuned by the authors to be as generally applicable as possible through the use of a dataset that reflects common organic components. This has won the software several awards and competitions. However, when faced with a relatively exotic system like fluorinated gases, the accuracy of COSMO-RS becomes untenable for scientific studies. Thus a procedure has been developed in this dissertation which may be applied to any such exotic molecules which one wishes to examine from a thermodynamic perspective. The procedure involves re-evaluating COSMO- RS global parameters with literature values to make it's accuracy acceptable by scientific standards. This project aims at bringing the COSMO-RS method in line with applying DES and R-134a fluorinated gas systems. The base program when tested against a database of 66 points comprised of DES- R134a and IL-R134a solubility values and henry constant values respectively produced an AARD error of 193%. The test set consisting of 10 solubility values of DES-R134a experimentally derived from literature can be seen in figure 20. Where the black dotted line represents the 1:1, x:y line. If all values

were found along this line then COSMO would be considered 100% accurate in these systems.

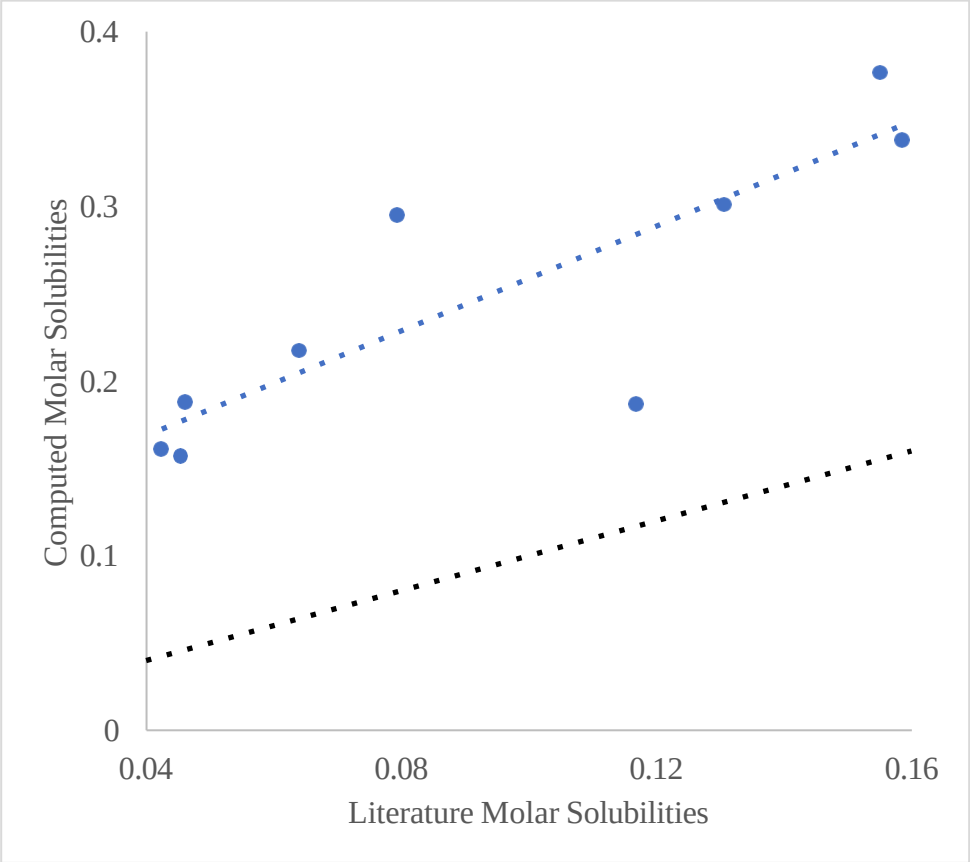

Figure 27: COSMO accuracy for R134a-DES solubilities.

Figure 27 is the same datapoints after the global re-parameterization which was computed to have and AARD of only 38%. The comparison between COSMO before and after suggests a nearly 500% increase in accuracy. The drastically reduced error is proof of the effectiveness of the parameterization procedure, and the flexibility of COSMO when

manipulated correctly. The datapoints are visibly much closer to the 1:1, x:y dashed line depicted in figure 21 than was witnessed in figure 20.

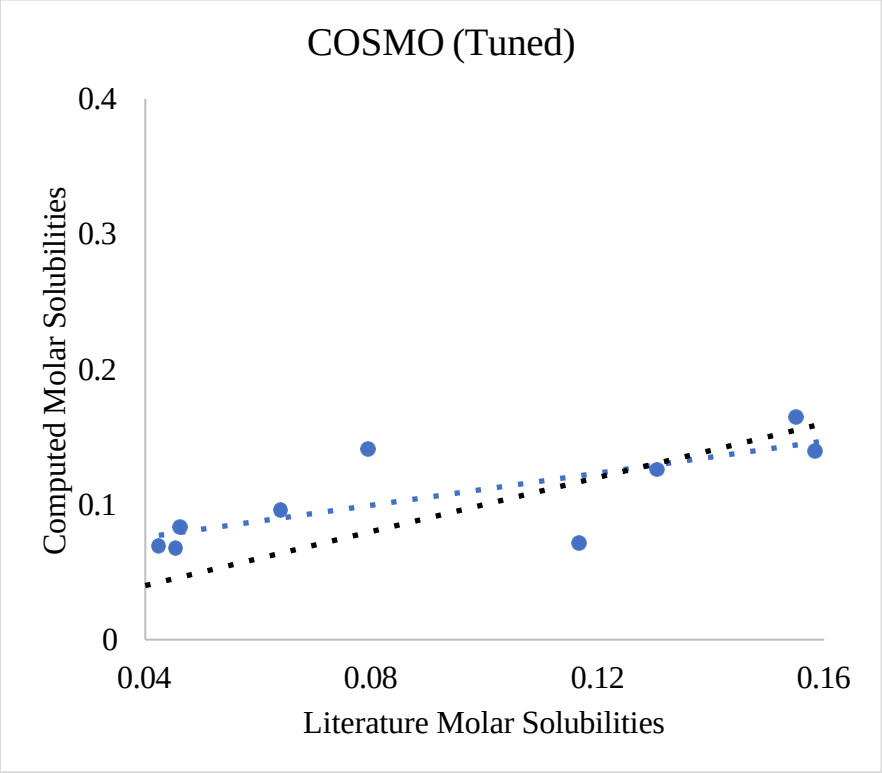

Figure 28: COSMO accuracy for R134a solubilities after re-parameterization.

The following is a description of the procedure for accomplishing this tuned COSMO. First the literature is scoured for experimental data on predictable thermodynamic property values such as solubilities, ln activity coefficients, henry constants, etc. For this project a total of 66 datapoints were found. This data set was divided into IL (56 datapoints) and DES (10 datapoints) data sets which would be used as a training and test dataset respectively. Next the global parameters were iteratively manipulated with the use of a Python script to determine the lowest objective function value

between the training set and complimentary predicted values. The objective function used in this project is available in equation A1. This form of equation was chosen as not to overtrain the system due to few significant outliers. The Python code is available in figure 22.

```python
from pathlib import Path

DEFAULT_TAB_FILE_PATH = Path.home() / 'R134a/Latest_R134a/Latest_R134a.tab'
# tab_file_path = input('Enter tab file Path (leave empty for default): ')
# if tab_file_path == '':
# tab_file_path = DEFAULT_TAB_FILE_PATH
tab_file_path = DEFAULT_TAB_FILE_PATH

# Get text from .tabTest file
tab_file = open(tab_file_path, 'r')
tab_file_text = tab_file.read()
tab_file.close()

tab_file_lines = tab_file_text.splitlines()  # Separate the text into lines

# Retrieve all r134a henry constants
h_list = []  # Create a list of all henry constants
for line in tab_file_lines:  # Find all lines with R134a in them
if 'R134a' in line:
h_str = line.split()[2]  # Grab the henry constant
h = float(h_str)  # Convert it it's number form
h_list.append(h)  # Add it to the henry constant list

# Get all literature values
lit_file = open('lit.txt', 'r')
lit_text = lit_file.read()
lit_file.close()

lit_numbers = []
for line in lit_text.splitlines():
lit_number = float(line)
lit_numbers.append(lit_number)

# Perform Objective Function
differences = []

for h, lit_number in zip(h_list, lit_numbers):

difference = abs(h - lit_number)

differences.append(difference)
objective_function = sum(differences) / len(h_list)

print('Solvent count:', len(h_list))

print('Lit Count:', len(lit_numbers))

print('Objective Function:', objective_function)
```

Figure 29: Python code

Table 18 contains the test data from the works of Lepre et al. [221] and Jovell et al. [222]. Table 18 contains the training dataset from the works of Sosa et al. [223], and Saali et al. [224]. The utilization of ionic liquid data for the training set was out of necessity due to the lack of available DES data with R134a. It is reasonable to assume that a more appropriate data set would produce even better results.

Table 18: Test Data Set.

Reference	Solvents	Literature Solubilities Molar	Cosmo (Tuned)	COSMO (Original)
[187]	[C2C1Im][TF2N]	0.117	0.072	0.187
[187]	[C8C1Im][TF2N]	0.131	0.126	0.301
[187]	[C8H4F13Im][TF2N]	0.158	0.140	0.338
[187]	[C8C1Im][BETI]	0.155	0.164	0.377
[187]	[C8H4F13Im][BETI]	0.160	0.154	0.365
[188]	N4/C4SO3/C4F9CO2H	0.079	0.141	0.295
[188]	[C2C1Im][C8F17SO3]/C4F9CO2H	0.064	0.096	0.218
[188]	[N1112(OH)][C4F9SO3]/C4F9CO2H	0.045	0.068	0.157
[188]	[N1112(OH)][C4F9CO2]/C4F9SO3H	0.042	0.069	0.161
[188]	[N1112(OH)][C8F17SO3]/C4F9CO2H	0.046	0.083	0.188

Table 19: Training data.

Reference	Solvent	Henry Constant	Temp (K)
[189]	[C2C1Im][C1CO2]	0.12	303.15
[189]	[C2C1Im][N(CF3SO2)2]	0.11	303.15
[189]	[C2C1Im][C4F9SO3]	0.10	303.15
[189]	[C2C1py][C4F9SO3]	0.10	303.15
[189]	[C2C1Im][N(C4F9SO2)2]	0.10	303.15
[189]	[C8C1Im][N(CF3SO2)2]	0.10	303.15
[189]	[C8C1Im][N(C2F5SO2)2]	0.09	303.15
[189]	[C8H4F13Im][N(CF3SO2)2]	0.09	303.15
[189]	[C8H4F13Im][N(C2F5SO2)2]	0.09	303.15
[189]	N4/C4F9SO3/C4F9CO2H	0.80	303.15
[189]	[C2C1Im][C8F17SO3]/C4F9CO2H	0.90	303.15
[189]	[C2C1Im][N(C4F9SO2)2]	1.10	303.15
[189]	[C2C1Im][C4F9SO3]	1.10	303.15
[189]	[N1112(OH)][C4F9SO3]/C4F9CO2H	1.18	303.15
[189]	[N1112(OH)][C4F9CO2]/C4F9SO3H	1.38	303.15
[189]	[N1112(OH)][C8F17SO3]/C4F9CO2H	1.32	303.15
[190]	[4,4,4,14-P][HFPS]	0.24	283.15
[190]	[6,6,6,14-P][TPES]	0.08	283.15
[190]	[bmim][HFPS]	0.27	283.15
[190]	[bmim][TPES]	0.18	283.15
[190]	[bmim][TTES]	0.27	283.15
[190]	[emim][BEI]	0.15	283.15
[190]	[emim][TF2N]	0.20	283.15
[190]	[Hmim][BF4]	0.38	283.15
[190]	[Hmim][PF6]	0.38	283.15
[190]	[Hmim][TF2N]	0.18	283.15
[190]	[4,4,4,14-P][HFPS]	0.39	298.15
[190]	[6,6,6,14-P][TPES]	0.16	298.15
[190]	[bmim][HFPS]	0.39	298.15
[190]	[bmim][TPES]	0.25	298.15
[190]	[bmim][TTES]	0.39	298.15
[190]	[emim][BEI]	0.25	298.15
[190]	[emim][TF2N]	0.32	298.15
[190]	[Hmim][BF4]	0.40	298.15

[190]	[Hmim][PF6]	0.48	298.15
[190]	[Hmim][TF2N]	0.27	298.15
[190]	[4,4,4,14-P][HFPS]	0.28	323.15
[190]	[6,6,6,14-P][TPES]	0.26	323.15
[190]	[bmim][HFPS]	0.69	323.15
[190]	[bmim][TPES]	0.48	323.15
[190]	[bmim][TTES]	0.69	323.15
[190]	[emim][BEI]	0.48	323.15
[190]	[emim][TF2N]	0.61	323.15
[190]	[Hmim][BF4]	0.74	323.15
[190]	[Hmim][PF6]	0.91	323.15
[190]	[Hmim][TF2N]	0.52	323.15
[190]	[4,4,4,14-P][HFPS]	1.17	348.15
[190]	[6,6,6,14-P][TPES]	0.43	348.15
[190]	[bmim][HFPS]	1.17	348.15
[190]	[bmim][TPES]	0.78	348.15
[190]	[bmim][TTES]	1.17	348.15
[190]	[emim][BEI]	0.78	348.15
[190]	[emim][TF2N]	1.00	348.15
[190]	[Hmim][BF4]	1.13	348.15
[190]	[Hmim][PF6]	1.13	348.15
[190]	[Hmim][TF2N]	0.69	348.15

8. Appendix B: COSMO-RS Computational Pathways

Thermodynamic properties of absorbed compounds, DES, and act of absorption will be predicted through COSMO-RS. If available, molecule files for analyte and DES components (HBAs and HBDs) will be gathered from the onboard database of COSMO-RS. Otherwise, molecules will be imported as SMILES files from PubChem. Files imported from PubChem will be run in TmoleX (version 4.5.3N) to solve for the lowest energetic geometric conformation and the sigma surface charges. All DFT calculations will be performed at the basis point density functional theory b-p DFT level and Karlsruhe (Ahlrichs) def2-TZVP (default-2 Valence Triple-Zeta Polarization) basis set [129]. HBA salts will be modelled in a single .cosmo extension file. The output files from TmoleX will be uploaded to COSMOConf18 for conformational analysis. The outputs of COSMOConf18 will be uploaded to COSMOthermX to predict thermodynamic properties including chemical potentials (μ). Equation 1 shows how separate functions of the sigma segments (E_{misfit}, E_{HB}, and p_s) are responsible for the prediction of chemical potential.

$$\mu_s(\sigma) = -\frac{RT}{a_{eff}} \ln\left[\int_s p(\sigma')^{\left(\frac{a_{eff}}{RT}(\mu_s(\sigma') - E_{misfit}(\sigma,\sigma') - E_{HB}(\sigma,\sigma'))\right)} d\sigma'\right] \quad (1)$$

Where $\mu_s(\sigma)$ is the chemical potential as a function of sigma (σ). σ and σ' are two interacting surface segments between two molecules prime and non-prime. a_{eff} is the effective contact area. E_{misfit} is the energetic penalty for charge and steric misfits of the segments. E_{HB} is the energy resulting from hydrogen bonding. $p_s(\sigma)$ is the distribution function. R is the gas constant and T is absorption temperature. These chemical potentials are further used as a basis for COSMO-RS calculations. Further description of the COSMO-RS software fundamentals may be found elsewhere [129]–[132].

Next the calculated sigma potentials are used to determine the chemical potential of compound i in the DES (S). This is achieved through equation 2 where the potential of the system is integrated over the surface of the compounds. C is a designated combinatorial term that accounts for area and volume geometric characteristics of differing molecules.

$$\mu_S^i = \mu_{C,S}^i + \int p^i(\sigma)\mu(\sigma)d\sigma \quad (2)$$

The activity coefficients ($\ln\gamma$) are calculated through equation 2 in COSMOthermX which represent the affinity between solvent and solute and are strong indicators of solubility [121], [133].

$$\ln \gamma_s^i = \frac{(\mu\dot{s} - \mu\dot{b})}{RT} \quad (3)$$

COSMOthermX uses the chemical potentials (μ) to determine ln γ_s^i of siloxane compound (i) in DES (s) at infinite dilution. R is the gas constant, and T is the absorption temperature of the system which was kept at 25°C as similar studies report lower temperatures equate to better solubilituies among DES and gaseous compounds [134], [135]. Equation 3 is used to convert ln γ_s^i into solubility capacity in some instances [136].

$$C_s^i = \frac{1}{\gamma_s^i} \quad (4)$$

In equation 4, Henry coefficients (H) used for the validation procedure are calculated through an iterative process of varying the pressures (P) with the concentration (C).

$$C=H*P \quad (5)$$

Similar to the ln activity coefficient, Gibbs free energy of solvation (G_{solv}) is computed as a difference in chemical potentials. G_{solv} is the result from the difference of the chemical potential of the siloxane compound i in its pure phase μ_p^i and its chemical potential in the solvent phase μ_s^i at infinite dilution. Equation 5 describes the process.

$$G_{solv} = \mu_s^i - \mu_p^i \quad (6)$$

The predicted solubility of analyte in DES is produced through equation 6. Where j is the gaseous analyte compound, p_j is the partial pressure of analyte in solvent system, p_j^o is the partial pressure of analyte in

its pure form, x_j is the solubility of analyte in solvent, and γ_j is the activity coefficient of analyte in solvent.

$$p_j = p_j^o x_j \gamma_j \quad (7)$$

Along with activity coefficients, another powerful indicator of solubility and interactions is the excess enthalpy of interaction (H_{int}) for the absorption [137]. Where ln gamma draws its importance from its relation to Hildebrand solubility, excess enthalpy of interaction (H_{int}) is a temperature derivative of Gibbs free energy, allowing for a more precise study of the contributions from each interaction type (hydrogen bond and van der Waals bond) [138], [139]. These interaction types are represented through COSMOthermX parameters used to measure the total enthalpy of mixing as expressed in equation 7.

The excess enthalpy of a system was solved through equation 4. Where H_{int} is the excess enthalpy of mixing or excess enthalpy of interaction for each molecule in the system, $H_{i,mix}$ and $H_{i,pure}$ are the enthalpies of the molecule i in the mixture and in pure form respectively. x_i is the composition of component i.

$$H_{int} = \sum x_i (H_{i,mix} - H_{i,pure}) \quad (8)$$

$$H_{int} = H_{mf} + H_{hb} + H_{vdw} \quad (9)$$

Where H_{mf} is the enthalpic penalty of a misfit factor which accounts for structural, steric hindrances, and charge misalignment [128]. H_{HB} is the enthalpic contribution from hydrogen bond interactions when mixing, and H_{vdw} is the Vander walls contribution [140].

Quantitative structure property relationships (QSPR) descriptors can be generated from sigma potential profiles reported in .cosmo files [141]. These moments (M) consist of σ polynomial function ($f_i(\sigma)$) which are reported in equation 8 and can be used in several property predictions in COSMOthermX like density and viscosity [131]. An analyte specific moment (M_i) is computed through equation 9 from the σ profile (p(σ)) of the siloxane and $f_i(\sigma)$.

$$f_i(\sigma) = \sigma^i \; for \; i \geq 0 \quad (10)$$

$$M_i^s = \int p(\sigma) f_i(\sigma) d\sigma \quad (11)$$

Some of these moments have been correlated with the chemical's properties while others remain as simple regression parameters. The zeroth order moment (M_0^s, where i=0) is the total surface area of the analyte "s", the first order moment (M_1^s, where i=1) is the total COSMO polarization charge on the surface of the given analyte, the second moment (M_2^s, where i=2) is a vector of total COSMO polarization energy of the molecule, the third moment (M_3^s, where i=3) correlates to the measure of sigma profile symmetry, and the hydrogen bond donating and hydrogen bond accepting

moments (M^{s}_{Hdon} and M^{s}_{Hacc} respectively) are measurements of the analytes ability to act as each, respectively [128].

9. Appendix C: EHS Analyses

The quantitative structure-activity relationship (QSAR) based software VEGA [60] was used to evaluate the EHS factors for each solvent based upon five properties:persistence, bioconcentrationfactor (BCF), mutagenicity, carcino genicity, and acute toxicity. Persistence is measured in days chemical is retained in the medium. Toxicity is measured in lethal dose 50 (LD50) of units mg/kg. BCF is measured in half life nits of L/kg. Mutagenicity is measured in revertants per microgram (rev/µg). Carcinogenicity is measured in concentrations per lifespan ([C]/time). VEGA has been used extensively in literature for EHS property analysis of novel solvents [51,61,62]. VEGA relies upon a k-nearest neighbors (KNN) algorithm to predict EHS properties based upon the structure of the input molecule and its database of experimental results [63]. VEGA model was run for each of the five properties studied for selected DES components in each appropriate projects for thoroughness and cross-checking validations. The persistence models were evaluated for soil, water, and air for thoroughness. For the DES included in the EHS report, the pure components that comprise the solvent are analyzed as the DES readily dissociate in the presence of moisture and are not covalently bound. Thus, their fate in the environment

would not be in the DES form but rather in the individual pure HBA and HBD forms. Furthermore, a cross validation of the results was performed through pure component safety data sheet (SDS) analysis. The National Fire Protection Association (NFPA) value rankings and the Occupational Safety and Health Administration (OSHA) Hazard Communication Standard (OHCS) categorization are used from literature for validation of VEGA results when available

10. Appendix D: Stream tables

Table 20: Eucalyptol Stream Table

	Units	FLASH-L	FLASH-V	LEANSOL	LEANSOL2	MIXED	PRODUCT	RICHSOL	S6	S9	S12	STRIP-B	STRIP-V	SYNGAS
From		FLASH	FLASH		PUMP	MIXER	ABSORBER	ABSORBER	B4	HEATX-1	HEATX-2	STRIPPER	STRIPPER	
To		HEATX-1		ABSORBER		PUMP		B4	FLASH	STRIPPER	MIXER	HEATX-2		ABSORBER
Stream Class		CONVEN	CONVEN	CONVEN	CONVEN	CONVEN	CONVEN	CONVEN	CONVEN	CONVEN	CONVEN	CONVEN	CONVEN	CONVEN
Phase		Liquid Phase	Vapor Phase	Liquid Phase	Liquid Phase	Liquid Phase	Vapor Phase	Liquid Phase		Liquid Phase	Liquid Phase	Liquid Phase	Vapor Phase	Vapor Phase
Temperature	C	80.0	80.0	30.0	32.2	30.0	31.2	41.7	36.8	80.0	30.0	397.0	355.4	30.0
Pressure	bar	1.0	1.0	10.0	10.0	1.0	10.0	10.0	1.0	1.0	1.0	1.0	1.0	15.0
Molar Vapor Fraction		0.0	1.0	0.0	0.0	0.0	1.0	0.0	0.3	0.0	0.0	0.0	1.0	1.0
Molar Liquid Fraction		1.0	0.0	1.0	1.0	1.0	0.0	1.0	0.7	1.0	1.0	1.0	0.0	0.0
Molar Solid Fraction		0.0	0.0	0.0	0.0	0.0	0.0	0.0	0.0	0.0	0.0	0.0	0.0	0.0
Mass Vapor Fraction		0.0	1.0	0.0	0.0	0.0	1.0	0.0	0.0	0.0	0.0	0.0	1.0	1.0
Mass Liquid Fraction		1.0	0.0	1.0	1.0	1.0	0.0	1.0	1.0	1.0	1.0	1.0	0.0	0.0
Mass Solid Fraction		0.0	0.0	0.0	0.0	0.0	0.0	0.0	0.0	0.0	0.0	0.0	0.0	0.0
Molar Enthalpy	cal/mol	-226006.7	-44576.5	-276526.8	-275736.9	-276211.5	-68.7	-162912.3	-162912.3	-226006.7	-276211.5	-159412.4	-83491.9	-28134.7
Mass Enthalpy	cal/gm	-426.2	-1437.7	-438.3	-437.6	-438.3	-33.3	-478.1	-478.1	-426.2	-438.3	-253.0	-291.3	-1312.7
Molar Entropy	cal/mol-K	-824.7	16.5	-1030.0	-1027.1	-1028.7	-4.4	-523.9	-523.3	-824.7	-1028.7	-783.6	-320.1	6.9
Mass Entropy	cal/gm-K	-1.6	0.5	-1.6	-1.6	-1.6	-2.1	-1.5	-1.5	-1.6	-1.6	-1.2	-1.1	0.3
Molar Density	mol/cc	0.0	0.0	0.0	0.0	0.0	0.0	0.0	0.0	0.0	0.0	0.0	0.0	0.0
Mass Density	gm/cc	1.0	0.0	1.0	1.0	1.0	0.0	1.1	0.0	1.0	1.0	0.8	0.0	0.0
Enthalpy Flow	cal/sec	-191179.9	-23074.5	-194811.6	-165446.8	-165731.5	-21.5	-222137.6	-222137.6	-191179.9	-165731.5	-95650.1	-20529.6	-27347.6

Average MW		530.3	31.0	630.9	630.1	630.1	2.1	340.8	340.8	530.3	630.1	630.1	286.7	21.4
Mole Flows	kmol/hr	3.0	1.9	2.5	2.2	2.2	1.1	4.9	4.9	3.0	2.2	2.2	0.9	3.5
H2		0.0	0.1	0.0	0.0	0.0	1.0	0.0	0.0	0.0	0.0	0.0	0.0	0.4
H2S		0.0	0.0	0.0	0.0	0.0	0.0	0.0	0.0	0.0	0.0	0.0	0.0	0.0
CO		0.1	0.6	0.0	0.0	0.0	0.0	0.3	0.3	0.1	0.0	0.0	0.5	0.5
CO2		0.0	0.3	0.0	0.0	0.0	0.0	0.1	0.1	0.0	0.0	0.0	0.0	0.2
DES12		0.8	0.0	1.0	1.0	1.0	0.0	0.5	0.5	0.8	1.0	1.0	0.4	0.0
Mass Flows	kg/hr	1614.9	57.8	1600.0	1361.1	1361.1	2.3	1672.7	1672.7	1614.9	1361.1	1361.1	253.7	75.0
Volume Flow	l/min	27.3	911.9	27.6	23.5	23.5	47.5	25.4	604.3	27.3	23.5	29.9	771.1	98.0

Table 21: 4-Cyanophenol stream table.

	Units	FLASH-L	FLASH-V	LEANSOL	PRODUCT	RICHSOL	S6	SYNGAS	LEANSOL	S9	S12	STRIP-B	STRIP-V
From		FLASH	FLASH		ABSORBER	ABSORBER	B4		PUMP	STRIPPER	HEATX-2	HEATX-1	HEATX-1
To				ABSORBER		B4	FLASH	ABSORBER		HEATX-1	PUMP	HEATX-2	
Stream Class		CONVEN	CONVEN	CONVEN	CONVEN	CONVEN	CONVEN	CONVEN	CONVEN	CONVEN	CONVEN	CONVEN	CONVEN
Phase		Liquid Phase	Vapor Phase	Liquid Phase	Vapor Phase	Liquid Phase		Vapor Phase	Liquid Phase		Liquid Phase	Liquid Phase	Vapor Phase
Temperature	C	35.5	35.5	30.0	30.4	35.5	31.3	30.0	33.7	100.0	30.0	398.9	341.0
Pressure	bar	1.0	1.0	15.0	14.0	14.0	1.0	15.0	15.0	1.0	1.0	1.0	1.0
Molar Vapor Fraction		0.0	1.0	0.0	1.0	0.0	0.4	1.0	0.0	0.0	0.0	0.0	1.0
Molar Liquid Fraction		1.0	0.0	1.0	0.0	1.0	0.6	0.0	1.0	1.0	1.0	1.0	0.0
Molar Solid Fraction		0.0	0.0	0.0	0.0	0.0	0.0	0.0	0.0	0.0	0.0	0.0	0.0
Mass Vapor Fraction		0.0	1.0	0.0	1.0	0.0	0.0	1.0	0.0	0.0	0.0	0.0	1.0
Mass Liquid Fraction		1.0	0.0	1.0	0.0	1.0	1.0	0.0	1.0	1.0	1.0	1.0	0.0
Mass Solid Fraction		0.0	0.0	0.0	0.0	0.0	0.0	0.0	0.0	0.0	0.0	0.0	0.0
Molar Enthalpy	cal/mol	-216351.2	-43737.8	-235080.2	-340.8	-154881.5	-154881.5	-28134.7	-234310.8	-203880.3	-235013.7	-129353.6	-65585.4
Mass Enthalpy	cal/gm	-348.0	-1392.8	-345.8	-156.0	-378.0	-378.0	-1312.7	-344.8	-328.0	-345.8	-190.4	-267.1
Molar Entropy	cal/mol-K	-885.4	16.7	-977.6	-5.0	-564.3	-563.3	6.9	-974.8	-846.6	-977.3	-753.8	-234.6
Mass Entropy	cal/gm-K	-1.4	0.5	-1.4	-2.3	-1.4	-1.4	0.3	-1.4	-1.4	-1.4	-1.1	-1.0
Molar Density	mol/cc	0.0	0.0	0.0	0.0	0.0	0.0	0.0	0.0	0.0	0.0	0.0	0.0
Mass Density	gm/cc	1.1	0.0	1.1	0.0	1.3	0.0	0.0	1.1	0.3	1.1	0.9	0.0
Enthalpy Flow	cal/sec	-213650.0	-24183.1	-211348.8	-112.7	-238583.6	-238583.6	-27347.6	-200506.0	-201334.7	-201107.5	-110691.4	-8643.3
Average MW		621.6	31.4	679.7	2.2	409.8	409.8	21.4	679.5	621.6	679.5	679.5	245.6
Mole Flows	kmol/hr	3.6	2.0	3.2	1.2	5.5	5.5	3.5	3.1	3.6	3.1	3.1	0.5
H2		0.0	0.0	0.0	1.0	0.0	0.0	0.4	0.0	0.0	0.0	0.0	0.0

H2S		0.0	0.0	0.0	0.0	0.0	0.0	0.0	0.0	0.0	0.0	0.0	0.1
CO		0.1	0.7	0.0	0.0	0.3	0.3	0.5	0.0	0.1	0.0	0.0	0.5
CO2		0.0	0.3	0.0	0.0	0.1	0.1	0.2	0.0	0.0	0.0	0.0	0.1
DES12		0.9	0.0	1.0	0.0	0.6	0.6	0.0	1.0	0.9	1.0	1.0	0.3
Mass Flows	kg/hr	2209.9	62.5	2200.0	2.6	2272.4	2272.4	75.0	2093.4	2209.9	2093.4	2093.4	116.5
Volume Flow	l/min	32.5	851.3	33.5	35.8	29.1	862.0	98.0	32.0	123.3	31.9	38.9	403.8

Table 22: Lidocaine Stream Tables

	Units	FLASH-L	FLASH-V	LEANSOL	LEANSOL2	MIXED	PRODUCT	RICHSOL	S9	S10	S12	STRIP-B	STRIP-V	SYNGAS
Description														
From					PUMP	MIXER	ABSORBER	ABSORBER	HEATX-1	B4	HEATX-2	STRIPPER	STRIPPER	
To		HEATX-1		ABSORBER		PUMP		B4	STRIPPER		MIXER	HEATX-2		ABSORBER
Stream Class		CONVEN	CONVEN	CONVEN	CONVEN	CONVEN	CONVEN	CONVEN	CONVEN	CONVEN	CONVEN	CONVEN	CONVEN	CONVEN
Phase		Liquid Phase	Vapor Phase	Liquid Phase	Liquid Phase	Liquid Phase	Vapor Phase	Liquid Phase	Liquid Phase		Liquid Phase	Liquid Phase	Vapor Phase	Vapor Phase
Temperature	C	120.0	120.0	30.0	32.4	30.0	30.5	34.6	100.0	31.3	30.0	386.2	100.3	30.0
Pressure	bar	1.0	1.0	15.0	11.0	1.0	10.0	10.0	1.0	1.0	1.0	1.0	1.0	15.0
Molar Vapor Fraction		0.0	1.0	0.0	0.0	0.0	1.0	0.0	0.0	0.4	0.0	0.0	1.0	1.0
Molar Liquid Fraction		1.0	0.0	1.0	1.0	1.0	0.0	1.0	1.0	0.6	1.0	1.0	0.0	0.0
Molar Solid Fraction		0.0	0.0	0.0	0.0	0.0	0.0	0.0	0.0	0.0	0.0	0.0	0.0	0.0
Mass Vapor Fraction		0.0	1.0	0.0	0.0	0.0	1.0	0.0	0.0	0.0	0.0	0.0	1.0	1.0
Mass Liquid Fraction		1.0	0.0	1.0	1.0	1.0	0.0	1.0	1.0	1.0	1.0	1.0	0.0	0.0
Mass Solid Fraction		0.0	0.0	0.0	0.0	0.0	0.0	0.0	0.0	0.0	0.0	0.0	0.0	0.0
Molar Enthalpy	cal/mol	-316760.5	-41931.7	-356921.8	-352287.8	-352933.8	-4308.8	-220117.3	-322996.1	-220117.3	-352933.8	-216320.3	-35585.5	-28134.7
Mass Enthalpy	cal/gm	-417.6	-1337.0	-450.7	-449.8	-450.7	-1043.4	-476.6	-425.8	-476.6	-450.7	-276.2	-1175.7	-1312.7
Molar Entropy	cal/mol-K	-1174.3	19.0	-1309.2	-1291.7	-1293.9	-3.7	-734.0	-1190.9	-733.2	-1293.9	-1004.1	20.8	6.9
Mass Entropy	cal/gm-K	-1.5	0.6	-1.7	-1.6	-1.7	-0.9	-1.6	-1.6	-1.6	-1.7	-1.3	0.7	0.3
Molar Density	mol/cc	0.0	0.0	0.0	0.0	0.0	0.0	0.0	0.0	0.0	0.0	0.0	0.0	0.0
Mass Density	gm/cc	1.0	0.0	1.0	1.0	1.0	0.0	1.2	1.0	0.0	1.0	0.8	0.0	0.0
Enthalpy Flow	cal/sec	-267274.7	-24387.1	-287922.8	-287525.9	-288053.2	-1522.5	-313747.9	-272536.1	-313747.9	-288053.2	-176553.7	-982.4	-27347.6
Average MW		758.5	31.4	792.0	783.2	783.2	4.1	461.8	758.5	461.8	783.2	783.2	30.3	21.4

Mole Flows	kmol/hr	3.0	2.1	2.9	2.9	2.9	1.3	5.1	3.0	5.1	2.9	2.9	0.1	3.5
Mole Fractions														
H2		0.0	0.0	0.0	0.0	0.0	0.9	0.0	0.0	0.0	0.0	0.0	0.0	0.4
H2S		0.0	0.0	0.0	0.0	0.0	0.0	0.0	0.0	0.0	0.0	0.0	0.0	0.0
CO		0.0	0.7	0.0	0.0	0.0	0.0	0.3	0.0	0.3	0.0	0.0	0.9	0.5
CO2		0.0	0.3	0.0	0.0	0.0	0.0	0.1	0.0	0.1	0.0	0.0	0.1	0.2
DES12		1.0	0.0	1.0	1.0	1.0	0.0	0.6	1.0	0.6	1.0	1.0	0.0	0.0
Mass Flows	kg/hr	2304.1	65.7	2300.0	2301.1	2301.1	5.3	2369.7	2304.1	2369.7	2301.1	2301.1	3.0	75.0
Mass Fractions														
Volume Flow	l/min	40.2	1140.7	39.4	39.2	39.2	53.5	33.1	39.8	798.0	39.2	48.0	51.4	98.0

Table 23: DPEG Stream Table

	Units	FLASH-L	FLASH-V	LEANSOL	LEANSOL2	MIXED	PRODUCT	S6	S8	S9	S12	STRIP-B	STRIP-V	SYNGAS
From		FLASH	FLASH		PUMP	B10	ABSORBER	B4	ABSORBER	HEATX-1	HEATX-2	STRIPPER	STRIPPER	
To		HEATX-1		ABSORBER		PUMP		FLASH	B4	STRIPPER	B10	HEATX-2		ABSORBER
Stream Class		CONVEN	CONVEN	CONVEN	CONVEN	CONVEN	CONVEN	CONVEN	CONVEN	CONVEN	CONVEN	CONVEN	CONVEN	CONVEN
Phase		Liquid Phase	Vapor Phase	Liquid Phase	Liquid Phase	Liquid Phase	Vapor Phase		Liquid Phase		Liquid Phase	Liquid Phase	Vapor Phase	Vapor Phase
Temperature	C	33.8	33.8	30.0	32.2	30.0	30.4	31.1	31.7	120.0	30.0	234.9	205.0	30.0
Pressure	bar	1.0	1.0	19.0	19.0	1.0	18.0	1.0	18.0	1.0	1.0	1.0	1.0	18.0
Molar Vapor Fraction		0.0	1.0	0.0	0.0	0.0	1.0	0.0	0.0	0.0	0.0	0.0	1.0	1.0
Molar Liquid Fraction		1.0	0.0	1.0	1.0	1.0	0.0	1.0	1.0	1.0	1.0	1.0	0.0	0.0
Molar Solid Fraction		0.0	0.0	0.0	0.0	0.0	0.0	0.0	0.0	0.0	0.0	0.0	0.0	0.0
Mass Vapor Fraction		0.0	1.0	0.0	0.0	0.0	1.0	0.0	0.0	0.0	0.0	0.0	1.0	1.0
Mass Liquid Fraction		1.0	0.0	1.0	1.0	1.0	0.0	1.0	1.0	1.0	1.0	1.0	0.0	0.0
Mass Solid Fraction		0.0	0.0	0.0	0.0	0.0	0.0	0.0	0.0	0.0	0.0	0.0	0.0	0.0
Molar Enthalpy	kcal/mol	-23.4	-79.6	-22.5	-22.2	-22.6	-14.7	-26.0	-26.0	-9.6	-22.6	15.4	-42.9	-28.2
Mass Enthalpy	kcal/kg	-85.1	-1997.8	-80.3	-79.2	-80.6	-892.2	-97.8	-97.8	-34.9	-80.6	54.9	-330.3	-1313.8
Molar Entropy	cal/mol-K	-45.3	4.9	-48.0	-47.0	-47.9	7.6	-44.5	-44.9	-5.8	-47.9	45.9	29.2	6.5
Mass Entropy	cal/gm-K	-0.2	0.1	-0.2	-0.2	-0.2	0.5	-0.2	-0.2	0.0	-0.2	0.2	0.2	0.3
Molar Density	kmol/cum	3.8	0.0	3.7	3.7	3.7	0.7	0.8	3.9	1.5	3.7	2.7	0.0	0.7
Mass Density	kg/cum	1038.5	1.6	1046.1	1043.5	1043.6	11.7	217.8	1041.7	404.2	1043.6	745.5	3.3	15.3
Enthalpy Flow	Gcal/hr	-0.3	0.0	-0.2	-0.2	-0.2	0.0	-0.3	-0.3	-0.1	-0.2	0.2	0.0	-0.1
Average MW		274.9	39.8	280.0	280.0	280.0	16.5	265.7	265.7	274.9	280.0	280.0	129.8	21.4
Mole Flows	kmol/hr	10.9	0.4	10.7	10.6	10.6	2.7	11.4	11.4	10.9	10.6	10.6	0.4	3.4

Mass Flows	kg/hr	3010.0	17.8	3000.0	2962.4	2962.4	44.2	3027.8	3027.8	3010.0	2962.4	2962.4	47.6	72.0
Volume Flow	cum/hr	2.9	11.4	2.9	2.8	2.8	3.8	13.9	2.9	7.4	2.8	4.0	14.3	4.7